Chem Soc Rev

RSC Publishing

TUTORIAL REVIEW

View Article Online
View Journal | View Issue

BODIPY dyes in photodynamic therapy

Anyanee Kamkaew,[a] Siang Hui Lim,[bc] Hong Boon Lee,[b] Lik Voon Kiew,[d] Lip Yong Chung[c] and Kevin Burgess*[a]

Cite this: *Chem. Soc. Rev.*, 2013, **42**, 77

BODIPY dyes tend to be highly fluorescent, but their emissions can be attenuated by adding substituents with appropriate oxidation potentials. Substituents like these have electrons to feed into photoexcited BODIPYs, quenching their fluorescence, thereby generating relatively long-lived triplet states. Singlet oxygen is formed when these triplet states interact with $^3O_2$. In tissues, this causes cell damage in regions that are illuminated, and this is the basis of photodynamic therapy (PDT). The PDT agents that are currently approved for clinical use do *not* feature BODIPYs, but there are many reasons to believe that this situation will change. This review summarizes the attributes of BODIPY dyes for PDT, and in some related areas.

Received 15th June 2012

DOI: 10.1039/c2cs35216h

www.rsc.org/csr

Introduction

Photodynamic therapy (PDT) is an emerging clinical modality for treatment of neoplastic and non-malignant lesions. Applications of PDT require a photosensitizing drug, light, and oxygen. A series of photochemical reactions generate *singlet* oxygen from the $^3O_2$ causing tissue damage in the regions where these three key components come together.[1,2] This is a highly localized effect because the half-life of singlet oxygen is low (0.6×10^{-6} s).[3] In cancer treatment, PDT can destroy the vasculature surrounding tumour cells, and activates immunological responses against them.[4] The main attribute of PDT is its potential for dual selectivity, *i.e.* preferential accumulation of the photosensitizer in diseased – over normal – tissues, and focusing light to confine damage to the targeted

[a] *Department of Chemistry, Box 30012, Texas A & M University, College Station, TX 77841-3012, USA. E-mail: burgess@tamu.edu*
[b] *Cancer Research Initiatives Foundation (CARIF), Subang Jaya Medical Centre, 47500 Subang Jaya, Selangor, Malaysia*
[c] *Department of Pharmacy, Faculty of Medicine, University of Malaya, 50603 Kuala Lumpur, Malaysia*
[d] *Department of Pharmacology, Faculty of Medicine, University of Malaya, Kuala Lumpur, 50603, Malaysia*

Anyanee Kamkaew

Anyanee Kamkaew received her BSc in Chemistry from Silpakorn University in Nakorn Pathom, Thailand, in 2007. She received a Development and Promotion of Science and Technology Talents Project (DPST) scholarship from Royal Government of Thailand in 2009 to pursue her PhD under the guidance of Prof. Kevin Burgess at Texas A&M University. Her current research of interest is in the field of organic and biomolecular synthesis to probe intramolecular delivery and targeting.

Siang Hui Lim

Siang Hui Lim received his BSc in Biomedical Sciences from University Kebangsaan Malaysia in Kuala Lumpur, then did his MSc research work in the field of Molecular Medicine in University Putra Malaysia in Selangor. Since 2007, he served as a Research Scientist in a non-profit cancer research institution in Malaysia, Cancer Research Initiatives Foundation (CARIF). His current research focuses on characterizing the photodynamic activity of potential photosensitizers and the antitumor activity of potential antineoplastic agents. He is currently pursuing his PhD in the field of photodynamic therapy focusing on improving the delivery of photosensitizers.

region.[5] PDT is relatively non-invasive, and treatments can be repeated without induction of resistance.[2]

One of the earliest clinical PDT agents is porfimer sodium (Photofrin®), a purified hematoporphyrin derivative. Porfimer sodium is a mixture of oligomeric porphyrin units (up to eight) linked by esters and ethers. It has received worldwide regulatory approval in several indications, including cancers of the esophagus, lung and bladder. Porfimer sodium is activated by red light at *ca.* 630 nm. Photons of this wavelength do not penetrate tissue beyond a few millimeters, hence porfimer sodium is only suitable for superficial tumours, or ones that can be reached *via* endoscopic/fiber optic procedures. Moreover, porfimer sodium has a low absorbance at 630 nm necessitating extended irradiation from a high-energy source, and this often leads to complications. Another disadvantage of porfimer sodium is that it is not cleared quickly leading to post-treatment skin photosensitivity.[6]

Recognition of the disadvantages of porfimer sodium has inspired efforts to develop more effective PDT photosensitizers. Desirable properties[7,8] for such agents include:

- low toxicity in the absence of light;
- low side-effect profiles (*e.g.* skin photosensitivity and pain after irradiation);
- appropriate lipophilic/hydrophilic balance for selective accumulation in tumour tissue;
- high extinction coefficients, particularly at long wavelengths for deep tissue penetration of light;
- low quantum yields for photobleaching; and
- high singlet-to-triplet intersystem crossing efficiencies.

Table 1 lists some newer photosensitizers that have been approved for anti-cancer PDT along with some of their salient physicochemical properties (comprehensive reviews on these compounds have been published elsewhere).[8] One of these

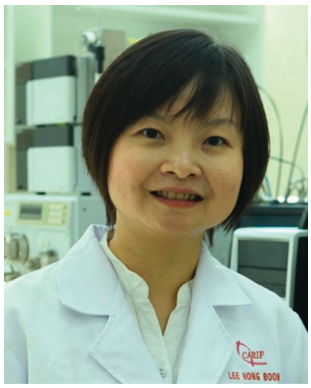

Hong Boon Lee

Hong Boon Lee obtained her BA (1996) and PhD (2000) in Organic Chemistry from the University of Cambridge, UK. Her PhD thesis under the tutelage of Prof. Shankar Subramanian, Department of Chemistry, focused on new methodologies in solid-phase synthesis of small molecules. She then won a post-doctoral research fellowship from the Wellcome Trust, UK, to make bioactive peptidomimetics under the guidance of Prof. Kevin Burgess at Texas A&M University, USA. Since 2002, Dr Lee has been conducting research at CARIF, Malaysia, where she combines chemistry and biology to discover and develop new anti-cancer compounds including photosensitizers for photodynamic therapy.

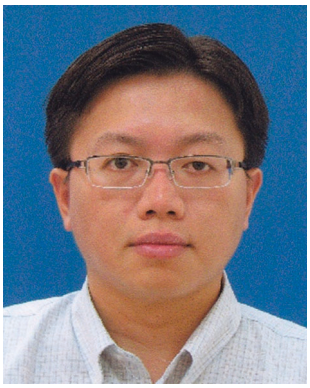

Lik Voon Kiew

Lik Voon Kiew received his doctorate from the University of Malaya, Malaysia, in 2008. He is currently a senior lecturer at the Pharmacology department, Faculty of Medicine of the University of Malaya, Malaysia. His current research interests include the development and in vitro/in vivo evaluation of cancer targeting drug carriers and anticancer photosensitizers.

Lip Yong Chung

Lip Yong Chung received his doctorate in pharmacy from the University of Cardiff, UK, in 1990. He joined Cardiff University as a research associate focusing on industry sponsored research and is currently a Professor in Pharmaceutical Sciences at the Faculty of Medicine of the University of Malaya, Malaysia. His current research interests include the design of bioactive molecules of pharmacological interest and the study of targeting biological systems.

Kevin Burgess

Suspecting that medicinal chemists have historically over-emphasised cytotoxicity data and under-emphasised the importance of chemical methods to target tumors, Kevin Burgess has become interested in the idea of using two targeting techniques simultaneously. Photodynamic therapy (PDT) is spatially targeted (to areas that are irradiated), and could be coupled with molecular fragments for active targeting of tumors. Burgess with co-workers at TAMU and in KL wrote this review to obtain a better understanding of what, if anything, had been done with BODIPY PDT agents in this regard.

Table 1 Spectroscopic and physicochemical properties of clinically approved photosensitizers

Photosensitizer	$\lambda_{max\ abs}$ (nm)	ε (M^{-1} cm^{-1})	$\lambda_{max\ emiss}$ (nm)	Φ_{Fl}	Φ_{PB}	Φ_{Δ}	Log $P_{o/w}$
Porfimer sodium (Photofrin®)	630[13]	3000[13]	NA	NA	5.4×10^{-5} (PB)[14]	0.25 (PB + 1% TX100; 630 nm; oxygen depletion with FFA)[15]	3.96 (calc.)[16]
Protoporphyrin IX (Levulan®)	635[13]	5000[13]	630 (ex 397 nm; PBS)[17]	0.011 (ex 397 nm; PBS)[17]	NA	0.54 (PB + 1% TX100; 630 nm; lysozyme inactivation; RB at 0.75)[18]	NA
Temoporfin (Foscan®)	650 (EtOH)[19] 652 (H_2O)[19]	39 000 (EtOH)[19] 23 000 (H_2O)[19]	655 (PBS)[20]	NA	1.54×10^{-5} (PBS + 10% FCS)[21]	0.31 (PBS + 10% FCS; >610 nm; DPBF; hypericin at 0.36)[21]	9.24[22]
Verteporfin (Visudyne®)	688 (PBS + 2% TX100)[23] 692 (PBS)[23]	31 200 (PBS + 2% TX100)[23] 13 500 (PBS)[23]	694 (PBS + 2% TX100)[23] 695 (PBS)[23]	0.049 (PBS + 2% TX100)[23] 0.002 (PBS)[23]	5.35×10^{-5} (PBS + 2% TX100)[23] 2.80×10^{-5} (PBS)[23]	0.82 (PB + 1% TX100; 692 nm; lysozyme inactivation; MB at 0.52)[18]	7.76 (calc.)[24]
Talaporfin (Laserphyrin®)	654 (PBS)[25]	40 000 (PBS)[25]	660 (PBS)[25]	NA	8.2×10^{-4} (PBS)[25]	0.77 (D_2O, oxygen depletion with FFA)[25]	−1.92[26]
Ce6 (Photolon®)	663 (PBS)[27]	38 000 (PBS)[27]	662 (PBS)[27]	0.18 (PBS)[27]	NA	0.75 (PB; 660 nm; lysozyme inactivation; MB at 0.52)[18]	0.78[27]

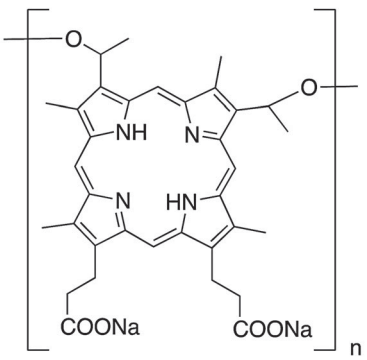

Hematoporphyrin
(Photofrin®) n=1-9
PB
$\lambda_{max\ abs}$ 630 nm
ε 1170 $M^{-1}cm^{-1}$
$^1O_2$ 0.28 (methylene blue, lysozyme inactivation)
indication: esophagus, lung and bladder cancer

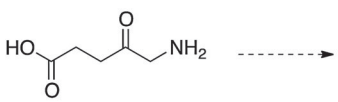

Aminolevulinic acid
(Levulan®)

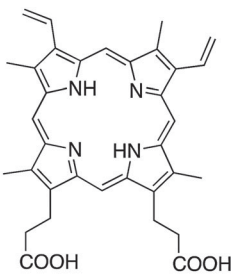

Protoporphyrin IX
PB
$\lambda_{max\ abs}$ 635 nm
ε 5000 $M^{-1}cm^{-1}$
$^1O_2$ 0.54 (methylene blue, lysozyme inactivation)
indication: non melanoma skin cancer

clinically applied photosensitizers, 5-aminolevulinic acid (ALA), is not a chromophore, but a precursor for the biosynthesis of the protoporphyrin IX (PpIX).[9] In tumours expression of ferrochelatase, the enzyme that converts PpIX to heme, is downregulated causing accumulation of the protoporphyrin PDT agent.[10] PpIX is rapidly cleared from the body, minimizing the risk of skin photosensitization.[11] However, ALA is hydrophilic and has limited penetration across certain biological barriers, so a lipophilic derivative, methyl-aminolevulinic acid, has also been developed.[12] Nevertheless, the absorption spectrum of PpIX at 630 nm is similar to that of porfimer sodium hence it also gives only superficial tissue penetration in PDT.

There are some clinically approved *chlorin*-based photosensitizers that are similar to PpIX. One of these, temoporfin (Foscan®), offers improved potency, less skin photosensitivity, and a longer maximum absorption wavelength.[28] However, temoporfin is so hydrophobic that it can precipitate upon administration.[29] Similarly verteporfin is activated by light at 690 nm, clears rapidly from the body, and only generates short-term skin photosensitivity.[30] This agent self-aggregates in aqueous solution,[31] hence it is applied in liposome formulations; this mode of delivery restricts the scope of use to, so far, age related macular degeneration caused by abnormal blood vessel growth of the retina.[32] Two other clinically approved chlorin-based photosensitizers are mono-aspartyl-L-chlorin e6 (also known as talaporfin) and chlorin e6-polyvinylpyrrolidone. Both these PDT agents are excellent singlet oxygen generators

but have high photobleaching rates that reduce their PDT efficiencies.[33]

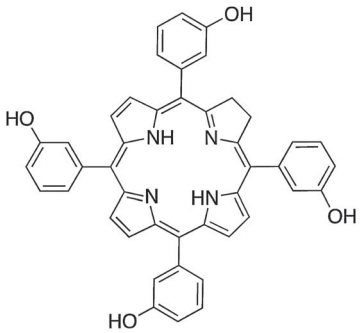

Temoporfin (Foscan®)
EtOH
$\lambda_{max\ abs}$ 650 nm
ε 39000 $M^{-1}cm^{-1}$
$^1O_2$ 0.30 (hypericin, DPPH)
indication: head and neck cancer

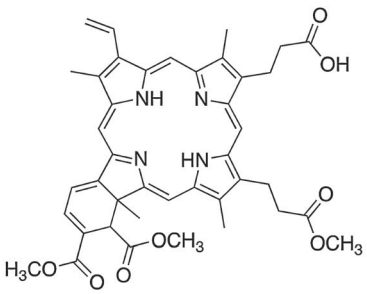

Verteporfin (Visudyne®)
PBS/Tx100
$\lambda_{max\ abs}$ 689 nm
ε 31200 $M^{-1}cm^{-1}$
$^1O_2$ 0.79 (methylene blue, lysozyme inactivation)
indication: age-related macular degeneration

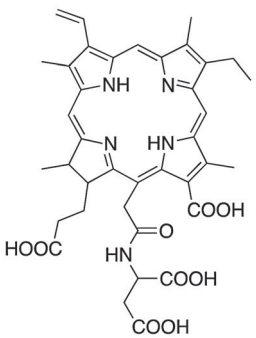

Talaporfin (Laserphyrin®)
PBS
$\lambda_{max\ abs}$ 654 nm
ε 40000 $M^{-1}cm^{-1}$
$^1O_2$ 0.48 (FFA, oxygen depletion)
indication: lung cancer

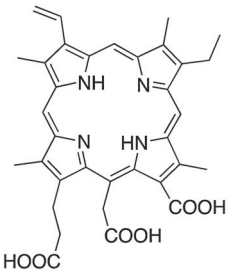

Chlorin e6-polyvinylpyrrolidone (Photolon®)
PBS
$\lambda_{max\ abs}$ 654 nm
ε 50000 $M^{-1}cm^{-1}$
$^1O_2$ 0.75 (methylene blue, lysozyme inactivation)
indication: skin and mucosal membrane cancer

The discussion above correctly implies that most of the clinically relevant PDT agents are cyclic tetrapyrroles (porphyrins, chlorins, and bacteriochlorins).[34,35] These can be synthetically inaccessible, and modifications to modulate their photophysical and biological properties are correspondingly difficult. Consequently, there is interest in non-porphyrin photosensitizers that might be made more easily.[36–38] Phenothiazinium-based structures are a well-known category of this type of PDT agent; they are easy to make but have low light-to-dark toxicity ratios.[39]

A new class of PDT agents has emerged over the past decade: these are based on the 4,4-difluoro-4-bora-3a,4a-diaza-*s*-indacene (BODIPY) core. BODIPYs have many ideal photosensitizer characteristics including high extinction coefficients, environment insensitivity, resistance to photobleaching,[40] and higher light–dark toxicity ratios[41] than phenothiazinium[39] PDT agents. Several review papers have covered the role of BODIPYs as fluorescence imaging probes,[42–46] but none have focused on derivatives for PDT. Fluorescence occurs *via* relaxation from singlet excited states, so high quantum yields for fluorescence are *undesirable* since this means that much of the energy absorbed on excitation does not cross to triplet states. Consequently, BODIPYs for PDT have to be modified to depress fluorescence and enhance singlet-to-triplet intersystem crossing. This review summarizes characteristics of selected members in this emerging class of BODIPY-based PDT agents.

Halogenated BODIPYs

BODIPY derivatives are amenable to extensive modifications around the 4,4-difluoro-4-bora-3a,4a-diaza-*s*-indacene core. Most of the dyes in this class have many ideal characteristics of PDT agents (low dark toxicities, cellular uptake, high extinction coefficients, low quantum yields for photobleaching) hence modifications are possible that enable absorbance at long wavelengths. However, most BODIPY dyes are efficiently excited into higher level *singlet* states, fluoresce from these, and do not cross to triplets; in fact, observation of triplet excited states in BODIPY dyes can be regarded as a novelty.[47,48] Photo-damage in PDT is thought to occur predominantly *via* triplet excited states, consequently BODIPY dyes for PDT tend to be modified to enhance intersystem crossing (ISC). Spin-coupling to heavy atoms is the most common of these modifications (the "heavy atom effect"), and the one most frequently encountered is halogenation. Appropriate placing of heavy atoms on the BODIPY core promotes spin–orbit coupling, hence ISC, but not energy loss from excited states. Heavy atoms are not typically added at positions that could disrupt the planarity of the dye as this would decrease conjugation.

"Tetramethyl-BODIPY" **1** does not contain a halogen, or significantly populate triplet states on excitation, and has a poor quantum yield (QY) for singlet oxygen ($^1O_2$) generation. Nagano's group was first to investigate a diiodo-analog, **2**, for singlet oxygen generation in PDT.[40] Formation of $^1O_2$ was inferred *via* a near IR absorbance at 1268 nm that emerged when **2** was excited at 514 nm. Measurements of rate and QY for $^1O_2$-generation in a standard way, using 1,3-diphenylisobenzofuran (DBPF), revealed high efficiencies for this process in both polar

and apolar solvents. Unsurprisingly, then, compound **2** was shown to have high light-to-dark photocytotoxicity ratios (HeLa cells). Nagano *et al.* suggested that high oxidation potentials are desirable because they may protect BODIPY from self-oxidation. They also argued that there are potential applications of PDT in membranes; apolar dyes like **2** are useful for studying effects in lipophilic media like this.

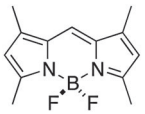

1

MeOH, $\Phi = 0.7$
$\lambda_{max\ abs}$ 502 nm
ε 120000 $M^{-1}cm^{-1}$
$\lambda_{max\ emiss}$ 508 nm
$^1O_2$ generation rel. rate 0.48 (methylene blue)
IC_{50} (HL-60 cells) >100 (0 J cm^{-2}), 4.4 ± 0.4 μM (4.1 J cm^{-2})
IC_{50} (HSC-2 cells) >100 (0 J cm^{-2}), 8.7 ± 2.0 μM (4.1 J cm^{-2})
IC_{50} (HK1 cell) 76.8 ± 10.6 μM (0 J cm^{-2}), 6.2 ± 1.2 μM (4.1 J cm^{-2})

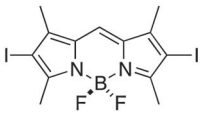

2

MeOH, $\Phi = 0.02$
$\lambda_{max\ abs}$ 534 nm
ε 110000 $M^{-1}cm^{-1}$
$\lambda_{max\ emiss}$ 548 nm
$^1O_2$ generation rel. rate 23.9 (methylene blue)
IC_{50} (HL-60 cells) >100 (0 J cm^{-2}), 62 ± 11 nM (4.1 J cm^{-2})
IC_{50} (HSC-2 cells) >100 (0 J cm^{-2}), 0.64 ± 0.06 μM (4.1 J cm^{-2})
IC_{50} (HK1 cell) >100 (0 J cm^{-2}), 0.57 ± 0.06 μM (4.1 J cm^{-2})

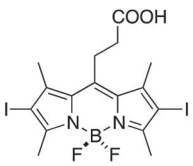

3

EtOH, $\Phi = 0.03$
$\lambda_{max\ abs}$ 525 nm
ε 93000 $M^{-1}cm^{-1}$
$\lambda_{max\ emiss}$ 540 nm
$^1O_2$ generation rel. rate 24.6 (methylene blue)
IC_{50} (HL-60 cells) >100 (0 J cm^{-2}), 45 ± 4 nM (4.1 J cm^{-2})
IC_{50} (HSC-2 cells) >100 (0 J cm^{-2}), 0.1 ± 0.06 nM (4.1 J cm^{-2})
IC_{50} (HK1 cell) 55.8 ± 0.8 μM (0 J cm^{-2}), 0.57 ± 0.1 μM (4.1 J cm^{-2})

Two studies have compared singlet oxygen generation of a range of iodinated BODIPYs. In the first,[41] iodination of *meso*-aryl substituents was found to have less impact than that of core-attached iodines. However, simple incorporation of a *meso*-ethylenecarboxylic acid group as in **3** improved the rate of singlet oxygen generation and light-induced photocytotoxicities (two of three cell lines, the other was the same over **2**). BODIPY **3** was found to localize in the mitochondria of HSC-2 cells, and to induce G_2/M arrest about 2 h after irradiation caused apoptosis. In general the physical parameters for singlet oxygen generation in this series correlated with their light-induced photocytotoxicities; this is noteworthy because such correlations are *not* always observed.

The second study of iodinated BODIPYs involved compounds like **4–6**[49] having iodine atoms at different positions around the BODIPY core, and measurement of QYs of oxygen generation for selected compounds. Surprisingly, introduction of iodines at the 3- and 5-positions *increases* fluorescence. Flash photolysis experiments showed monoexponential decay of the excited states of these dyes, consistent with predominant recovery to the starting material state indicative of high stability against photobleaching.

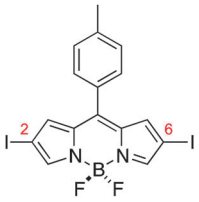

4

c-hexane, $\Phi = 0.012$
$\lambda_{max\ abs}$ 548.5 nm
ε 43000 $M^{-1}cm^{-1}$
$\lambda_{max\ emiss}$ 567.5 nm
$^1O_2$ QY 0.83 ± 0.07

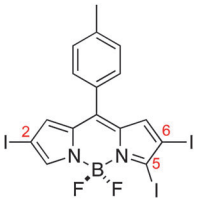

5

c-hexane, $\Phi = 0.060$
$\lambda_{max\ abs}$ 563.5 nm
ε 48000 $M^{-1}cm^{-1}$
$\lambda_{max\ emiss}$ 577.5 nm
$^1O_2$ QY 0.86 ± 0.09

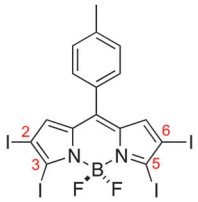

6

c-hexane, $\Phi = 0.099$
$\lambda_{max\ abs}$ 581 nm
ε 116000 $M^{-1}cm^{-1}$
$\lambda_{max\ emiss}$ 593 nm
$^1O_2$ QY 0.87 ± 0.06

Triplet excited states for BODIPY dyes are pertinent to triplet–triplet annihilation, hence some groups have studied iodinated systems like the styryl-substituted one, **7**, and the dimers **8–9**.[50] Triplet lifetimes indicated for these structures were measured *via* time-resolved spectroscopy. Estimates of triplet quantum QY were quoted based on 1 − (fluorescence QY), but this is an overestimate because it assumes that non-radiative decay processes are not operative.

A second study from Zhao and Li featured insertion of thiophene units between the iodine and the BODIPY core. This gave

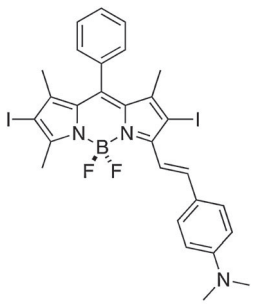

7

toluene, $\Phi = 0.095$
$\lambda_{max\ abs}$ 629 nm
ε 72800 $M^{-1}cm^{-1}$
$\lambda_{max\ emiss}$ 706 nm
triplet QY 0.905

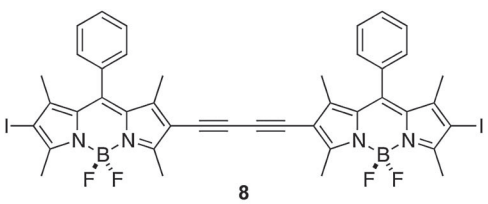

8

toluene, $\Phi = 0.11$
$\lambda_{max\ abs}$ 576 nm
ε 180000 $M^{-1}cm^{-1}$
$\lambda_{max\ emiss}$ 623 nm
triplet QY 0.895

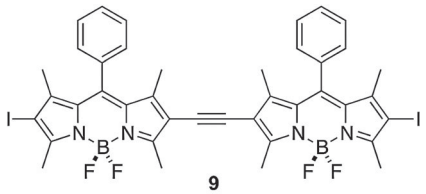

9

toluene, Φ = 0.093
$\lambda_{max\ abs}$ 575, 618 nm
ε 90900, 89500 $M^{-1}cm^{-1}$
$\lambda_{max\ emiss}$ 646 nm
triplet QY 0.907

dyes **10** and **11** that have exceptionally long triplet lifetimes, slight red-shifted absorption and fluorescence maxima, and markedly decreased extinction coefficients. These dyes also exhibit significant fluorescence indicating incomplete ISC.[51] Data specifically relating to the PDT properties of **7–11** have not been reported.

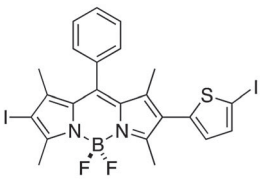

10

toluene, Φ = 0.075
$\lambda_{max\ abs}$ 532 nm
ε 69700 $M^{-1}cm^{-1}$
$\lambda_{max\ emiss}$ 609 nm
triplet QY 0.925

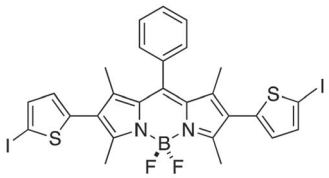

11

toluene, Φ = 0.12
$\lambda_{max\ abs}$ 526 nm
ε 49000 $M^{-1}cm^{-1}$
$\lambda_{max\ emiss}$ 612 nm
triplet QY 0.876

Thiophene is less aromatic than benzene, and its HOMO/LUMO energy levels are more suitable for conjugation with some unsaturated fragments. Extended heterocycles containing thiophene fragments can have similar useful characteristics. For instance, in **12** and **13** the heteroaryl-fused "KFL-4" BODIPY cores[52,53] have long wavelength absorption maxima, high molar extinction coefficients, high QYs for $^1O_2$ generation, and have higher photostabilities than the clinically approved PDT agent (mTHPC). Moreover, these brominated compounds have residual fluorescence that might enable them to be used simultaneously for imaging and PDT.

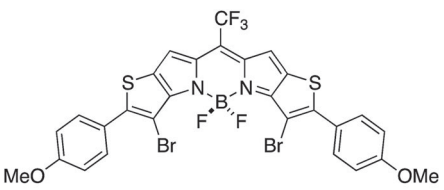

12

CH_3Cl, Φ = 0.45
$\lambda_{max\ abs}$ 720 nm
ε 89000 $M^{-1}cm^{-1}$
$\lambda_{max\ emiss}$ 754 nm
$^1O_2$ generation rel. rate 1.2 (DPBF)

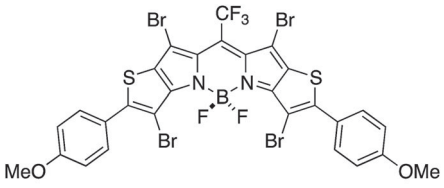

13

CH_3Cl, Φ = 0.11
$\lambda_{max\ abs}$ 766 nm
ε 75000 $M^{-1}cm^{-1}$
$\lambda_{max\ emiss}$ 820 nm
$^1O_2$ generation rel. rate 0.5 (DPBF)

Compound **7** above is an example of a "styryl-substituted" BODIPY. Akkaya's group, pioneers of this area, showed compounds like this are conveniently formed *via* Knoevenagel reactions since 2,7-methyl substituents on BODIPYs are slightly acidic.[54–57] In the first contribution on the PDT characteristics of these compounds, Akkaya's team made three brominated systems that also have oligoethylene glycol fragments to promote water-solubilities.[58] Compound **14** was the most studied of these; it had an EC_{50} (conc. required for 50% of the maximal effect; excitation at 625 nm) of 200 nM and the cytotoxicity was attributed to cell-membrane damage as indicated *via* fluorescence microscopy.

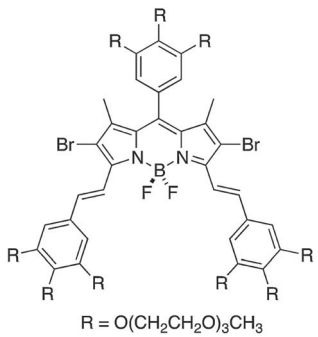

R = $O(CH_2CH_2O)_3CH_3$

14

EtOH
$\lambda_{max\ abs}$ 660 nm
ε 102000$M^{-1}cm^{-1}$
$\lambda_{max\ emiss}$ 680 nm
EC_{50} (K562 cells) 200 nM (2.5 mW cm^{-2})

In a similar study, but featuring diiodo-BODIPY dyes, Ng and co-workers found that **15** was the most promising of four related potential PDT agents. They implied that this had the lowest EC_{50} in the series (7 nM on HT29 carcinoma cells) possibly because it permeated into cells, and accumulated inside, giving the most intense fluorescence. Fluorescence microscopy experiments indicated that this compound localized in the endoplasmic reticulum (ER, an organelle involved in lipid and protein synthesis).

The research on compound **15** described above was followed by more studies on styryl-substituted BODIPYs, but this time on ones with two different substituents. It was hypothesized that the unsymmetrical substitution pattern would promote

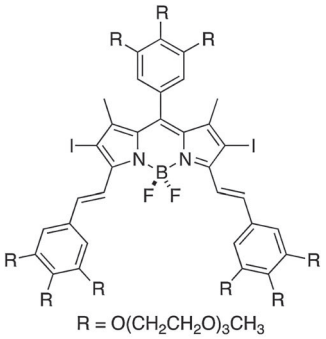

15

DMF, Φ = 0.090
$\lambda_{max\ abs}$ 667 nm
ε 70795 $M^{-1}cm^{-1}$
$\lambda_{max\ emiss}$ 703 nm
IC_{50} (HT29 cells) 7 nM (48 J cm^{-2})

amphiphilic character.[59] Dimethylamine **16** was the most studied in this series; it had a low EC_{50} (17 nM) and localized in lysosomes, less in mitochondria, and, unlike **15**, not in the ER. Overall, the authors concluded that the functional groups on the alkene were more important to the localization behavior of the dyes than the lack of symmetry in the system. This paper is an excellent reference for data on standards for singlet oxygen generation.[6,60]

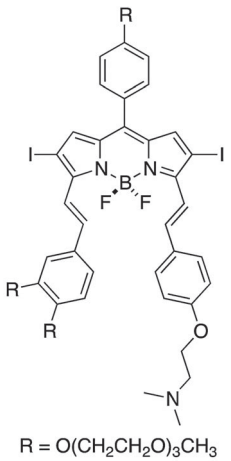

16

DMF, Φ = 0.18
$\lambda_{max\ abs}$ 665 nm
ε 81283 $M^{-1}cm^{-1}$
$\lambda_{max\ emiss}$ 695 nm
IC_{50} (HT29 cells) 17 nM (48 J cm^{-2})

An attractive feature of Akkaya's route to styryl-substituted dyes is the diversity of aromatic aldehydes that can be condensed to obtain these products. For instance, the pyrene-containing systems **17** were prepared to facilitate non-covalent, supramolecular interactions between these compounds and single-walled carbon nanotubes. Nanotubes of this kind are internalized by mammalian cells, hence their interaction with the pyrene potentially could be used for intracellular delivery of the PDT agent. Complexation of the nanotubes with the agent was, in the event, observed and accompanied by a small decrease in the singlet oxygen generation efficiency, but cytotoxicity studies have not been reported so far.

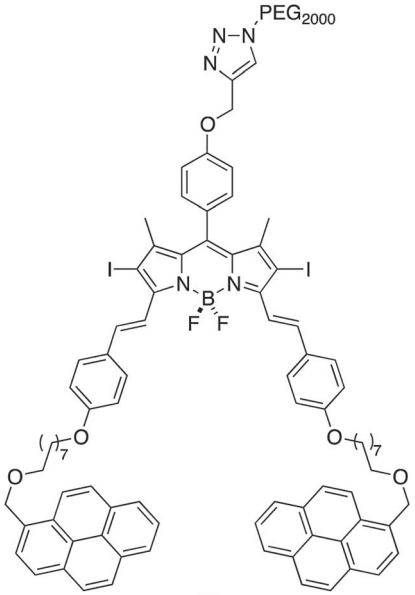

17

isopropanol
$\lambda_{max\ abs}$ 666 nm

Halogenated aza-BODIPY PDT agents

Aza-BODIPYs like **18**[61,62] have the BODIPY *meso*-carbon substituted by nitrogen, and this has some surprising effects. Notably, aza-BODIPYs have absorbance and fluorescence emissions of around 650 and 675 nm, and these may be displaced to even longer wavelengths in compounds containing an electron donating group *para*-oriented relative to the alkene (*e.g.* OMe in **18**). Bromination of aza-BODIPY 2,6-positions results in at least

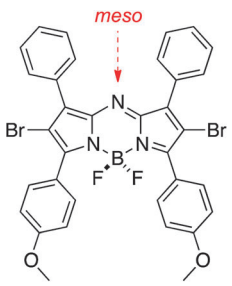

18

$CHCl_3$, Φ = 0.1
$\lambda_{max\ abs}$ 679 nm
ε 75000 $M^{-1}cm^{-1}$
$\lambda_{max\ emiss}$ 714 nm
$^1O_2$ QY 0.74
triplet QY 0.72
EC_{50} (MRC5-SV40 cells)
ND (0 J cm^{-2}), 37 ± 30 nM (8 J cm^{-2}), 14 ± 10 nM (16 J cm^{-2})
EC_{50} (HeLa cells)
ND (0 J cm^{-2}), 63 ± 20 nM (8 J cm^{-2}), 41 ± 30 nM (16 J cm^{-2})

a four-fold reduction in fluorescence QY, and an increased population of triplet states upon excitation giving at least 1000× differences between light and dark cytotoxicities. That *para*-substituent also modulates PDT activity; for instance, the corresponding system without the methoxide generated less singlet oxygen than **18**, even when present at 100× the concentration. Molar extinction coefficients of these systems are significantly better than those of porphyrins. Unfortunately, the aqueous solubilities of aza-BODIPYs tend to be modest so they are often delivered in cellular assays using a cremophor (a common excipient used in drugs to increase water solubilities, *cf.* a cremophor is used in formulations of paclitaxel for the same reason).

Compound **18** has a QY for singlet oxygen generation of 74%.[63] Time resolved spectroscopy revealed that its triplet quantum yield was 72% (a lifetime of 21 μs) and that the dye was exceptionally photostable.[63] The tetraiododibromo derivative **19** had a similar triplet QY (78%; a lifetime of 1.6 μs).[64] Quantum mechanical calculations (DFT) on these systems have been used to understand their HOMO–LUMO levels and singlet-to-triplet energy gaps.[65]

Dibromo-aza-BODIPY **18** (designated **ADPM06** in papers) has been extensively studied in cells and *in vivo* assays. It has a nanomolar EC_{50} for light-induced cytotoxicity in a range of different human tumour cell lines, with no discernable selectivity for any particular type. Encouragingly, these cell types include some drug-resistant and metastatic lines. Cells can die *via* necrotic or apoptotic pathways; **18** administered at EC_{50} concentrations caused apoptotic cell death. Moreover, even though cell death in PDT can be reduced under depleted oxygen levels (*e.g.* hypoxia in cancer cells), **18** retained significant activity under these conditions.[60] Apoptosis is initiated in PDT mediated by **18** as a result of active oxygen species generated around the ER. This is accompanied by activation of several inhibitor and executioner caspases. Positron emission tomography studies using ^{18}F-labeled agents showed that a marked decrease in tumor proliferation (breast and glioma models) occurred 24 h post-PDT treatment with **18**.[60] In fact, ablation of breast tumors was observed in 71% of mice treated with **18** at 2 mg kg^{-1} after irradiation; this is comparable to "cure-rates" for more established PDT agents in mice xenograft models. The inherent fluorescence of **18** facilitated studies to determine the organ distribution and clearance of this compound; the data are consistent with that of an ideal initiator of PDT. There was no accumulation of **18** in the skin, an important property for PDT agents. Positron emission tomography and magnetic imaging studies showed that this PDT agent caused a decrease in tumour-vasculature perfusion and -metabolic activity.[66]

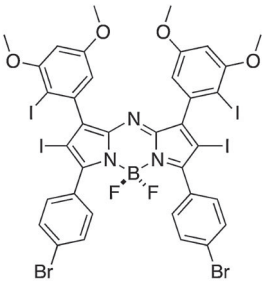

19

DMSO
$\lambda_{max\ abs}$ 666 nm
ε 69900 $M^{-1}cm^{-1}$
$\lambda_{max\ emiss}$ 694 nm
$^1O_2$ QY 0.70
triplet QY 0.78

Applications of PDT are not limited to chemotherapy of cancer; another, though rarer, use of these agents is as antibacterials. O'Shea and co-workers hypothesized that the quaternary ammonium salt **20** may implant into bacterial membranes as a result of its positive charge and amphiphilic character. Fluorescence studies with the non-halogenated analog **20** demonstrated that this stains both Gram-negative (*E. coli*) and -positive (*S. aureus*) bacteria, and yeast cells (*C. albicans*) with a bias to the membrane regions. Encouragingly, a human cell line (MDA-MB-231) showed only minimal uptake in the same timeframe. Strong antibacterial activity on these microbes was observed when they were irradiated with **21**; total eradication occurred at concentrations of 1–5 μg mL^{-1}.

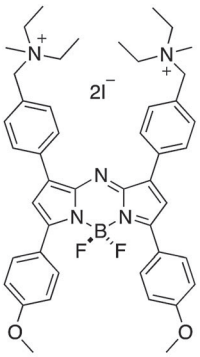

20

$CHCl_3$, Φ = 0.22
$\lambda_{max\ abs}$ 702 nm
ε = 69000 $M^{-1}cm^{-1}$
$\lambda_{max\ emiss}$ 732 nm

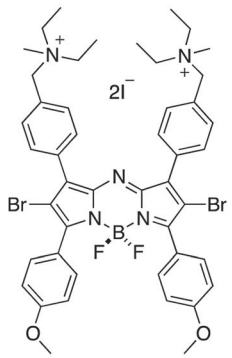

21

$CHCl_3$, Φ = 0.10
$\lambda_{max\ abs}$ 681 nm
ε = 64000 $M^{-1}cm^{-1}$
$\lambda_{max\ emiss}$ 722 nm

PDT characteristics modulated by photoinduced electron transfer (PET)

Several groups converged on the idea that photoinduced electron transfer (PET; unfortunately, this is also a widely used abbreviation for positron emission tomography) can be used to selectively quench intersystem crossing to triplet states. They have applied this hypothesis in several different and ingenious ways.

Some PDT side-effects may arise from prolonged light sensitivity. O'Shea recognized that aza-BODIPY dyes with a non-conjugated but proximal amine may undergo rapid relaxation *via* PET processes *when the amine is not protonated*. However, a larger portion of the amine would be protonated in the relatively acidic (pH 6.5–6.8) interstitial fluid that surrounds tumours, PET would selectively diminish in those regions, and the cytotoxic effect would be greater around cancerous cells than healthy ones.[67] Dye **22** was the pivotal one used to investigate this hypothesis. This agent was shown to generate

more singlet oxygen in acidic than in neutral media, and an EC_{50} value of 5.8 nM was recorded for light-induced cytoxicity. However, to the best of our knowledge, photocytotoxicities of this agent *in vivo* have not yet been compared with closely related compounds that lack the amine groups, so the clinical potential of **22** is still an open question.

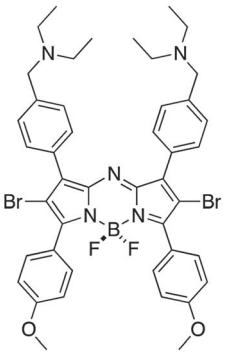

22
$CHCl_3$
$\lambda_{max\ abs}$ 684 nm
ε = 70800 $M^{-1}cm^{-1}$
$\lambda_{max\ emiss}$ 728 nm
$^1O_2$ acidic rate increase 10.6
EC_{50} (MRC5-SV40 cells) 4.5 ± 0.7 μM (0 J cm^{-2}), 5.8 ± 3 nM(16 J cm^{-2})

Another way to use PET modulation of singlet-to-triplet conversion is *via* an appropriately situated crown ether.[68] Intracellular sodium ion concentrations are apparently around 3× higher in tumor cells than in healthy ones, so coordination of these to a crown might selectively increase the PET effect in tumour cells. Thus Akkaya and co-workers combined *meso*-crown ether with pyridyl–styryl substituents in molecule **23** to sense higher sodium ion and proton concentrations in tumour cells, respectively. The authors observed cumulative effects of both stimuli in singlet oxygen generation, but conceded that the concentrations required to achieve a desirable response were greater than intracellular levels; no cell studies were reported.[69]

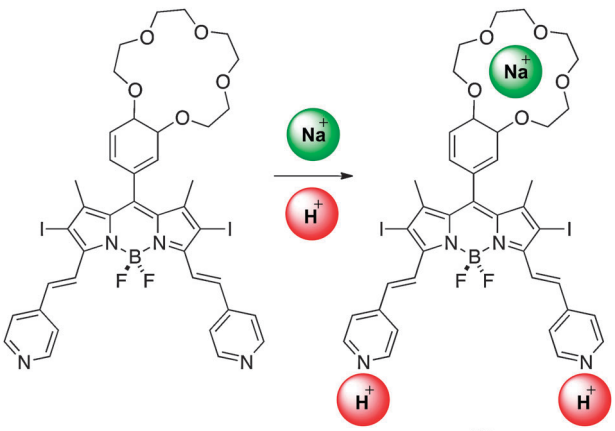

23
CH_3CN
$\lambda_{max\ abs}$ 630 nm
$^1O_2$ generation rel. rate 1
CH_3CN
$\lambda_{max\ abs}$ 660 nm
$^1O_2$ generation rel. rate 6.1

An insightful assertion by Nagano *et al.* was mentioned earlier in this review: that electron withdrawing BODIPY-substituents should protect BODIPYs from oxidation. A recent study from that group featured a range of BODIPY dyes with different electron withdrawing groups at the 2- and 6-positions.[70] Observation of singlet oxygen production confirmed that these dyes are most stable with electron withdrawing groups. A rough inverse correlation between levels of singlet oxygen production and the electron withdrawing abilities of these substituents was also noted. Observed QYs for singlet oxygen generation were probably not high on an absolute scale (the paper did not mention what they were) but the study does point to a fundamental issue: singlet oxygen generation can be modulated by tuning the oxidation potential of the BODIPY core. This concept was used very effectively in the next study from the Nagano lab, described below.

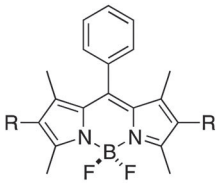

24
photostability
R = COOR' > CN > SO_3H > CONHR' > H > COOH > CH_2CH_2COOH

All the applications of PDT so far target cells as a whole, wherein the mechanisms by which the cell biology is disrupted are not of primary importance.[71] On a molecular scale, however, it is possible to use highly localized singlet oxygen generation to disable specific proteins; this is the technique of chromophore assisted light inactivation (CALI). Nagano's group had the idea that a hydrophobic BODIPY-based sensitizer might bury itself in a lipophilic cavity of a protein receptor when brought into proximity *via* binding to a conjugated ligand. This strategy is likely to be most effective when singlet oxygen production is enhanced by placing the sensitizer in a lipophilic environment. The specific case studied was inositol 1,4,5-trisphosphate (IP_3) coupled to a 2,6-diiodo-BODIPY; the hypothesis was that ligand binding would place the dye into a hydrophobic cavity that is easily seen in the receptor that binds IP_3 (IP_3R). They showed that the electron donating substituent in structure **25** modulated the properties of the sensitizer such that the production of singlet oxygen was slow except in relatively apolar solvents.

An attribute of this particular system is that binding to IP_3R gives a measurable biochemical output, *i.e.* increased Ca^{2+} concentration. Thus binding of the 2,6-diiodo-BODIPY conjugate gave dose-dependent release of Ca^{2+} with an EC_{50} value of 3 μM, while 2,6-diiodo-BODIPY conjugated with the enantiomeric IP_3-ligand did not give the same Ca^{2+} release. Permeablized cells were then used to input a calcium ion sensor and the appropriate conjugates; only the ones with an environment-activated photosensitizer conjugated to the appropriate IP_3-ligand enantiomer gave calcium release that was negatively modulated by treatment with light (Fig. 1).

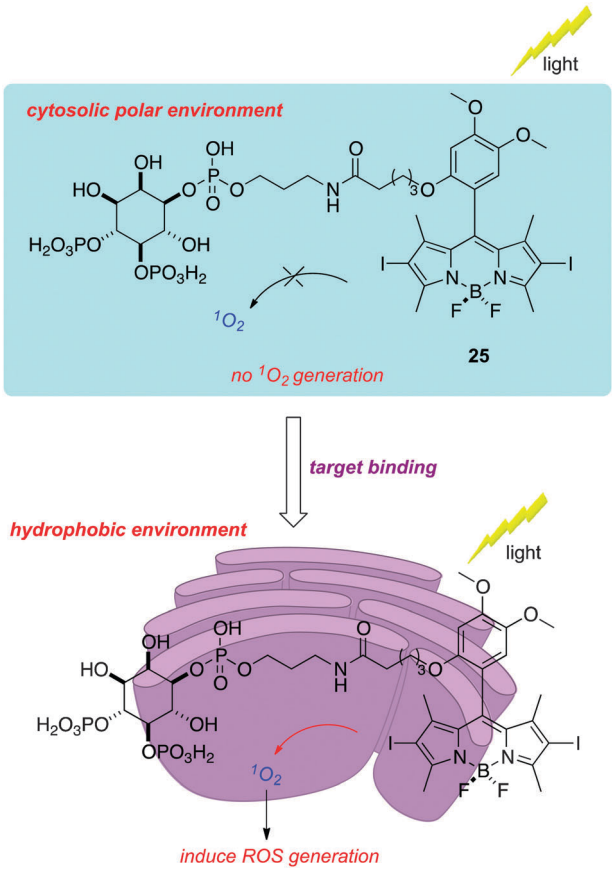

Fig. 1 Binding of a functionalized BODIPY to the inositol 1,4,5-trisphosphate receptor places the PDT agent in a hydrophobic environment where singlet oxygen generation is favored, leading to inactivation of the protein.

Halogen-free BODIPY sensitizers

There is nothing special about halogen atoms in design of BODIPY derivatives for triplet-sensitization; any substituent with molecular orbitals having appropriate multiplicity and energy levels might function in this way. Surprisingly, some BODIPY fragments have emerged as appropriate substituents to induce triplet-sensitization. Thus, dimers of BODIPY dyes wherein the chromophores are directly connected may, on excitation, undergo more efficient ISC to triplet states than the corresponding monomers.[72]

Computational studies have been used to predict orthogonal chromophores that may give electronic mixing in the excited states

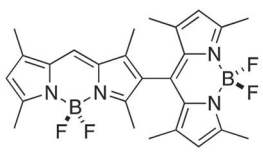

26
$CHCl_3$, Φ = 0.03
$\lambda_{max\ abs}$ 514 nm
ε 119400$M^{-1}cm^{-1}$
$\lambda_{max\ emiss}$ 527 nm
$^1O_2$ QY 0.51
EC_{50} (K562cells) ND (0 mW cm^{-2}), 50 nM (2.5 mW cm^{-2})

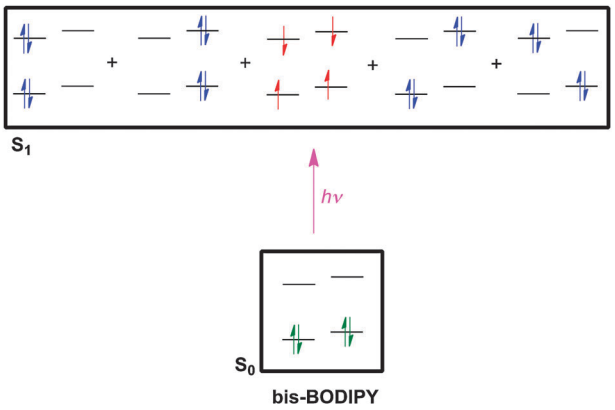

Fig. 2 Excitation of bisBODIPY systems like **26** gives singlet excited states (blue electrons), but a triplet state (red) is also favored.

to generate triplets. Selection of the appropriate computational method is important; here multiconfigurational self-consistent field, MCSFF, was used. Just as predicted, bisBODIPY systems like **26** were less fluorescent than their constituent monomers, and gave relatively high singlet QYs. An EC_{50} of 50 nM was measured for human erythroleukemia cells (Fig. 2).[73]

Attempts to extend conjugation using the styryl approach *failed* to give triplet oxygen production at higher wavelengths. We suggest that this could be due to accelerated photobleaching of a long-lived triplet excited state.[74]

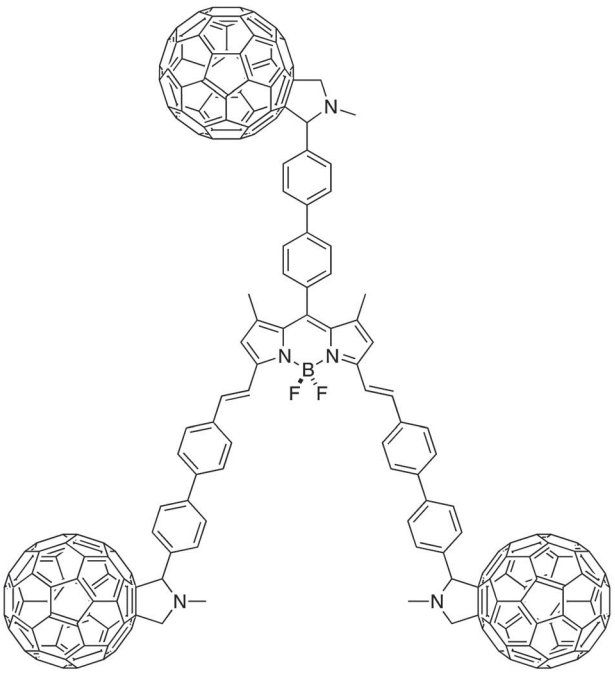

27
toluene, Φ = 0.009
$\lambda_{max\ abs}$ 657 nm
ε 64600 $M^{-1}cm^{-1}$
$\lambda_{max\ emiss}$ 667 nm
triplet QY 0.85

BODIPY derivative **27** is an organic triplet photosensitizer; it is particularly interesting because no halogens or other heavier elements are involved.[75] It appears that the BODIPY fluorescence is quenched *via* intramolecular energy transfer to the styryl protected C_{60}-dyads, accounting for the long-lived triplet excited state (123.2 μs) of this material.

BODIPY dyes for observing reactive oxygen species

There are BODIPY-derivatives designed to be sensors for the generation of reactive oxygen species. These are not necessarily PDT agents, but they can be used to monitor consequences of PDT treatment. One useful probe of this kind is the commercially available C11-BODIPY. For example, this probe was used to demonstrate that oxidants were present in a cell culture up to 30 min after illumination in a PDT experiment. A dark control showed that hydrogen peroxide only activated the probe when it was in direct contact with the cells so the researchers were able to deduce that the reactive oxygen species involved in the PDT experiment were not confined to peroxide anions.[76]

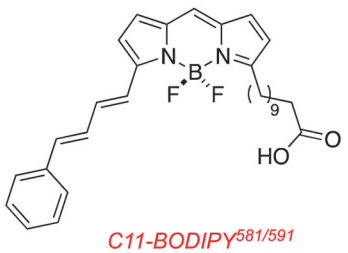

C11-BODIPY$^{581/591}$

probe to detect reactive oxygen species (ROS) in cells and membranes

Conclusions

Many studies have focused on BODIPY core modifications to facilitate singlet oxygen generation. The intrinsic absorption maxima of simple BODIPY dyes (*ca.* 510–530 nm) are shorter than ideal, so many of the featured modifications also aim to extend conjugation in these molecules. For instance, Akkaya's methyl-BODIPY condensation reaction has been used several times, including studies by other groups, for this purpose. One of the most promising avenues of research, pioneered mainly by O'Shea, centers on aza-BODIPY compounds as PDT agents; these are less synthetically accessible, but have red-shifted absorption maxima. In our view, aza-BODIPY agents are probably closer to clinical development than any subcategory in the BODIPY class.

An interesting consequence of the PDT work is Nagano's CALI technique to eliminate selected receptors on a molecular level. This approach is mostly intended for *in vitro* and cellular studies, so wavelength of absorption is not critical. BODIPY dyes can also be used as sensors for reactive oxygen species in studies involving other types of agents.

A priority for future research must be to develop clinically useful PDT agents. Possibly this will be coupled with *active*-targeting. Thus it will be interesting to see future studies featuring BODIPYs conjugated with ligands for cell-surface receptors that are over-expressed on tumour cells. It is surprising that we did not encounter reports of this strategy, even employing common small molecule targeting agents like RGD peptidomimetics and folic acid.

Abbreviations

$\lambda_{max\ abs}$	Absorption maxima (Q-band)
ε	Molar extinction coefficient
$\lambda_{max\ emiss}$	Fluorescence emission maxima
Φ_{Fl}	Fluorescence quantum yield
Φ_{PB}	Photobleaching quantum yield
Φ_{Δ}	Singlet oxygen generation quantum yield
Log $P_{o/w}$	Log octanol/water partition coefficient
PB	Phosphate buffer pH ~ 7.4
EtOH	Ethanol
PBS	Phosphate buffered saline
TX100	Triton X100
FFA	Furfuryl alcohol
MB	Methylene blue
RB	Rose Bengal
NA	Not available

Acknowledgements

We thank The National Institutes of Health (GM087981), The Robert A. Welch Foundation (A-1121), and HIR-MOHE grant (UM.C/625/1/HIR/MOHE/MED/17), Ministry of Higher Education, Malaysia, for financial support.

References

1 P. Agostinis, K. Berg, A. Cengel Keith, H. Foster Thomas, W. Girotti Albert, O. Gollnick Sandra, M. Hahn Stephen, R. Hamblin Michael, A. Juzeniene, D. Kessel, M. Korbelik, J. Moan, P. Mroz, D. Nowis, J. Piette, C. Wilson Brian and J. Golab, *CA Cancer J. Clin.*, 2011, **61**, 250–281.
2 D. E. J. G. J. Dolmans, D. Fukumura and R. K. Jain, *Nat. Rev. Cancer*, 2003, **3**, 380–387.
3 J. Moan and K. Berg, *Photochem. Photobiol.*, 1991, **53**, 549–553.
4 A. Juarranz, P. Jaen, F. Sanz-Rodriguez, J. Cuevas and S. Gonzalez, *Clin. Transl. Oncol.*, 2008, **10**, 148–154.
5 A. P. Castano, T. N. Demidova and M. R. Hamblin, *Photodiagn. Photodyn. Ther.*, 2004, **1**, 279–293.
6 A. Hajri, S. Wack, C. Meyer, M. K. Smith, C. Leberquier, M. Kedinger and M. Aprahamian, *Photochem. Photobiol.*, 2002, **75**, 140–148.
7 M. J. Garland, C. M. Cassidy, D. Woolfson and R. F. Donnelly, *Future Med. Chem.*, 2009, **1**, 667–691.
8 R. R. Allison and C. H. Sibata, *Photodiagn. Photodyn. Ther.*, 2010, **7**, 61–75.
9 J. C. Kennedy and R. H. Pottier, *J. Photochem. Photobiol., B*, 1992, **14**, 275–292.
10 M. Wachowska, A. Muchowicz, M. Firczuk, M. Gabrysiak, M. Winiarska, M. Wańczyk, K. Bojarczuk and J. Golab, *Molecules*, 2011, **16**, 4140–4164.
11 J. Webber, D. Kessel and D. Fromm, *J. Photochem. Photobiol., B*, 1997, **37**, 151–153.
12 A. Godal, N. O. Nilsen, J. Klaveness, J. E. Branden, J. M. Nesland and Q. Peng, *J. Environ. Pathol., Toxicol. Oncol.*, 2006, **25**, 109–126.

13 W. M. Sharman, C. M. Allen and J. E. van Lier, *Drug Discovery Today*, 1999, **4**, 507–517.
14 J. D. Spikes, *Photochem. Photobiol.*, 1992, **55**, 797–808.
15 S. Kimel, B. J. Tromberg, W. G. Roberts and M. W. Berns, *Photochem. Photobiol.*, 1989, **50**, 175–183.
16 M. Tanaka, M. Kinoshita, Y. Yoshihara, N. Shinomiya, S. Seki, K. Nemoto, T. Hirayama, T. Dai, L. Huang, M. R. Hamblin and Y. Morimoto, *Photochem. Photobiol.*, 2012, **88**, 227–232.
17 G. I. Lozovaya, Z. Masinovsky and A. A. Sivash, *Origins Life Evol. Biospheres*, 1990, **20**, 321–330.
18 J. M. Fernandez, M. D. Bilgin and L. I. Grossweiner, *J. Photochem. Photobiol., B*, 1997, **37**, 131–140.
19 M. F. Grahn, A. McGuinness, R. Benzie, R. Boyle, M. L. de Jode, M. G. Dilkes, B. Abbas and N. S. Williams, *J. Photochem. Photobiol., B*, 1997, **37**, 261–266.
20 I. Belitchenko, V. Melnikova, L. Bezdetnaya, H. Rezzoug, J. L. Merlin, A. Potapenko and F. Guillemin, *Photochem. Photobiol.*, 1998, **67**, 584–590.
21 C. Hadjur, N. Lange, J. Rebstein, P. Monnier, H. van den Bergh and G. Wagnieres, *J. Photochem. Photobiol., B*, 1998, **45**, 170–178.
22 M. Chen, X. Liu and A. Fahr, *Int. J. Pharm.*, 2011, **408**, 223–234.
23 B. Aveline, T. Hasan and R. W. Redmond, *Photochem. Photobiol.*, 1994, **59**, 328–335.
24 J. K. Macalpine, R. Boch and D. Dolphin, *J. Porphyrins Phthalocyanines*, 2002, **6**, 146–155.
25 J. D. Spikes and J. C. Bommer, *J. Photochem. Photobiol., B*, 1993, **17**, 135–143.
26 D. Kessel, *Photochem. Photobiol.*, 1989, **49**, 447–452.
27 H. A. Isakau, M. V. Parkhats, V. N. Knyukshto, B. M. Dzhagarov, E. P. Petrov and P. T. Petrov, *J. Photochem. Photobiol., B*, 2008, **92**, 165–174.
28 M. O. Senge and J. C. Brandt, *Photochem. Photobiol.*, 2011, **87**, 1240–1296.
29 T. Kiesslich, J. Berlanda, K. Plaetzer, B. Krammer and F. Berr, *Photochem. Photobiol. Sci.*, 2007, **6**, 619–627.
30 J. M. Houle and A. Strong, *J. Clin. Pharmacol.*, 2002, **42**, 547–557.
31 B. M. Aveline, T. Hasan and R. W. Redmond, *J. Photochem. Photobiol., B*, 1995, **30**, 161–169.
32 A. F. Cruess, G. Zlateva, A. M. Pleil and B. Wirostko, *Acta Ophthalmol.*, 2009, **87**, 118–132.
33 Y. Hongying, W. Fuyuan and Z. Zhiyi, *Dyes Pigm.*, 1999, **43**, 109–117.
34 E. D. Sternberg, D. Dolphin and C. Brückner, *Tetrahedron*, 1998, **54**, 4151–4202.
35 E. S. Nyman and P. H. Hynninen, *J. Photochem. Photobiol., B*, 2004, **73**, 1–28.
36 M. Wainwright and R. M. Giddens, *Dyes Pigm.*, 2003, **57**, 245–257.
37 F. Harris, L. K. Chatfield and D. A. Phoenix, *Curr. Drug Targets*, 2005, **6**, 615–627.
38 M. Wainwright, *Photodiagn. Photodyn. Ther.*, 2005, **2**, 263–272.
39 M. Wainwright, D. A. Phoenix, L. Rice, S. M. Burrow and J. Waring, *J. Photochem. Photobiol., B*, 1997, **40**, 233–239.
40 T. Yogo, Y. Urano, Y. Ishitsuka, F. Maniwa and T. Nagano, *J. Am. Chem. Soc.*, 2005, **127**, 12162–12163.
41 S. H. Lim, C. Thivierge, P. Nowak-Sliwinska, J. Han, H. Van den Bergh, G. Wagnieres, K. Burgess and H. B. Lee, *J. Med. Chem.*, 2010, **53**, 2865–2874.
42 A. Loudet and K. Burgess, *Chem. Rev.*, 2007, **107**, 4891–4932.
43 N. Boens, V. Leen and W. Dehaen, *Chem. Soc. Rev.*, 2012, **41**, 1130–1172.
44 A. Loudet and K. Burgess, in *Handbook of Porphyrin Science With Applications to Chemistry, Physics, Materials Science, Engineering, Biology and Medicine*, ed. K. Kadish, K. Smith and R. Guilard, World Scientific, 2010, p. 203.
45 G. Ulrich, R. Ziessel and A. Harriman, *Angew. Chem., Int. Ed.*, 2008, **47**, 1184–1201.
46 R. Ziessel, G. Ulrich and A. Harriman, *New J. Chem.*, 2007, **31**, 496–501.
47 B. Hinkeldey, A. Schmitt and G. Jung, *ChemPhysChem*, 2008, **9**, 2019–2027.
48 T. N. Singh-Rachford, A. Haefele, R. Ziessel and F. N. Castellano, *J. Am. Chem. Soc.*, 2008, **130**, 16164–16165.
49 M. J. Ortiz, A. R. Agarrabeitia, G. Duran-Sampedro, J. Banuelos Prieto, T. A. Lopez, W. A. Massad, H. A. Montejano, N. A. Garcia and I. Lopez Arbeloa, *Tetrahedron*, 2012, **68**, 1153–1162.
50 W. Wu, H. Guo, W. Wu, S. Ji and J. Zhao, *J. Org. Chem.*, 2011, **76**, 7056–7064.
51 Y. Chen, J. Zhao, L. Xie, H. Guo and Q. Li, *RSC Adv.*, 2012, **2**, 3942–3953.
52 K. Umezawa, A. Matsui, Y. Nakamura, D. Citterio and K. Suzuki, *Chem.–Eur. J.*, 2009, **15**, 1096–1106.
53 K. Umezawa, Y. Nakamura, H. Makino, D. Citterio and K. Suzuki, *J. Am. Chem. Soc.*, 2008, **130**, 1550–1551.
54 A. Coskun, M. D. Yilmaz and E. U. Akkaya, *Org. Lett.*, 2007, **9**, 607–609.
55 E. Deniz, G. C. Isbasar, O. A. Bozdemir, L. T. Yildirim, A. Siemiarczuk and E. U. Akkaya, *Org. Lett.*, 2008, **10**, 3401–3403.
56 Z. Ekmekci, M. D. Yilmaz and E. U. Akkaya, *Org. Lett.*, 2008, **10**, 461–464.
57 O. Buyukcakir, O. A. Bozdemir, S. Kolemen, S. Erbas and E. U. Akkaya, *Org. Lett.*, 2009, **11**, 4644–4647.
58 S. Atilgan, Z. Ekmekci, A. L. Dogan, D. Guc and U. Akkaya Engin, *Chem. Commun.*, 2006, 4398–4400.
59 H. He, P.-C. Lo, S.-L. Yeung, W.-P. Fong and D. K. P. Ng, *Chem. Commun.*, 2011, **47**, 4748–4750.
60 W. M. Gallagher, L. T. Allen, C. O'Shea, T. Kenna, M. Hall, A. Gorman, J. Killoran and D. F. O'Shea, *Br. J. Cancer*, 2005, **92**, 1702–1710.
61 J. Killoran, L. Allen, J. F. Gallagher, W. M. Gallagher and D. F. O'Shea, *Chem. Commun.*, 2002, 1862–1863.
62 A. Gorman, J. Killoran, C. O'Shea, T. Kenna, W. M. Gallagher and D. F. O'Shea, *J. Am. Chem. Soc.*, 2004, **126**, 10619–10631.
63 P. Batat, M. Cantuel, G. Jonusauskas, L. Scarpantonio, A. Palma, D. F. O'Shea and N. D. McClenaghan, *J. Phys. Chem. A*, 2011, **115**, 14034–14039.
64 N. Adarsh, R. R. Avirah and D. Ramaiah, *Org. Lett.*, 2010, **12**, 5720–5723.
65 A. D. Quartarolo, N. Russo and E. Sicilia, *Chemistry*, 2006, **12**, 6797–6803.
66 A. T. Byrne, A. E. O'Connor, M. Hall, J. Murtagh, K. O'Neill, K. M. Curran, K. Mongrain, J. A. Rousseau, R. Lecomte, S. McGee, J. J. Callanan, D. F. O'Shea and W. M. Gallagher, *Br. J. Cancer*, 2009, **101**, 1565–1573.
67 S. O. McDonnell, M. J. Hall, L. T. Allen, A. Byrne, W. M. Gallagher and D. F. O'Shea, *J. Am. Chem. Soc.*, 2005, **127**, 16360–16361.
68 O. A. Bozdemir, R. Guliyev, O. Buyukcakir, S. Selcuk, S. Kolemen, G. Gulseren, T. Nalbantoglu, H. Boyaci and E. U. Akkaya, *J. Am. Chem. Soc.*, 2010, **132**, 8029–8036.
69 S. Ozlem and E. U. Akkaya, *J. Am. Chem. Soc.*, 2008, **131**, 48–49.
70 T. Komatsu, D. Oushiki, A. Takeda, M. Miyamura, T. Ueno, T. Terai, K. Hanaoka, Y. Urano, T. Mineno and T. Nagano, *Chem. Commun.*, 2011, **47**, 10055–10057.
71 T. Yogo, Y. Urano, A. Mizushima, H. Sunahara, T. Inoue, K. Hirose, M. Iino, K. Kikuchi and T. Nagano, *Proc. Natl. Acad. Sci. U. S. A.*, 2008, **105**, 28–32.
72 B. Ventura, G. Marconi, M. Broering, R. Kruger and L. Flamigni, *New J. Chem.*, 2009, **33**, 428–438.
73 Y. Cakmak, S. Kolemen, S. Duman, Y. Dede, Y. Dolen, B. Kilic, Z. Kostereli, L. T. Yildirim, A. L. Dogan, D. Guc and E. U. Akkaya, *Angew. Chem., Int. Ed.*, 2011, **50**, 11937–11941.
74 S. Duman, Y. Cakmak, S. Kolemen, E. U. Akkaya and Y. Dede, *J. Org. Chem.*, 2012, **77**, 4516–4527.
75 L. Huang, X. Yu, W. Wu and J. Zhao, *Org. Lett.*, 2012, **14**, 2594–2597.
76 D. V. Sakharov, E. D. R. Elstak, B. Chernyak and K. W. A. Wirtz, *FEBS Lett.*, 2005, **579**, 1255–1260.

Journal of Medicinal Chemistry Article

J. Med. Chem. **2010,** *53,* 2865–2874 **2865**
DOI: 10.1021/jm901823u

In Vitro and In Vivo Photocytotoxicity of Boron Dipyrromethene Derivatives for Photodynamic Therapy

Siang Hui Lim,[†] Cliferson Thivierge,[‡] Patrycja Nowak-Sliwinska,[§] Junyan Han,[‡] Hubert van den Bergh,[§] Georges Wagnières,[∥] Kevin Burgess,[‡] and Hong Boon Lee*,[†]

[†]*Cancer Research Initiatives Foundation (CARIF), Sime Darby Medical Centre, 47500 Subang Jaya, Selangor, Malaysia,* [‡]*Department of Chemistry, Texas A&M University, College Station, Texas 77842,* [§]*Institute of Bio-Engineering, and* [∥]*Institute of Chemical Sciences and Engineering, Medical Photonics Group, Swiss Federal Institute of Technology (EPFL), 1015 Lausanne, Switzerland*

Received December 10, 2009

To understand the effects of substitution patterns on photosensitizing the ability of boron dipyrromethene (BODIPY), two structural variations that either investigate the effectiveness of various iodinated derivatives to maximize the "heavy atom effect" or focus on the effect of extended conjugation at the 4-pyrrolic position to red-shift their activation wavelengths were investigated. Compounds with conjugation at the 4-pyrrolic position were less photocytotoxic than the parent unconjugated compound, while those with an iodinated BODIPY core presented better photocytotoxicity than compounds with iodoaryl groups at the meso-positions. The potency of the derivatives generally correlated well with their singlet oxygen generation level. Further studies of compound **5** on HSC-2 cells showed almost exclusive localization to mitochondria, induction of G_2/M-phase cell cycle block, and onset of apoptosis. Compound **5** also extensively occluded the vasculature of the chick chorioallantoic membrane. Iodinated BODIPY structures such as compound **5** may have potential as new photodynamic therapy agents for cancer.

Introduction

Photodynamic therapy (PDT[a]) is now a well-recognized modality for cancer treatment, but to date, only a small number of PDT drugs, namely, porfimer sodium, temoporfin, and aminolevulinic acid, have been approved mainly for treatment of skin, gynecological, gastrointestinal, and some head and neck cancers.[1] PDT involves site-specific activation of an administered photosensitizer using light of a wavelength matched to the λ_{max} of the photosensitizer[2,3] in order to generate cytotoxic reactive oxygen species (e.g., $^1O_2$) that eradicate tumors via cellular damage, via vasculature damage or by recruiting members of the inflammatory and immune response system.[2,3] These photosensitizers, as well as the majority of those currently being investigated in clinical trials, share a common cyclic tetrapyrrole structure,[4] probably due to the fact that modern PDT has evolved from naturally derived porphyrins such as hematoporphyrin. Aside from cyclic tetrapyrrole structures, a number of naturally occurring and synthetic dyes that are non-porphyrin have also been evaluated for their photosensitizing ability against cancer. The focus has been primarily on cationic structures such as methylene blue, Nile blue, and Nile red analogues and the chalcogenopyrylium class of photosensitizers. These classes of compounds, however, suffer from a major drawbacks due to their inherent dark cytotoxicity.

One alternative class of non-porphyrin photosensitizers that has emerged recently is the BODIPY chromophore. BODIPYs have many characteristics of an ideal photosensitizer including high extinction coefficients, high quantum efficiencies of fluorescence, relative insensitivity to environment, and resistance to photobleaching. Nagano and co-workers reported the synthesis of a simple diiodo-substituted BODIPY with possible applications that included PDT. The diiodo-substituted BODIPY at the 4-pyrollic position produces the supposed internal heavy atom effect and subsequently enhanced the intersystem crossing efficiency from a singlet to a triplet state that controls the singlet oxygen production.[5] O'Shea and co-workers prepared a series of azadipyrromethenes with high absorption in the far-red wavelengths and demonstrated their efficacy in light-induced toxicity in a panel solid tumor cell line.[6] One of the azadipyrromethenes was later shown to effectively eradicate the subcutaneously xenografted MDA-231 breast tumors in nude mice.[7] Akkaya and co-workers introduced another class of water-soluble BODIPY dyes with extended conjugation at the 5-pyrollic positions.[8] These photosensitizers were shown to have strong absorptions in the 650−680 nm therapeutic window and good photoinduced cytotoxicity in K562 leukemia cells at submicromolar concentrations even under low fluence rate LED irradiation.

*To whom correspondence should be addressed. Phone: +603-5639-1874. Fax: +603-5639-1875. E-mail: hongboon.lee@carif.com.my.

[a] Abbreviations: BODIPY, boron dipyrromethene; PDT, photodynamic therapy; CAM, chorioallantoic membrane; EDD, embryo development day; Rh123, rhodamine 123; DPBF, 1,3-diphenylisobenzofuran; MTT, methylthiazolyldiphenyltetrazolium bromide; DMSO, dimethyl sulfoxide.

Published on Web 03/03/2010

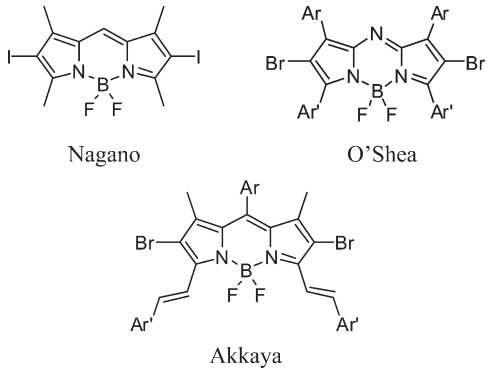

This study investigates the effects of two structural variations of BODIPY on their photocytotoxicity in terms of photophysical properties and in vitro and in vivo efficacies. In the first variation, functionalizations such as meso-substitution and sulfonation to improve hydrophilicity were tested to fine-tune the activity of iodinated BODIPY-based structures such as Nagano's compound (**6** in Figure 1). Because photosensitizers that absorb in the longer wavelengths may be activated deeper in the tissues and may therefore be clinically favored, a second variation consisting of compounds with extended conjugation at the 4-pyrollic position, which is a structural variation that has not been studied prior to this, was included in this study. First, the PDT efficacy of these BODIPY-based photosensitizers on a panel of leukemia and solid tumor cell lines, with particular attention on their structure−activity relationships, was studied. The effect of the most active derivative on an oral cancer cell line, HSC-2, was further investigated for intracellular localization, cell cycle arrest, and onset of apoptosis experiments, as well as in a preclinical in vivo model using the chick chorioallantoic

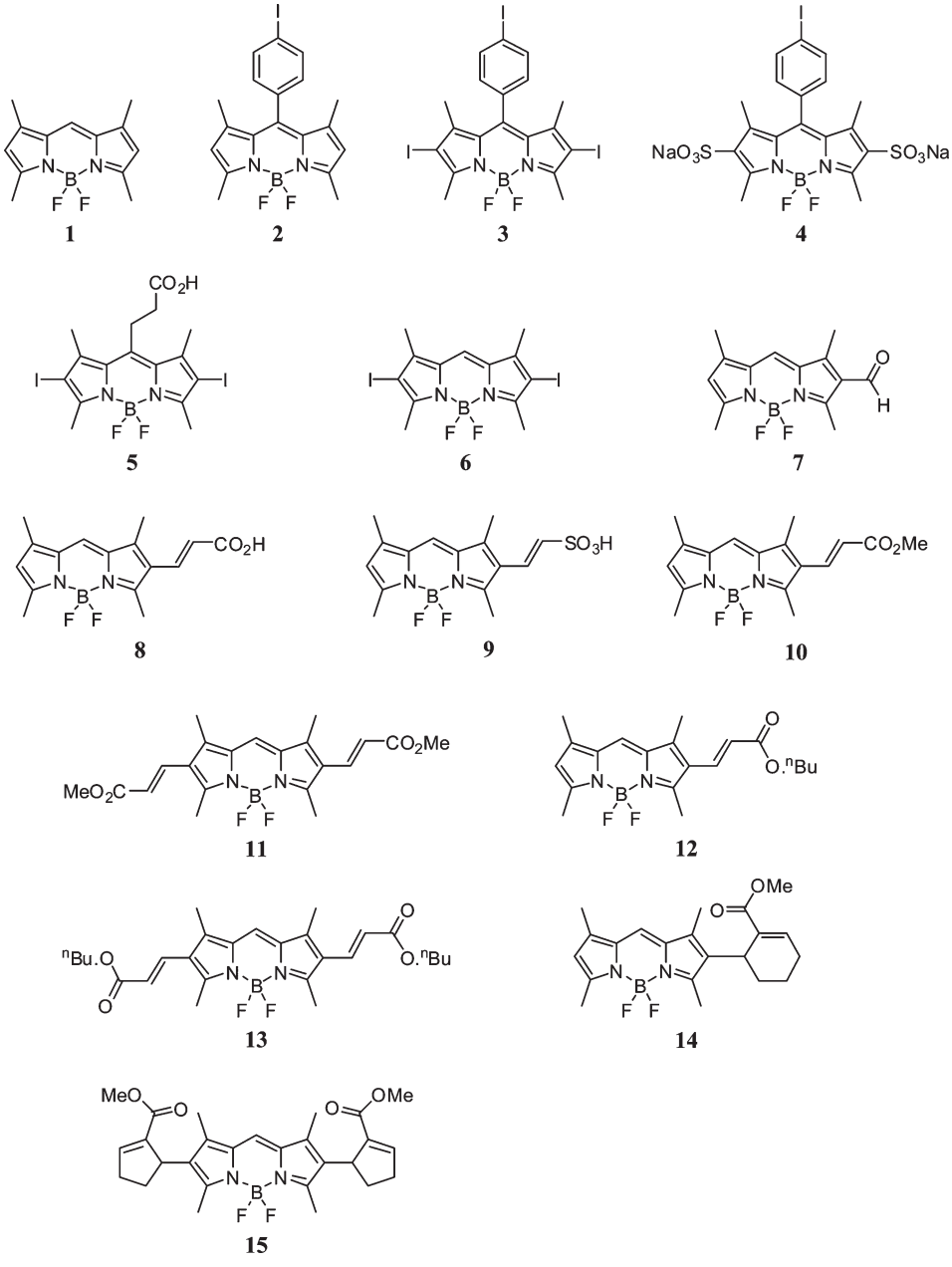

Figure 1. Structures of BODIPY.

membrane (CAM), in ovo, for PDT efficacy in terms of vascular occlusion.[9]

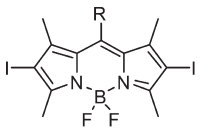

Structural variation 1

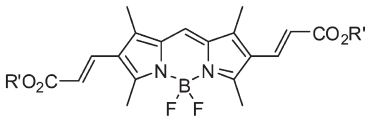

Structural variation 2

Results and Discussion

Structural Variations and Photophysical Properties. Two structural variations around the BODIPY core of compound **1** were investigated in this study (Figure 1). The first (compounds **2**−**6**) investigated the effectiveness of various iodinated derivatives in order to maximize the "heavy atom effect". To fine-tune the activity of iodinated BODIPY-based structures, additional functionalizations such as meso-substitution with alkyl or aryl groups as well as sulfonation to improve hydrophilicity were tested. Compound **5** contains a carboxylic acid handle and could be easily attached to other molecules later if required. For the second variation (compounds **7**−**15**), the effect of extended conjugation at the 4-pyrollic position was examined. Extended conjugation at the 4-pyrrolic positions increases the absorption wavelength of the compounds to the red, permitting the use of longer excitation wavelength that penetrates deeper into biological tissues for effective treatment.

Table 2 summarizes the photophysical data of compounds **1**−**15**. The absorption and emission wavelengths of compounds **1**−**15** range from 500 to 600 nm. As expected for compounds **8**−**15**, extending the conjugation with an acrylate shifts the $\lambda_{abs\,max}$ to the red by 20−30 nm while attaching two acrylates red-shifts the $\lambda_{abs\,max}$ by 50−60 nm, compared to compound **1**. The $\lambda_{abs\,max}$ values for iodinated compounds **3**, **5**, and **6** are also red-shifted compared to compound **1** but not for compounds **2** and **4**, which are aryl-iodinated at the meso position. In addition, all compounds have high extinction coefficients and high quantum efficiencies of fluorescence except for a few structures. Among the exceptions, compounds **3**, **5**, and **6** have much lower quantum efficiency of fluorescence and a correspondingly higher singlet oxygen generation rate (Table 3) compared to the other BODIPYs studied here, probably as a result of the enhanced intersystem crossing efficiency from the lowest singlet excited state to the triplet state contributed by the internal heavy-atom effect. As in the case of the $\lambda_{abs\,max}$ values above, compounds **2** and **4** which contain a para-iodoaryl group at the meso position did not demonstrate the same loss in fluorescence yields or the same increase in singlet oxygen generation rate as compounds **3**, **5**, and **6** probably because in the former group, first, the iodine atom is not directly attached to the BODIPY core and, second, the iodoaryl plane is twisted relative to the BODIPY plane,[10] overall causing the aryl iodine atom to only, at most, elicit an intramolecular external heavy-atom effect.[6]

In Vitro Photocytotoxic and Comparative Singlet-Oxygen Generation. The in vitro photocytotoxic activity of compounds **1**−**15** against a promyelocytic leukemia cell line (HL-60), an oral squamous carcinoma cell line (HSC-2), and a nasopharyngeal carcinoma cell line (HK1) following irradiation with 4.1 J/cm^2 of a broad spectrum light was determined using a modified methylthiazolyldiphenyltetrazolium bromide (MTT) assay. Parallel assays without light irradiation were also carried out to determine cytotoxicity in the dark. Results were expressed as IC_{50}, the concentration of compound (in μM) that inhibits proliferation rate by 50% compared to control untreated cells. The parent compound, denoted as **1**, was also prepared and tested for comparison. From the assay, all compounds had negligible or undeterminable unirradiated cytotoxicity up to 100 μM. Upon irradiation with 4.1 J/cm^2 of light, compounds **1**−**6** and **10**−**15** demonstrated photosensitized cytotoxicity with IC_{50} values in the submicromolar to tens of micromolar range. Compounds **5** and **6**, which had two iodine atoms directly attached to the BODIPY core, showed the highest activity among the analogues, with IC_{50} values that are up to 100 times lower than that of compound **1** (0.045 μM vs 4.4 μM in HL-60). In contrast, compounds **7**−**9** displayed poor activity with undeterminable IC_{50} up to 100 μM.

The influence of the iodine atom on the photocytotoxic activity of the compounds was evident from studying compounds **1**−**6**. Meso-substitution with a para-iodoaryl group in compound **2** does not alter the photocytotoxicity significantly compared to compound **1**, while further substitution with iodine atoms on the two pyrrolic 4-carbon to yield either compound **3** from **2** or compound **6** from **1** improved the activity by 10- and 100-fold, respectively, in all three cell lines, alluding to the importance of iodine atom substitution on the pyrrollic carbons rather than on the meso-aryl position. Compound **5**, which has an additional carboxylic acid

Table 1. Damage Score of PDT-Induced Vasculature Network Occlusion

occlusion score	findings
0	No occlusion
1	Partial closure of capillaries of diameter of $< 10\ \mu$m
2	Closure of capillary system, partial closure of blood vessel of diameter of $< 30\ \mu$m, and size reduction of larger blood vessels
3	Closure of vessels of diameter of $< 30\ \mu$m and partial closure of larger blood vessels
4	Total closure of vessels of diameter of $< 70\ \mu$m and partial closure of larger vessels
5	Total occlusion of vessels in the irradiated area

Table 2. Photophysical Properties of BODIPY Derivatives

compd	$\lambda_{abs\,max}$ (nm)	ε ($M^{-1}\,cm^{-1}$)	$\lambda_{em\,max}$ (nm)	Φ_{fl} [a]	ref dye[b]	solvent
1	505	83 000	516	0.80	1	EtOH
2	504	82 000	510	0.64	1	$CHCl_3$
3	537	89 000	552	0.05	2	CH_2Cl_2
4	498	100 000	509	0.34	1	H_2O
5	525	93 000	540	0.03	2	EtOH
6	534	110 000	548	0.02	1	MeOH
7	494	81 000	504	0.95	1	EtOH
8	531	27 000	570	0.42	2	EtOH
9	529	[c]	560	0.25	2	EtOH
10	527	63 000	549	0.73	2	EtOH
11	559	13 000	580	0.51	3	EtOH
12	528	62 000	551	0.73	2	EtOH
13	560	30 000	580	0.52	3	EtOH
14	517	63 000	527	0.78	2	EtOH
15	530	72 000	539	0.92	2	EtOH

[a] Φ_{fl} represents quantum efficiency of fluorescence. [b] Reference dyes used for quantum yield determination (solvent, Φ_{fl}): (1) fluorescein (0.1 M NaOH, 0.92); (2) rhodamine 6G (EtOH, 0.94); (3) rhodamine B (EtOH, 0.97). [c] Value not determined.

Table 3. Comparative Singlet Oxygen Generation and in Vitro Photo Cytotoxicity Induced by BODIPY

		activity IC_{50} (μM)[b]					
		HL-60		HSC-2		HK1	
BODIPY	singlet oxygen generation, relative rate[a]	0 J/cm^2	4.1 J/cm^2	0 J/cm^2	4.1 J/cm^2	0 J/cm^2	4.1 J/cm^2
1	0.48	> 100	4.4 ± 0.4	> 100	8.7 ± 2.0	76.8 ± 10.6	6.2 ± 1.2
2	0.15	> 100	2.7 ± 1.2	> 100	5.1 ± 0.8	> 100	5.7 ± 0.1
3	13.9	10	0.42 ± 0.06	10	0.5 ± 0.1	95.5 ± 7.9	0.69 ± 0.08
4	0.07	> 100	54.3 ± 8.3	> 100	59.4 ± 6.2	> 100	59.0 ± 7.1
5	24.6	> 100	0.045 ± 0.004	> 100	0.10 ± 0.06	55.8 ± 0.8	0.57 ± 0.1
6	23.9	> 100	0.062 ± 0.011	> 100	0.64 ± 0.06	> 100	0.57 ± 0.06
7	0.07	> 100	> 100	> 100	> 100	> 100	> 100
8	0.01	> 100	> 100	> 100	> 100	> 100	> 100
9	0.00	> 100	> 100	> 100	> 100	> 100	> 100
10	0.57	> 100	4.8 ± 0.7	> 100	5.4 ± 0.6	> 100	5.3 ± 0.6
11	0.41	> 100	5.2 ± 0.6	> 100	11.1 ± 7.4	> 100	8.5 ± 0.5
12	0.73	> 100	0.49 ± 0.07	> 100	0.6 ± 0.1	99.6 ± 0.6	1.1 ± 0.6
13	0.17	> 100	57.7 ± 6.6	> 100	37.7 ± 15.7	> 100	> 100
14	0.24	> 100	4.9 ± 0.6	> 100	4.1 ± 0.2	> 100	5.0 ± 0.6
15	0.29	> 100	3.8 ± 0.7			> 100	4.8 ± 0.9

[a] Comparative singlet oxygen generation of photosensitizers relative to methylene blue. [b] IC_{50}, the concentration of compound that inhibits the proliferation rate by 50% compared with control untreated cells. Values represent the mean ± SD of three determinations assessed 24 h using standard MTT assay. Cells were incubated with compound for 2 h prior to irradiation with 4.1 J/cm^2.

tether at the meso position, has similar to marginally better activity than compound **6** in all three cell lines. An attempt to improve the water solubility of compound **2** by substituting with sodium sulfonate to yield compound **4** resulted in 10 times loss in activity.

For the effect of extended conjugation at 4-pyrrolic positions on photocytotoxic activity of BODIPYs, compounds **7**−**15** were studied. Extending the 4-pyrollic carbon with a single aldehyde (**7**) or the hydrophilic allylic carboxylic acid (**8**) and allylic suphonic acid (**9**) resulted in loss of activity of greater than 100 μM IC_{50} values. Single extensions at the 4-pyrrolic position with acrylate esters affected the activity differently depending on the length of the alkyl ester group, where the methyl compound **10** showed no change in activity while *n*-butyl compound **12** demonstrated 10-fold improvement in activity compared to compound **1**. For compounds with double extension with the same groups at the 4-pyrollic positions, the methyl compound **11** remained unaltered in its activity compared to compound **1**, but interestingly, the *n*-butyl compound **13** showed 10-fold loss in activity compared to **1** or 100-fold loss compared to the singly extended counterpart **12**. The explanation for the reversal in structure−activity relationship of the *n*-butyl acrylate esters compared with the methyl acrylate esters from the single- to the double-extension (compounds **10** and **12** compared with compounds **11** and **13**) is not obvious and could just be due to the poorer solubility of the doubly extended *n*-butyl derivative **13**. Compounds **14** and **15**, which were failed attempts to prepare the analogous ring-constrained conjugated structures, were also tested and showed similar activities compared to compound **1**, further suggesting the minor role that 4-pyrrolic extended conjugation or the lack of it plays in modulating the photocytotoxicity of the BODIPY structures.

Subsequently, the relative rate of singlet oxygen generation was measured for compounds **1**−**15** by monitoring the reaction of known singlet oxygen acceptor 1,3-diphenylisobenzofuran (DPBF) with photosensitizers generated singlet oxygen.[11] This was achieved by following the loss of DPBF absorbance at 410 nm at an initial concentration of 50 μM over a period of 1 h. A light source filtered at 510 nm wavelength was used to minimize the photobleaching of DPBF. As a result, this would have caused an underestimation of singlet oxygen generation rate of the compounds with $\lambda_{abs\,max}$ lower than 510 nm, as the light transmission through the filter begins to drop below 510 nm. Each of the compounds was tested at an equivalent concentration of reference sensitizer methylene blue. The results from this study ranged from 0.01- to over 24-fold of singlet oxygen generation rate compared to that of methylene blue. Importantly, the rate of reactive oxygen generation measured generally correlated with the potency of these compounds and there may be a main factor affecting the photocytotoxicity of these BODIPY compounds.

Photosensitizer Cellular Localization. To ascertain the intracellular localization of the BODIPYs, compound **5**, owing to its good potency data, was chosen and examined by spinning disk confocal microscopy using dual staining techniques (Figure 2). Costaining images and topographic profiles of HSC-2 cell line loaded with compound **5** and a mitochondria-specific dye rhodamine 123 (Rh123) revealed an almost identical overlap, suggesting that compound **5** localized particularly well in mitochondria (Figure 2A,B). In comparison, compound **5** displayed only partial colocalization with endoplasmic reticulum and lysosomes, according to the confocal images and topographic profiles of compound **5** with ER-Tracker (Figure 2C,D) and with LysoTracker (Figure 2E,F), respectively. Staining of the cytoplasmic or nuclear membrane by compound **5** was not detected, indicating that it does not react nonspecifically with biological membranes. Furthermore, the nucleus remained free of compound **5** (dark nuclear area), signifying that this class of compounds would not be expected to directly damage DNA.

Mitochondria perform vital cellular functions and are involved in multiple signaling cascades in regulation of metabolism, cell cycle control development, and cell death.[12] In PDT, mitochondria are an important target. During mitochondria-photosensitization in PDT, cytochrome *c* is released from mitochondria to directly effect rapid cell death

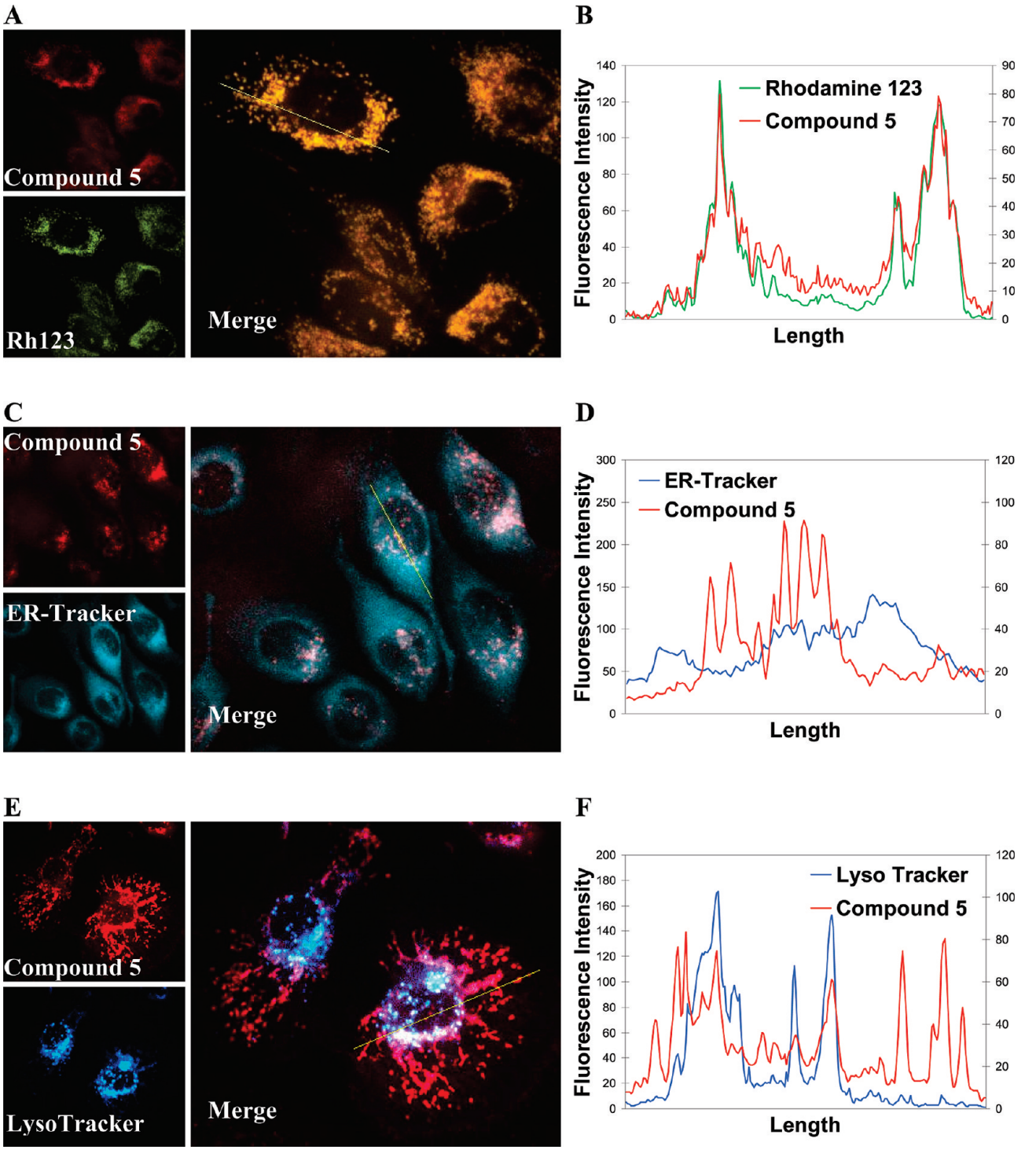

Figure 2. Intracellular localization of compound **5** in HSC-2 cells. Spinning disk confocal images (A, C, E) and fluorescence topographic profiles (B, D, F) of HSC-2 cells double-stained with 100 nM compound **5** and respective organelle probes. (A, B) Mitochondria were labeled with 100 nM Rh123 and excited at 494 nm. (C, D) Endoplasmic reticulum were labeled with 100 nM ER-Tracker and excited at 365 nm. (E, F) Lysosomes were labeled with 500 nM of LysoTracker and excited at 365 nm. Compound **5** was excited at 575 nm. Line indicates the longitudinal transcellular axis analyzed to generate the topography fluorescence profiles. Objective magnification is ×63.

through downstream effector pathways of apoptosis, bypassing other upstream apoptotic signaling pathways that require synthesis of new proteins. This mechanism of action is particularly useful in the treatment of cancer types that are chemoresistant because of mutations in upstream pro-apoptotic signaling pathways.[13]

Cell Cycle Arrest and Apoptosis. To study the mechanism of action of compound **5** that contributed to its photocytoxicity, the effect of compound **5** on cell cycle and apoptosis of HSC-2 cells was investigated using flow cytometric method. The cell cycle profile of HSC-2 cells treated with compound **5** was analyzed in a time course experiment. At 0.25 μM, compound **5** was found to induce G_2/M arrest in HSC-2 cells as early as 2 h following light irradiation (Figure 3). HSC-2 cells in G_2/M phase gradually increased from 26.1% in the control group to 39.8%, 48.4%, 55.5%, respectively, at 2, 4, and 6 h after light

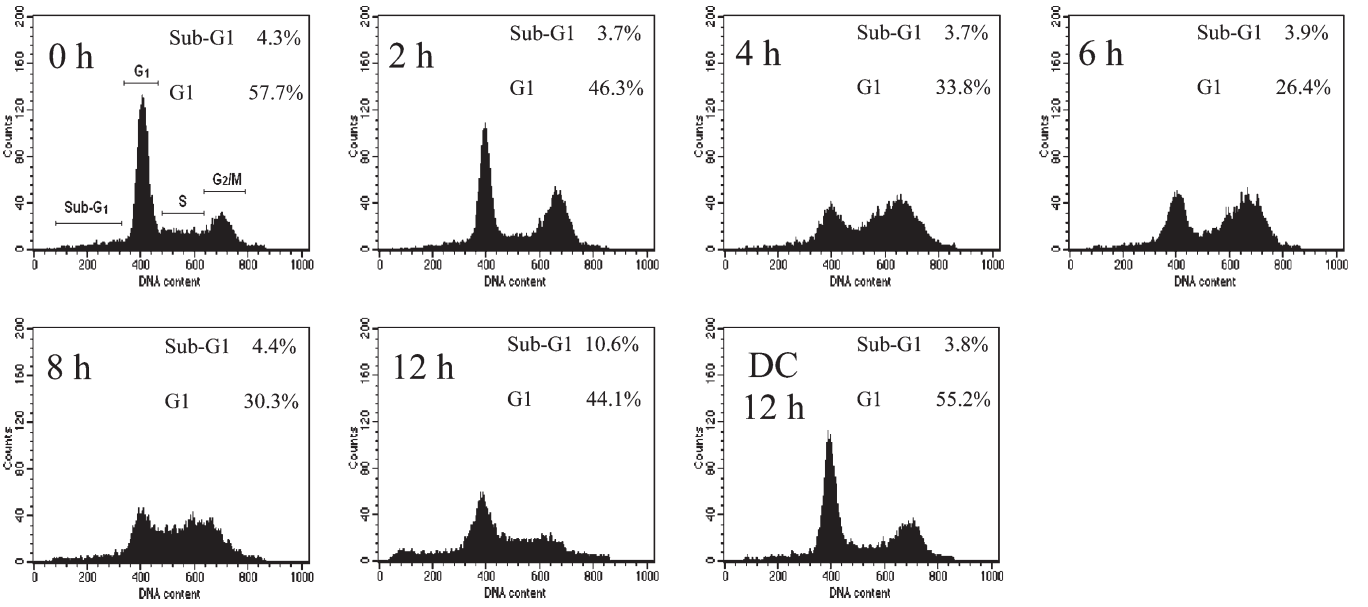

Figure 3. Effects on HSC-2 cell cycle phase at various intervals postirradiation analyzed using flow cytometry after treatment with 0.25 μM compound **5** and irradiated with a light dose of 4.1 J/cm^2. DC represents unirradiated dark control.

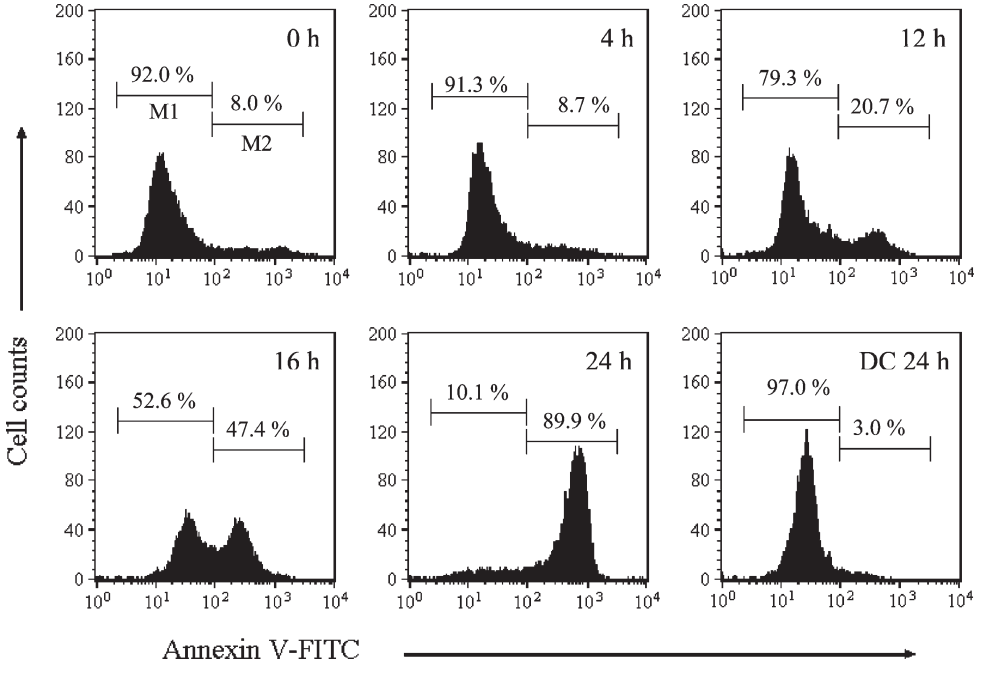

Figure 4. Representative histograms of the event of annexin V−fluorescein isothiocyanate (FITC) binding to phosphatidylserine as an indicator of apoptosis in HSC-2 cells treated with 0.5 μM compound **5** and irradiated with a light dose of 4.1 J/cm^2. M1 represents viable cell population, M2 represents apoptotic cell population, and DC represents unirradiated dark control.

irradiation. Concomitant with the increased proportion of G_2/M phase cells, HSC-2 cells in the G_1 phase were reduced from 57.7% to 46.3%, 33.8%, and 26.4% while the proportion of HSC-2 cells in S phase remained fairly constant. At 8 and 12 h, the proportion of cells arresting in the G_2/M phase was reduced to 48.8% and 26.0%, respectively, after light irradiation. Following the reduction of the proportion of cells arresting in G_2/M phase, an increase of sub-G_1 cells population from 8 to 12 h (from 4.4% to 10.6%) was observed. The proportion of cells treated with compound **5** without irradiation remains unchanged compared to control.

In the present study, the maximal level of G_2/M cell-cycle arrest was observed at 6 h after PDT. Thereafter, the recovery of the cell cycle profile to one with a reduced G2/M peak may be due to the redistribution of cells to sub-G_1, indicating the onset of apoptosis of arrested cells. A similar G_2/M arrest was also observed in hypericin-based PDT, a naturally occurring photosensitizer currently undergoing research.[14,15] Photosensitization of Hela cervical cancer cells with hypericin resulted in phosphorylation of mitochondria Bcl-2 that correlated with G_2/M cell cycle arrest, followed by the onset of apoptosis.[14]

In addition to cell cycle analysis, the onset of apoptosis was also quantified in flow cytometry experiments by measuring the externalization of membrane phosphatidylserine through annexin V−FITC staining, an event that is

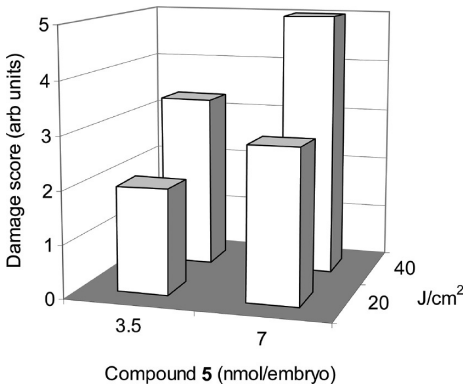

Figure 5. Effects of drug concentration and light dose on vascular occlusion efficacy of compound **5** in the CAM model. Error bars represent standard error mean from at least 10 embryos.

considered characteristic of cells undergoing apoptosis (Figure 4). Flow cytometric analysis of HSC-2 cells treated with 0.5 μM compound **5** showed the onset of apoptosis by 12 h following irradiation with 20.7% of the cells stained positive for annexin V compared to less than 10% at 0 or 4 h time points. The proportion of cells undergoing apoptosis continued to increase rapidly to 47.4% by 16 h, and at 24 h the apoptotic cell proportion was at 89.9%.

PDT-Induced Vascular Occlusion. One of the ways PDT causes damage during cancer treatment is by shutdown of blood vessels feeding the tumor.[16] Hence, the ability of compound **5** to exert in vivo vasculature disruption was investigated using the in ovo CAM model. In the present study, the ability of compound **5** to induce occlusion of blood vessels in the CAM by PDT was performed at 3.5−7.0 nmol/embryo with a light dose of 20−40 J/cm^2. The degree of vascular occlusion was scored 24 h after treatment according to Table 1. The score for photosensitizer-mediated PDT-induced vascular occlusion is shown in Figure 5, and the angiograms representing the vascular occlusion score are shown in Figure 6. As expected, the degree of vascular occlusion increased with drug and light dose. The average CAM vasculature damage score when irradiated at 20 J/cm^2 on embryos treated with 3.5 and 7.0 nmol/embryo of compound **5** was at approximately 2 and 3, respectively. When the light dose increased to 40 J/cm^2, the damage score increased accordingly to 3.5 and 5. Meanwhile, the control eggs that received 20 μL of vehicle (cremophor EL 2.5%, EtOH 2.5% in saline) and exposed to a similar light dose showed no detectable vascular alteration in the treated area. This indicated that the vascular occlusion observed in embryos treated with compound **5** was neither caused by the vehicle components nor was it thermally induced. Finally, treatment with compound **5** alone without irradiation did not induce any vascular occlusion, as nonirradiated areas remained perfused after 24 h.

As the main respiratory organ of the chick embryo, CAM is a well-vascularized membrane that is suitable as a model for PDT. It is easily accessible, inexpensive, and relatively easy to handle for photosensitizer administration, light irradiation, fluorescence analysis of administered photosensitizer, and microscopy examination of PDT-induced vascular damage.[9,17] CAM is a viable model that has been successfully used to evaluate the photodynamic-induced vascular occlusion efficacy of some photosensitizers that are in clinical trials as well as those that are already clinically

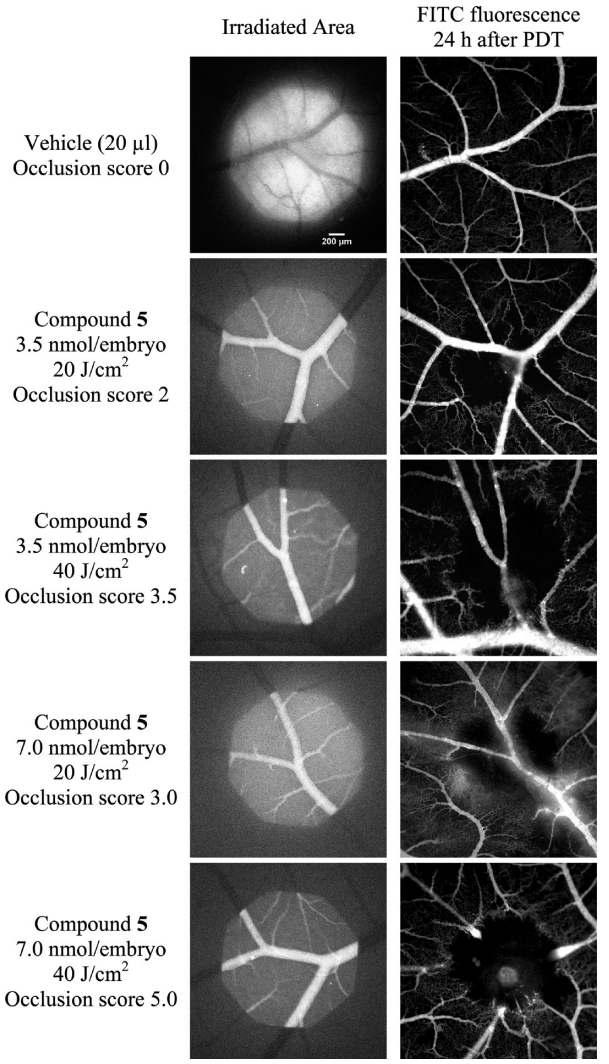

Figure 6. Representative angiographies of blood vessels supplying the CAM at beginning and 24 h after PDT, illustrating the vascular occlusion efficacy induced by compound **5** at 3.5−7 nmol/embryo. Irradiation was performed at 510−560 nm of excitation with 20−40 J/cm^2 light dose. Cremophor EL (2.5%) and EtOH (2.5%) in saline were used as a control vehicle. Objective magnification is×4.

approved such as palladium bacteriopheophorbide, porfimer sodium, lutetium texaphyrin, 5-aminolevulinic acid, and verteporfin.[18,19] For example, a PDT experiment in the CAM model using verteporfin at a dose that is similar to the recommended clinical dosage for the treatment of age-related macular degeneration has been shown to cause complete occlusion of the large neovessels, an observation that correlates well with clinical setting.[9] In addition, in a BALB/c mouse model where PDT treatment by verteporfin resulted in suppression of tumor growth, antivascular effects were also observed, whereby a decrease in the blood volume at the tumor site was noted.[20,21] The results from the study demonstrated that compound **5** was able to induce complete closure of larger vessels, which is considered favorable in PDT treatment of cancer.

Conclusions

We have demonstrated the in vitro photocytotoxic activity of BODIPY derivatives against cell lines from leukemia and two types of solid tumor. Structure−activity relationship

study indicated the importance of having iodine atoms directly substituted on the BODIPY pyrollic carbon-4 position rather than at the meso-aryl position, in accordance with the high singlet oxygen generation rate of these compounds. Extended conjugation at the 4-pyrollic positions shifts the $\lambda_{max\,abs}$ to the red but did not confer extra potency except for the compound with a single *n*-butyl acrylate ester (**12**). Hydrophilic analogues substituted with groups such as carboxylic acid, sulfonic acid, or sodium sulfonate generally drastically diminished the activity. An exception here was the doubly iodinated compound **5** with an aliphatic carboxylic acid which showed up to 100-fold lower IC_{50} value in HL-60 compared to the parent compound **1**, perhaps because of the structural difference where the carboxylic acid group is not directly conjugated with the BODIPY core. Fluorescence microscopy studies showed that compound **5** localized exclusively within the mitochondria. This, together with data from cell cycle analysis and onset of apoptosis studies, suggests that compound **5** probably induced cell death through mitochondria-dependent apoptosis rather than through damage to nucleic materials. In addition, an emulsion of compound **5** was able to occlude the vasculature network in the CAM in vivo model, further showing its potential as an effective PDT agent.

Although photosensitizers with > 600 nm excitation wavelengths allow deeper access into biological tissues for effective treatment of abnormal tissues of bigger volume, the shorter absorption wavelength of the BODIPY-based photosensitizers studied here, such as compound **5**, may be preferred in the treatment of superficial tissues. In a clinical PDT of cancer in the esophagus and bronchi with porfimer sodium II, treatment regime with light corresponding to the 514 nm excitation wavelength exhibited similar effectiveness as that with 630 nm in terms of tumor eradication but, significantly, with less damage of the deep tissue which could cause perforation in the esophagus.[22] Overall, our results suggest that BODIPY structures, especially compound **5**, have potential to be explored as a clinically useful agent for PDT of cancer.

Experimental Section

Materials. ER-Tracker Blue-White DPX, LysoTracker Blue DND-22, rhodamine 123, SYTOX Green were purchased from Molecular Probes, Invitrogen (OR). Annexin V−FITC apoptosis detection kit 1 was purchased from BD Biosciences (CA). All cell culture reagents were purchased from Gibco, Invitrogen (Auckland, New Zealand). RNase A, dimethyl sulfoxide, propidium iodide, methylene blue, 1,3-diphenylisobenzofuran, and methylthiazolyldiphenyltetrazolium bromide were purchased from Sigma (St. Louis, MO). Fluorescein isothiocyanate dextran (FITC-dextran, 20 kDa) was purchased from Sigma-Aldrich (Buchs, Switzerland). Indian ink was purchased from Pebeo S.A. (Romanel-sur-Morges, Switzerland). Cremophor EL and absolute ethanol (Fluka Biochemika, Buchs, Switzerland) were used as dosing vehicles. NaCl, 0.9%, pH 7.4 (saline), was purchased from B Braun Medical AG (Emmertbrücke, Switzerland).

Photosensitizers. The synthesis of many of the compounds studied here has already been reported elsewhere except for compounds **3**, **5**, and **7** which is shown in Scheme 1. Compound **1** was prepared using a new method whereby 3,5-dimethylpyrrole-2-carbaldehyde was treated with 1.2 equiv of $POCl_3$ followed by addition of $BF_3 \cdot OEt_2$.[23] Compound **2** was prepared from condensation of 2,4-dimethylpyrrole with 4-iodobenzene acid in $POCl_3$ and reaction of the resultant dipyrromethene intermediate with $BF_3 \cdot OEt_2$.[24] Compounds **3** and **4** were prepared from compound **2** through iodination using I_2/HIO_3 and disulfonation

Scheme 1[a]

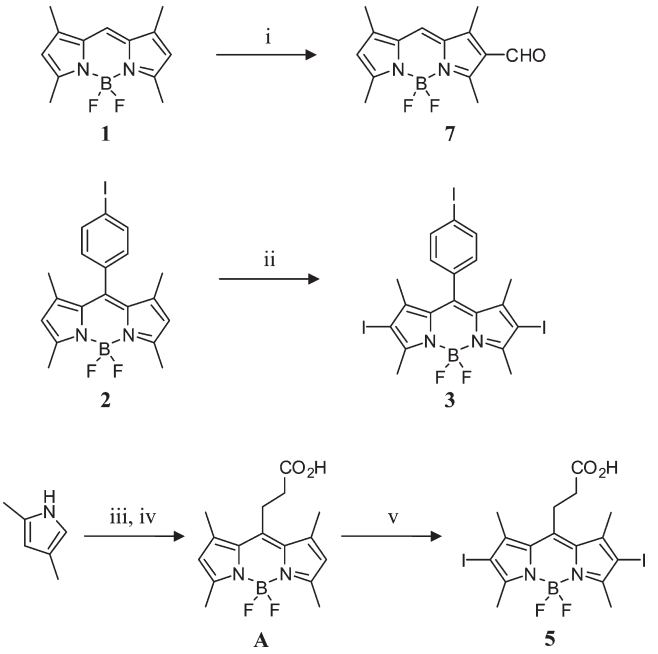

[a] Reagents and conditions: (i) $POCl_3$, DMF, 1,2-dichloroethane, 85 °C, 17 h; (ii) I_2, HIO_3, EtOH, 60 °C, 20 min; (iii) succinic anhydride, $BF_3 \cdot OEt_2$, toluene, 80 °C, 5 h; (iv) $BF_3 \cdot OEt_2$, Et_3N, 20 °C, 16 h; (v) I_2, HIO_3, MeOH, 25 °C, 30 min.

using chlorosulfonic acid,[25] respectively. Compound **5** was prepared from 2,4-dimethylpyrrole and succinic anhydride in the presence of $BF_3 \cdot OEt_2$ (to yield compound **A**), followed by iodination of the resultant BODIPY. Compound **6** was obtained from diiodination of compound **1**.[5] Compound **7** was obtained from treating compound **1** with dry dimethylformamide and $POCl_3$. Compounds **8**−**15** were prepared using palladium-catalyzed activation of the parent compound **1** using Heck-type coupling with the respective acrylate structures.[26] The experimental details for measuring the photophysical properties and synthesis of compounds **3**, **5**, and **7** are included in the Supporting Information. All compounds were dissolved in dimethyl sulfoxide (DMSO) at 10 mM, aliquoted, and stored at −20 °C prior to use.

Cells. HL-60 human promyelocytic leukemia cells were obtained from American Type Culture Collection (VA) and maintained in RPMI 1640 medium supplemented with 10% FBS. HSC-2 oral cavity human squamous carcinoma cells were obtained from Health Science Research Resources Bank (Japan Health Sciences Foundation, Japan). HK1 nasopharyngeal epithelial carcinoma cell line was a gift from University of Hong Kong Culture Collection (University of Hong Kong, Hong Kong). Both cell lines were grown in MEM medium supplemented with 10% FBS.

Photoinduced Cytotoxicity Assay. Approximately 15 000 HL-60 cells/well or 3000 cells/well for HSC-2 and HK1 cells in phenol-red-free culture medium containing 10% fetal bovine serum were seeded in a 96-well plate. HSC-2 and HK1 cells were allowed to adhere overnight before test compounds were introduced. Photosensitizer stock solutions (10 mM in DMSO) were diluted with medium, and concentrations varying from 0.001 to 100.0 μM were tested on the cells. The control wells received 0.01% of DMSO, equivalent to the highest amount of DMSO used as vehicle in the compound-treated wells. Following 2 h of treatment, cells were irradiated with a light dose of 4.1 J/cm^2 from a broad spectrum light source and fluence rate of 6.8 mW/cm^2 and were further incubated for 24 h before cell viability was assessed using MTT assay. Following incubation, 15 μL of MTT solution (5 mg/mL) was added into each well and incubated for

4 h at 37 °C. The medium was then removed, and 100 μL of DMSO was added to dissolve the formazan crystal formed. Absorbance, as a measure of viable cell number, was read at 570 nm with an OpsysMR microplate spectrometer (Thermo-Labsystems, Chantilly, VA). The dark toxicity of each photosensitizer was also determined in every experiment.

Comparative Singlet-Oxygen Generation Measurements. An amount of 8 mL of aerated isopropanol containing 50 μM of DPBF and the photosensitizer (0.5 μM or 5 μM) in a 6-well plate was irradiated at 6.8 mW/cm^2 of filtered light source of >510 nm wavelength with a Roscolux medium yellow no. 10 filter (Rosco, NY) at room temperature for 1 h. Aliquots of 200 μL were removed from the mixture at various fixed intervals, and the absorbance was measured at 410 nm. The rate of singlet oxygen production was determined from the reduction in intensity of absorbance recorded over time. Irradiation of DPBF−isopropanol solution in the absence of photosensitizer as a negative control and solution containing methylene blue as a comparative control was also carried out. The relative singlet oxygen generation rate for each of the photosensitizers was determined by using methylene blue as a reference.

Cellular Localization. HSC-2 cells grown on round glass coverslips in 12-well plates were co-incubated with 100 nM photosensitizer together with organelle-specific fluorescence probes. The endoplasmic reticulum was labeled with 100 nM of ER-Tracker Blue-White DPX, the lysosomes were stained with 500 nM of LysoTracker Blue DND-22, and the mitochrondria were tracked with 100 nM Rh123, each for 15−30 min of incubation at room temperature. After incubation, cells were gently rinsed in PBS to remove free dyes, and the stained cells were observed using Olympus DSU spinning disk confocal microscope configured with a PlanApo 63× oil objective (Olympus Optical Corp. Ltd., Tokyo, Japan) and iXon EM + digital camera (Andor Technology, South Windsor, CT). Fluorescent images of *XY* sections at 0.2 μm were collected sequentially using Olympus Cell software. Organelle-specific fluorescence probes were respectively excited at 330−385 nm wavelengths to illuminate ER-tracker and LysoTracker, at 460−490 nm for Rh123 and at 520−550 nm for the photosensitizer.

Annexin V−FITC Apoptosis Analysis. HSC-2 cells grown in 60 mm dishes at 50% confluency were treated with 0.5 μM compound **5**. Following 2 h of incubation, cells were irradiated with 4.1 J/cm^2 of broad spectrum light. At various treatment intervals, floating cells in the medium were pooled together with the adherent cells after trypsinization and were washed twice with cold phosphate buffered saline (PBS). The cells were resuspended with 1× binding buffer at 1×10^6 cells/mL. A 100 μL of cell suspension was transferred to a flow cytometry tube followed by 5 μL of annexin V−FITC and 5 μL of 200 μg/mL propidium iodide in PBS. The cells were gently mixed and incubated for 15 min at room temperature in the dark before analysis on a FACSCalibur flow cytometer equipped with a 488 nm argon laser. The fluorescence data of 1×10^4 cells were collected with the FL1 detector with 530/30 band-pass filter to collect annexin−FITC fluorescence and with the FL3 detector with a 630 nm long-pass filter to collect propidium iodide fluorescence.

Cell Cycle Analysis. HSC-2 cells were treated with 0.25 μM compound **5** and collected as above. Cells were then fixed in 70% ice-cold ethanol (v/v in PBS) overnight at 4 °C. Following fixation, the cells were washed twice in cold PBS. The pellet was then resuspended in PBS solution containing 20 μg/mL RNase A and 1 μM SYTOX Green for 30 min. The cells were analyzed on a FACSCalibur flow cytometer with 488 nm argon laser. The DNA−SYTOX Green fluorescence of 1×10^4 cells were collected with the FL1 detector with 530/30 band-pass filter.

PDT on the CAM Vasculature (in Ovo). Freshly obtained fertilized chicken eggs were incubated with the narrow apex down in a 90° swinging incubator (Savimat MG 200, Chauffry, France) at 37 °C and 65% relative humidity. On embryo development day (EDD) 3, an opening on the eggshell, about 4 mm in diameter, was bored at the apex and sealed with adhesive tape to avoid contamination and desiccation of the egg contents. The eggs were further incubated in stationary position with the apex upright until EDD-9.

Microscopic observation of CAM vasculature and the light irradiation during PDT were performed with an epifluorescence Eclipse 600 FN microscope equipped with a CFI Achromat 4×/0.1 objective (Nikon, Japan). Illumination was provided by a 100 W mercury arc lamp (Osram, GmbH, Augsburg, Germany). Light doses were adjusted with neutral density filters and measured with a calibrated Field-Master GS power analyzer (Coherent, Santa Clara, CA). For exciting and detecting compound **5**, the microscope was equipped with a G-2A filter set (excitation, 510−560 nm) (Nikon, Japan). For detecting FITC, a B-2E/C filter set (excitation, 465−495 nm) was used (Nikon, Japan). Fluorescence angiograms (1280 × 1024 pixels with 4095 gray level, i.e., 12 bits) were acquired with an F-view II 12-bit monochrome Peltier-cooled digital CCD camera driven with analySIS DOCU software from Soft Imaging System (Münster, Germany). The fluorescence images were stored in a 16-bit TIF file.

On EDD-9, the egg opening was extended to ∼30 mm in diameter. Embryo was intravenously administered with a single bolus of 3.5−7 nmol/embryo of photosensitizer in dosing vehicle (cremophor EL 5%, EtOH 5% in saline) at the CAM main vasculature. A minute after injection, a site with vessels of diameter between 5 and 100 μm was irradiated at a light dose of 20−40 J/cm^2 filtered at 510−560 nm with an irradiation area of 0.02 cm^2 and fluence rate of 40 mW/cm^2. The site was photographed at the beginning and at the end of irradiation. Subsequently, the egg opening was sealed with parafilm and the embryo was further incubated for 24 h before assessing the PDT damage induced.

Fluorescence angiograms were performed in order to assess the PDT-induced vasculature damage. Blood vessels were perfused with 10 μL of 25 mg/mL FITC−dextran followed by injection of Indian ink in order to decrease the embryo's interfering fluorescence from deeper located vessels. This interfering luminescence may change rapidly with time because of the embryo's movement. Prior to injection, the Indian ink was filtered using a sterile cellulose acetate membrane (0.2 μm pores, Renner GmbH, Darmstadt, Germany). The vasculature network at the site of irradiation was illuminated by exciting the FITC at 465−495 nm wavelengths on the epifluorescence microscope. The vasculature network was imaged, and the damage induced by PDT was scored according to the criteria as defined by Lange et al. (Table 1).[8] At least 10 embryos were assessed for each treatment group.

Acknowledgment. This work was supported by grants from the Cancer Research Initiatives Foundation. We thank David Lyn (Matrix Optics, Malaysia) for help with the cellular localization experiments.

Note Added after ASAP Publication. This paper was published on March 3, 2010 with an error in the O'Shea structure. The revised version was published on March 8, 2010.

Supporting Information Available: General procedures for spectroscopic measurements, synthesis procedures, and characterization data for compounds **1**−**15**. This material is available free of charge via the Internet at http://pubs.acs.org.

References

(1) Allison, R. R.; Downie, G. H.; Cuenca, R.; Hu, X. H.; Childs, C. J. H.; Sibata, C. H. Photosensitizers in clinical PDT. *Photodiagn. Photodyn. Ther.* **2001**, *1*, 27–42.
(2) Dolmans, D. E.; Fukumura, D.; Jain, R. K. Photodynamic therapy for cancer. *Nat. Rev. Cancer* **2003**, *3*, 380–387.

(3) Hopper, C. Photodynamic therapy: a clinical reality in the treatment of cancer. *Lancet Oncol.* **2000**, *1*, 212–219.
(4) Nyman, E. S.; Hynninen, P. H. Research advances in the use of tetrapyrolic photosensitizers for photodynamic therapy. *J. Photochem. Photobiol., B* **2004**, *73*, 1–28.
(5) Yogo, T.; Urano, Y.; Ishitsuka, Y.; Maniwa, F.; Nagano, T. Highly efficient and photostable photosensitizer based on BODIPY chromophore. *J. Am. Chem. Soc.* **2005**, *127*, 12162–12163.
(6) Gorman, A.; Killoran, J.; O'Shea, C.; Kenna, T.; Gallagher, W. M.; O'Shea, D. F. In vitro demonstration of the heavy-atom effect for photodynamic therapy. *J. Am. Chem. Soc.* **2004**, *126*, 10619–10631.
(7) Byrne, A. T.; O'Connor, A. E.; Hall, M.; Murtagh, J.; O'Neill, K.; Curran, K. M.; Mongrain, K.; Rousseau, J. A.; Lecomte, R.; McGee, S.; Callanan, J. J.; O'Shea, D. F.; Gallagher, W. M. Vascular-targeted photodynamic therapy with BF2-chelated tetraaryl-azadipyrromethene agents: a multi-modality molecular imaging approach to therapeutic assessment. *Br. J. Cancer* **2009**, *101*, 1565–1573.
(8) Atilgan, S.; Ekmekci, Z.; Dogan, A. L.; Guc, D.; Akkaya, E. U. Water soluble distyryl-boradiazaindacenes as efficient photosensitizers for photodynamic therapy. *Chem. Commun.* **2006**, *42*, 4398–4400.
(9) Lange, N.; Ballini, J. P.; Wagnières, G.; van den Bergh, H. A new drug screening procedure for photosensitizing agents used in photodynamic therapy for CNV. *Invest. Ophthalmol. Visual Sci.* **2001**, *42*, 38–46.
(10) Burghart, A.; Kim, H.; Welch, M. B.; Thoresen, L. H.; Reibenspies, J.; Burgess, K. 3,5-Diaryl-4,4-difluoro-4-bora-3a,4a-diaza-*s*-indacence (BODIPY) dyes: synthesis, spectroscopic, electrochemical, and structural properties. *J. Org. Chem.* **1999**, *64*, 7813–7819.
(11) Kochevar, I. E.; Redmond, R. W. Photosensitized production of singlet oxygen. *Methods Enzymol.* **2000**, *319*, 20–28.
(12) McBride, H. M.; Neuspiel, M.; Wasiak, S. Mitochodria: more than just a powerhouse. *Curr. Biol.* **2006**, *16*, R551–R56.
(13) Morgan, J.; Oseroff, A. R. Mitochondria-based photodynamic anti-cancer therapy. *Adv. Drug Delivery Rev.* **2001**, *49*, 71–86.
(14) Vantiegham, A.; Xu, Y.; Assefa, Z.; Piette, J.; Vandenheede, J. R.; Merlevede, W.; de Witte, P. A. M.; Agostinis, P. Phosphorylation of Bcl-2 in G_2/M phase-arrested cells following photodynamic therapy with hypericin involves a CDK1-mediated signal and delays the onset of apoptosis. *J. Biol. Chem.* **2002**, *277*, 37718–37731.
(15) Lee, H. B.; Ho, A. S. H.; Teo, S. H. p53 status does not affect photodynamic cell killing induced by hypericin. *Cancer Chemother. Pharmacol.* **2005**, *58*, 91–98.
(16) Chen, B.; Pogue, B. W.; Hoopes, P. J.; Hasan, T. Vascular and cellular targeting for photodynamic therapy. *Crit. Rev. Eukaryotic Gene Expression* **2006**, *16*, 276–305.
(17) Vargas, A.; Zeisser-Labouébe, M.; Lange, N.; Gurny, R.; Delie, F. The chick embryo and its chorioallantoic membrane (CAM) for the in vivo evaluation of drug delivery systems. *Adv. Drug Delivery Rev.* **2007**, *59*, 1162–1176.
(18) Rück, A.; Böhmler, A.; Steiner, R. PDT with TOOKAD studied in the chorioallantoic membrane of fertilized eggs. *Photodiag. Photodyn. Ther.* **2005**, *2*, 79–90.
(19) Hammer-Wilson, M. J.; Cao, D.; Kimel, S.; Berns, M. W. Photodynamic parameters in the chick chorioallantoic membrane (CAM) bioassay for photosensitizers administered intraperitoneally (IP) into the chick embryo. *Photochem. Photobiol. Sci.* **2002**, *1*, 721–728.
(20) Ichikawa, K.; Takeuchi, Y.; Yonezawa, S.; Hikita, T.; Kurohane, K.; Namba, Y.; Oku, N. Antiangiogenic photodynamic therapy (PDT) using Visudyne causes effective suppression of tumour growth. *Cancer Lett.* **2004**, *205*, 39–48.
(21) Kurohane, K.; Tominaga, A.; Sato, K.; North, J. R.; Namba, Y.; Oku, N. Photodynamic therapy targeted to tumour-induced angiogenic vessels. *Cancer Lett.* **2001**, *167*, 49–56.
(22) Grosjean, P.; Wagnieres, G.; Fontolliet, C.; van den Bergh, H.; Monnier, P. Clinical photodynamic therapy for superficial cancer in the oesophagus and the bronchi: 514 nm compared with 630 nm light irradiation after sensitization with photofrin II. *Br. J. Cancer* **1998**, *77*, 1989–1995.
(23) Wu, L.; Burgress, K. A new synthesis of symmetric boraindacene (BODIPY) dyes. *Chem. Commun.* **2008**, *40*, 4933–4935.
(24) Tahtaoui, C.; Thomas, C.; Rohmer, F.; Klotz, P.; Duportail, G.; Mély, Y.; Bonnet, D.; Hibert, M. Convenient method to access new 4,4-dialkoxy- and 4,4-dialkoxy-diaza-*s*-indacene dyes: synthesis and spectroscopic evaluation. *J. Org. Chem.* **2007**, *72*, 269–272.
(25) Li, L.; Han, J.; Nguyen, B.; Burgess, K. Synthesis and spectral properties of functionalized, water-soluble BODIPY derivatives. *J. Org. Chem.* **2008**, *73*, 1963–1970.
(26) Thivierge, C.; Bandichhhor, R.; Burgess, K. Spectral dispersion and water solubilization of BODIPY dyes via palladium-catalyzed C−H functionalization. *Org. Lett.* **2007**, *9*, 2135–2138.

Supporting Information

In Vitro and *In Vivo* Photo-cytotoxicity of Boron Dipyrromethene Derivatives for Photodynamic Therapy

*S. Hui Lim[1], Cliferson Thivierge[2], Patrycja Nowak-Sliwinska[3], Junyan Han[2], Hubert van den Bergh[3], Georges Wagnières[4], Kevin Burgess[2], H. Boon Lee[1]**

Table of Contents

1. General Procedures

NMR spectra were recorded on a VXP-300 MHz and Inova-500 MHz spectrometers (^{1}H at 300 MHz or 500 MHz and ^{13}C at 75 or 125 MHz) at room temperature unless otherwise mentioned. Chemical shifts of ^{1}H NMR spectra were recorded and reported in ppm from the solvent resonance ($CDCl_3$ 7.26 ppm, CD_3OD 3.31 ppm). Data are reported as follows: chemical shift, multiplicity (s = singlet, bs = broad singlet, d = doublet, t = triplet, q = quartet, br = broad, m = multiplet), coupling constants, and number of protons. Proton decoupled ^{13}C NMR spectra were also recorded in ppm from solvent resonance ($CDCl_3$ 77.16, CD_3OD 49.0 ppm). Analytical thin layer chromatography (TLC) was performed on EM Reagents 0.25 mm silica-gel 60-F plates, and visualized with UV light. Flash chromatography was performed using silica gel (230–600 mesh). MS were measured under ESI, MALDI or APCI conditions. All solvents and reagents were used as received unless noted otherwise.

2. Synthesis and Characterization

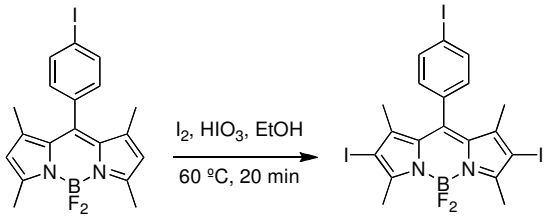

2 **3**

A mixture of **2** (107 mg, 0.238 mmol), I_2 (151 mg, 0.476 mmol), HIO_3 (84.0 mg, 0.476 mmol) in 10 mL EtOH was warmed to 60 °C for 20 min. The mixture was then cooled to room temperature. The precipitate was filtered and washed thoroughly with MeOH to yield 135 mg (81 %) of product as an orange powder. ^{1}H NMR (300 MHz, $CDCl_3$) δ 7.88 (d, J = 8.4 Hz, 2H), 7.02 (d, J = 8.4 Hz, 2H), 2.64 (s, 6H), 1.43 (s, 6H). ^{13}C could not be obtained due to the tendency of the compound to crash out of solution during analysis. MS (APCI) calcd for $C_{19}H_{15}BF_2I_3N_2$ $[M\text{-}H]^-$ 700.84, found 701.38. R_f = 0.29 (49:1 hexanes/EtOAc). Compound is photosensitive and should be stored over extended periods accordingly.

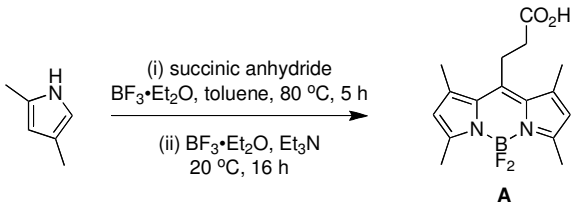

A

A solution of 2,4-dimethylpyrrole (1.0 mL, 10 mmol), succinic anhydride (400 mg, 4.0 mmol), and BF_3• Et_2O (0.50 mL, 4.0 mmol) in 30 mL toluene was heated to 80 °C under N_2 for 5 h. The mixture was cooled to 25 ºC and BF_3·Et_2O (5.0 mL, 40 mmol) and Et_3N (10 mL, 80 mmol) were then added. After stirring for 16 h at 20 ºC under N_2 the reaction

was quenched with 60 mL of 0.1 M HCl aqueous solution. Extraction was performed and the organic fractions were combined and dried over magnesium sulfate. The organic solvent was removed under reduced pressure and the product was purified via flash silica column with 85 % ethyl acetate:hexane to afford the desired product as an orange solid (203 mg, 18 %). ^{1}H NMR (300 MHz, $CDCl_3$) δ 6.07 (s, 2H), 3.29-3.35 (m, 2H), 2.62-2.68(m, 2H), 2.52 (s, 6H), 2.44 (s, 6H), ^{13}C NMR (75 MHz, $CDCl_3$), δ 176.6 154.8, 142.8, 140.3, 131.2, 122.0, 35.1, 23.4, 16.4, 14.5. MS (ESI) calcd for $C_{16}H_{19}BF_2N_2O_2$ $[M-H]^-$ 319.15, found 319.15. R_f = 0.50 (1:1 EtOAc/hexanes).

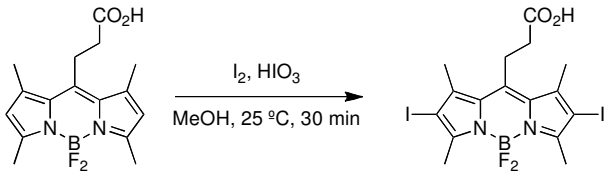

A **5**

Tetramethyl-BODIPY acid **A** (600 mg, 1.87 mmol) was suspended in 200 mL of MeOH. I_2 (1.24 g, 4.87 mmol) was added followed by iodic acid (660 mg, 3.75 mmol) in ~3 mL water was added over 5 min. The mixture was stirred for 30 min at 25 ºC. The MeOH was then removed under reduced pressure and the crude product was purified via flash silica column with 50 % ethyl acetate:hexane to afford the desired product as a red solid (574 mg, 54 %). ^{1}H NMR (300 MHz, $CDCl_3$) δ 3.28-3.32 (m, 2H), 2.45-2.52 (m, 2H), 2.50 (s, 6H), 2.43 (s, 6H), ^{13}C NMR (75 MHz, $CDCl_3$), δ 175.1 156.3, 142.5, 142.3, 131.1, 87.0, 34.9, 24.2, 19.3, 16.5. MS (ESI) calcd for $C_{16}H_{17}BF_2I_2N_2O_2$ $[M+K]^+$ 610.9, found 611.6. R_f = 0.55 (1:1 EtOAc:hexanes).

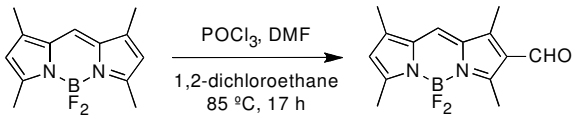

1 7

Dry DMF (22 μL, 0.24 mmol) was placed in a flame-dried flask. The flask was cooled to 0 ºC and distilled $POCl_3$ (18 μL, 0.23 mmol) was added. The mixture was warmed to room temperature and stirred for 15 min. The mixture was added *via* canula to another flame-dried flask containing **1** (20 mg, 0.081 mmol) in 1,2-dichloroethane (2 mL). The mixture was refluxed for 17 h, at which point complete conversion of **1** was indicated by TLC. Reaction was cooled to room temperature and sodium acetate trihydrate (121 mg, 0.89 mmol) was added in a minimum amount of water. The mixture was heated to reflux for 30 min and then cooled to room temperature. The mixture was washed twice with 2 mL of water and once with 2 mL of brine. The organic layer was dried over $MgSO_4$ and filtered. The filtrate was evaporated under reduced pressure to yield a crude orange powder which was further purified by silica gel flash column eluting with CH_2Cl_2 to yield 21 mg (99 %) of product as an orange powder. ^{1}H NMR (300 MHz, $CDCl_3$) δ 10.04 (s, 1H), 7.23 (s, 1H), 6.22 (s, 1H), 2.78 (s, 3H), 2.60 (s, 3H), 2.51 (s, 1H), 2.31 (s, 1H). ^{13}C NMR (125 MHz, CDCl3), δ 185.7, 163.7, 157.4, 145.6, 140.7, 136.6, 131.2, 125.9, 122.2, 121.6, 15.4, 13.0, 11.6, 10.6. MS (ESI) calcd for $C_{14}H_{15}BF_2N_2O$ $[M+H]^+$ 277.13, found 277.46. R_f = 0.24 (4:1 hexanes/EtOAc).

molecular pharmaceutics

Article

pubs.acs.org/molecularpharmaceutics

Photodynamic Characterization of Amino Acid Conjugated 15[1]-Hydroxypurpurin-7-lactone for Cancer Treatment

Siang Hui Lim,[†,‡] Mun Li Yam,[†] May Lynn Lam,[†] Fadzly Azhar Kamarulzaman,[†] Norazwana Samat,[†] Lik Voon Kiew,[§] Lip Yong Chung,[‡] and Hong Boon Lee*[,†,‡]

[†]Cancer Research Initiatives Foundation (CARIF), Sime Darby Medical Centre, Subang Jaya, Selangor, Malaysia

[§]Department of Pharmacology, Faculty of Medicine, and [‡]Department of Pharmacy, Faculty of Medicine, University of Malaya, Kuala Lumpur, Malaysia

Supporting Information

ABSTRACT: This study aims to improve the photodynamic properties and biological effectiveness of 15[1]-hydroxypurpurin-7-lactone dimethyl ester (G2), a semisynthetic photosensitizer, for the PDT treatment of cancer. The strategy we undertook was by conjugating G2 with aspartic acid and lysine amino acid moieties. The photophysical properties, singlet oxygen generation, distribution coefficiency (Log *D* in octanol/PBS pH 7.4), and photostability of these analogues and their *in vitro* bioactivities such as cellular uptake, intracellular localization, and photoinduced cytotoxicity were evaluated. In addition, selected analogues were also investigated for their PDT-induced vasculature occlusion in the chick chorioallantoic membrane model and for their antitumor efficacies in Balb/C mice bearing 4T1 mouse mammary tumor. From the study, conjugation with aspartic acid improved the aqueous solubility of G2 without affecting its photophysical characteristics. G2-Asp showed similar *in vitro* and *in vivo* antitumor efficacies compared to the parent compound. Given the hydrophilic nature of G2-Asp, the photosensitizer is a pharmaceutically advantageous candidate as it can be formulated easily for systemic administration and has reduced risk of aggregation in vascular system.

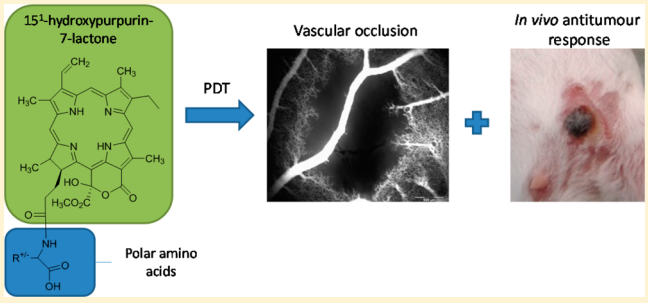

KEYWORDS: *cancer, photodynamic therapy, tetrapyrrole photosensitizer, amino acid conjugation, vascular occlusion*

INTRODUCTION

In our search for new photosensitizers for photodynamic therapy (PDT) of cancer, 15[1]-hydroxypurpurin-7-lactone methyl ethyl diester was isolated from a Malaysian plant *Aglaonema simplex* belonging to the Araceae plant family. It exhibited strong photocytotoxic activity in HL60 leukemia and in HSC-2 and HSC-3 oral cancer cell lines.[1] Before this, a structurally similar hydroxypurpurin-7-lactone was isolated from the leaves of a bamboo plant *Phyllostachys bambusoided* and it induced rapid apoptosis in CMK-7 human leukemia cell line upon irradiation with light.[2]

In order to prepare sufficient material for further studies, a closely related analogue 15[1]-hydroxypurpurin-7-lactone dimethyl ester was semisynthesized using chlorophyll-a as a precursor. 15[1]-Hydroxypurpurin-7-lactone dimethyl ester, code-named as G2 (Figure 1), exhibited PDT activity by inducing the closure of capillaries and small neovessels in a chick chorioallantoic membrane (CAM) model.[3] Compared with a known photosensitizer pheophorbide-*a* (PhA), G2 showed stronger photocytotoxicity with more pronounced apoptosis, when tested against human head and neck cancer cells.[4] Even though the potency data for G2 as a photosensitizer was promising, solubilization of G2 was challenging throughout the experimental evaluation because of its hydrophobic nature. Precipitation of the compound was a major problem, and formulation of G2 for intravenous injection in the CAM experiments was only successful with the addition of a small amout of Cremophor EL as an emulsifier.

Compound derivatization as a way to improve the overall efficacy of a photosensitizer has been an interesting subject, as reviewed by Sternberg et al.[5] To date, numerous modified porphyrin-based photosensitizers have been synthesized. These include porphyrins coupled to various molecules such as phosphates,[6] peptides,[7] fullerene,[8] and antibody.[9] Another example of modification is the conjugation of porphyrin-based compounds to amino acids.[10−12] The attachment of amino acid moieties to a photosensitizer improves solubility and facilitates its entry into the cells.[13] It has also been reported that photosensitizers conjugated with amino acids showed improved *in vitro* and *in vivo* biological activities.[13,14] In addition, ionically charged photosensitizers can localize in specific organelles in the target cells, affecting modes of cell death and overall potency.

Received: May 13, 2014
Revised: July 18, 2014
Accepted: July 31, 2014
Published: July 31, 2014

dx.doi.org/10.1021/mp500351s | *Mol. Pharmaceutics* 2014, 11, 3164−3173

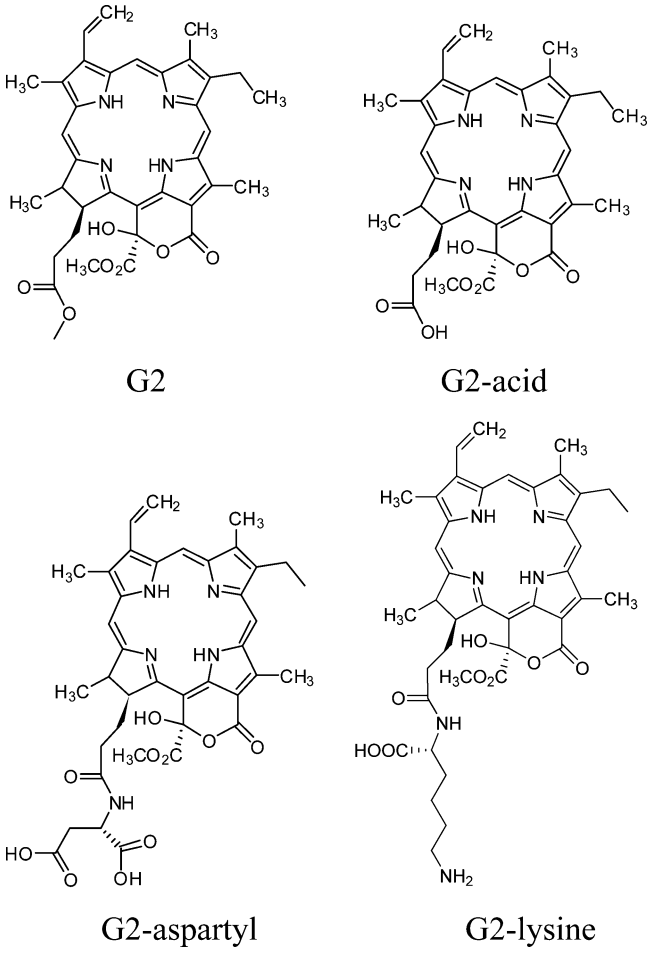

Figure 1. Structures of G2 analogues.

This study reports on efforts to prepare hydrophilic derivatives of G2 as a way to improve aqueous solubility while maintaining its biological activity. The strategy we undertook was to conjugate G2 with ionic amino acid moieties to prepare G2-Asp and G2-Lys. The preparation and characterization of the G2 analogues in comparison with G2, in terms of physiochemical properties as well as their biological activities, are included. G2 compound in its acid form (G2 acid), an intermediate during the synthesis of the analogues, was also evaluated. The most promising analogues were investigated for their PDT-induced antitumor efficacies in Balb/C mice bearing 4T1 mouse mammary tumor.

EXPERIMENTAL SECTION

Materials. HSC-2 human oral squamous carcinoma cell line was purchased from Health Science Research Resources Bank (Japan Health Sciences Foundation, Japan), and 4T1 mouse mammary carcinoma cell line was purchased from from the American Tissue Culture Collection (Virginia, USA). Cell culture reagents including minimum essential medium (MEM), RPMI (Roswell Park Memorial Institute medium) 1640 medium, fetal bovine serum (FBS), penicillin−streptomycin, and trypsin were purchased from Gibco, Invitrogen (Auckland, New Zealand). 1,3-Diphenylisobenzofuran (DPBF), propidium iodide, RNase A, fluorescein isothiocyanate dextran (FITC−dextran, 20 kDa), and dimethyl sulfoxide (DMSO) were purchased from Sigma-Aldrich (St. Louis, USA) while thiazoyl blue tetrazolium bromide (MTT) was purchased from Amresco (OH, USA). Ethanol, isopropanol, octanol-1, and acetonitrile were purchased from Fisher Scientific (Leics, U.K.). Tiletamine-zolazepam (Zoletil) was purchased from Virbac (Carros, France). Ketamine (Ketamil) and xylazine (Xylazil-100) were obtained from Troy Laboratories (NSW, Australia). ER-Tracker Blue-white DPX, LysoTracker Blue DND-22, and rhodamine 123 were purchased from Molecular Probes, Invitrogen (OR, USA)

Equipment. UV−visible absorption and fluorescence emission spectra were recorded with the cuvette platform of SpectraMax M4 (Molecular Devices, CA, USA) using 1 cm path length quartz cuvettes. Meanwhile, the absorbance and fluorescence intensity of samples in a 96-well plate were measured with the microplate platform of SpectraMax M4. Photoirradiation for all *in vitro* experiments was performed with a light source containing a Halotone 300 W halogen lamp (Philips Electronic, The Netherlands). An 8 cm water column was used to filter off the infrared radiation, and a Roscolux #26 Light Red (>580 nm) (Rosco, NY, USA) filter was placed in the irradiation path before the sample. The irradiation intensity was measured with a calibrated Nova-Oriel power meter (Newport Corp, CA, USA).

Photosensitizers. 15^1-Hydroxypurpurin-7-lactone dimethyl ester (G2), 15^1-hydroxypurpurin-7-lactone methyl ester (G2 acid), aspartyl-15^1-hydroxypurpurin-7-lactone methyl ester (G2-Asp), and lysyl-15^1-hydroxypurpurin-7-lactone methyl ester G2 acid (G2-Lys) were prepared following literature protocols from a crude acetone extract of *Spirulina pacifica*. Details of the semisynthesis of these compounds and their spectroscopic data are included in the Supporting Information. PhA was purchased from Frontier Scientific (UT, USA). Working stock concentrations of these compounds were mentioned in their respective experiments.

Photophysical Properties. Compounds were dissolved in ethanol or in PBS at 10 μM for the measurements of UV−visible and fluorescence emission spectra. The UV−visible spectral data was collected at wavelengths from 300 to 800 nm. The compounds were excited at their respective maximal absorption (λ_{max}) for the measurement of the fluorescence emission spectrum, which was recorded from 600 to 800 nm. The extinction coefficient (ε) for each compound was determined, and the fluorescence quantum efficiency (Φ_{fl}) was calculated using PhA in ethanol (Φ_{fl} = 0.28) as reference.[15]

Relative Rate of Singlet Oxygen Generation. Compounds at 0.5 to 5 μM were prepared in 8 mL of 50 μM DPBF in aerated isopropanol. This mixture in a 6-well plate was irradiated at 5.3 mW/cm^2. 200 μL of the solution was sampled in a covered 96-well plate in duplicate at fixed intervals over 1 h, and the absorbance was read at 410 nm using a microplate reader. An irradiated well without photosensitizer was also performed as a negative control. The singlet oxygen generation rate was deduced from the reduction of DPBF absorbance over time, and the quantum yield was determined by using PhA (Φ_Δ = 0.52) as reference.[16]

Distribution Coefficient (Log *D*). Octanol-1 and phosphate buffered saline (PBS) (pH 7.4) were presaturated with each other by shaking vigorously a mixture of both in separate bottles and leaving the bottles overnight to settle down. A stock solution of compounds in known concentrations (5 to 20 μM) in octanol-1 was prepared. This solution was shaken vigorously with the same volume of PBS (pH 7.4) in a 2 mL microcentrifuge tube. Another set of experiments was prepared by diluting the octanol-1 stock solution into half its

dx.doi.org/10.1021/mp500351s | *Mol. Pharmaceutics* 2014, 11, 3164−3173

concentration and shaking the same volume of this diluted stock solution with a second volume of PBS. To facilitate equilibration, tubes were centrifuged at 400*g* for 10 min. Both the octanol-1 and aqueous phases were carefully sampled for absorbance measurement, and the compound concentrations in both phases were interpolated from a standard curve of the compound determined at 400 nm. The distribution coefficient or Log *D* was then calculated using the following equation:

$$\text{Log } D = \log(\text{concentration}_{\text{octanol-1}}/\text{concentration}_{\text{PBSpH7.4}})$$

Photostability Studies. For photostability assay, 10 μM concentrations of compounds in 100 μL of PBS (pH 7.4) were irradiated with light of wavelength >580 nm at 8.9 mW/cm^2 for various durations. Following irradiation, the sample absorbance was recorded at 400 nm using a microplate reader.

Photocytotoxicity Determined Using MTT Assay. For *in vitro* studies, compounds were prepared in DMSO at 10 mM, aliquoted, and stored at −20 °C prior to use. The oral cancer cell line HSC-2 was grown and maintained in MEM supplemented with 10% fetal bovine serum and 1% penicillin−streptomycin. For assays, HSC-2 cells were seeded into 96-well plates at 4000 cells/well in phenol red free MEM containing 5% fetal bovine serum and 1% penicillin−streptomycin and incubated overnight for cell attachment before photosensitizers were added at concentrations varying from 0.01 to 10 μM. Following 2 h of incubation, cells were irradiated with 5.3 J/cm^2 of light, at wavelength >580 nm and at a fluence rate of 8.9 mW/cm^2 for 10 min. Cells were further incubated for 24 h before cell viability was determined. Following incubation, 20 μL of MTT (5 mg/mL in PBS) was added to each well and incubated for 4 h. The supernatant was removed, and the purple formazan formed was dissolved with 100 μL of DMSO. Absorbance was read at 570 nm using a microplate reader. A set of dark controls without irradiation was performed concurrently.

Cellular Uptake of Photosensitizer. HSC-2 cells were seeded into 96-well plates at 4000 cells/well and incubated overnight. Cells were treated with compounds at 10 μM for the indicated periods. Following incubation, the content of each well was removed and the wells were washed twice with PBS. Each well was then incubated with 200 μL of acetonitrile:water (4:1) for 30 min at room temperature to lyse the cells and to extract the photosensitizers. Subsequently, 100 μL of the extract was transferred to a black 96-well plate and their fluorescence intensity (excitation/emission at 400/675 nm) was measured using a microplate reader. The concentrations of the photosensitizer were determined from a calibration curve.

Intracellular Localization. The intracellular localization of the G2 analogues was analyzed by confocal microscopy using dual staining techniques as previously reported.[17] Briefly, cells grown on round glass coverslips were coincubated with 100 nM of test compound together with each organelle-specific fluorescence probe, respectively. The endoplasmic reticulum was labeled with 100 nM ER-Tracker Blue-White DPX, the lysosomes were stained with 500 nM LysoTracker Blue DND-22, and the mitochrondria were tracked with 100 nM Rh123, each for 15−30 min of incubation at room temperature. Following incubation, cells were rinsed gently with PBS to remove free dyes, and the stained cells were observed using an Olympus DSU spinning disk confocal microscope configured with a PlanApo 60× oil objective and XM10 monochrome cooled CCD camera (Olympus Optical Corp. Ltd., Tokyo, Japan). Fluorescence images of XY sections at 0.2 μm were collected sequentially using Olympus Cell software. Organelle-specific fluorescence probes were respectively excited at 330−385 nm wavelengths to illuminate ER-Tracker and Lyso-Tracker, at 460−490 nm for Rh123, and at 400−440 nm for the test compound. The intracellular localization of the test compound was determined by comparing its fluorescence topographic profile with the topographic profile of each organelle-probe generated from a longitudinal transcellular axis.

PDT on the CAM Vasculature (*in Ovo*). Freshly fertilized chicken eggs (variety Lohmann Brown obtained from Hing Hong Sdn Bhd, Selangor, Malaysia) were incubated with the narrow apex facing down in a swinging Octagon 40DX incubator (Brinsea Products Inc., Stanford, England). On embryo development day (EDD) three, an eggshell opening about 4 mm in diameter was bored at the apex and sealed with adhesive tape to avoid contamination and desiccation of the egg contents. The eggs were further incubated in stationary position with the apex upright. On EDD-9, the egg opening was extended to ∼30 mm in diameter and a single bolus of 6 nmol/embryo of photosensitizer in dosing vehicle (CrEL 5%, EtOH 5% in saline) was intravenously administered at the CAM main vasculature. One minute after injection, a site with vessels between 5 and 100 μm in diameter was irradiated with a light dose of 20−40 J/cm^2. Irradiation was performed with light of 400−440 nm wavelength with an irradiation area of 0.02 cm^2 and fluence rate of 130 mW/cm^2. Subsequently, the egg opening was sealed with parafilm and was further incubated for 24 h before assessing the PDT-induced damage. Fluorescence angiograms were performed in order to assess the PDT-induced vasculature damage. Blood vessels were perfused with 10 μL of 25 mg/mL FITC−dextran followed by injection of India ink in order to decrease the embryo's interfering fluorescence from deeper located vessels. The vasculature network at the site of irradiation was illuminated by exciting FITC at 465−495 nm wavelengths on the fluorescence microscope. The vasculature network was imaged, and the damage induced by PDT was scored using a previously defined arbitrary damage scale as listed in Table 1.[18]

Table 1. Damage Score of PDT-Induced Vasculature Network Occlusion

occlusion score	findings
0	no occlusion
1	Partial closure of capillaries of diameter <10 μm
2	closure of capillary system, partial closure of blood vessel of diameter <30 μm, and size reduction of larger blood vessels
3	closure of vessels of diameter <30 μm and partial closure of larger blood vessels
4	total closure of vessels of diameter <70 μm and partial closure of larger vessels
5	total occlusion of vessels in the irradiated area

Microscopic observation of CAM vasculature and the light irradiation during PDT were performed with an MVX10 macro zoom fluorescence microscope equipped with an MV PLAPO 2XC lens (Olympus, Japan). Illumination was provided by a 75 W xenon lamp (Olympus, Japan). Light doses were adjusted with neutral density filters and measured with a Nova-Oriel power meter. For exciting and detecting G2 analogues, a 400−440 nm excitation filter set (U-FBVW; Olympus, Japan) was used. For detecting FITC, a 460−480 nm excitation filter set (U-MGFPHQ; Olympus, Japan) was used. Fluorescence

angiograms were acquired with an XM10 monochrome cooled CCD camera driven by Cell^M Software from Olympus Soft Imaging Solution (Münster, Germany).

***In Vivo* PDT Efficacy Studies.** All animal experiments were conducted in accordance with protocols reviewed by Animal Care and Use Committee (ACUC), Faculty of Medicine, University of Malaya (animal ethics approval reference number FAR/14/07/2010/LSH). Female Balb/C mice aged between 7 and 8 weeks with a minimum weight of 17 g were maintained in a controlled environment of 12 h light−dark cycles with free access to food and water. Tumor allografts were initiated by injecting 5×10^5 of 4T1 mouse mammary carcinoma cells in 0.1 mL of RPMI 1640 medium into the mammary fat pad at the lower left quadrant of the mice's abdomen. Compound stock solutions were prepared at 15 mg/mL in 1:1 mixture of CrEL:EtOH and further diluted 10× to 1.5 mg/mL with saline before use. CrEL is a nonionic surfactant consisting of a mixture of castor oil and ethylene oxide derivatives, and it has been used to solubilize lipophilic photosensitizers via the formation of micelles.[19] As this was an early preclinical test on photosensitizer efficacies, the formation of the micelles and their characteristics were not determined. Treatments were initiated when tumors reached an approximate volume of 100 mm^3. Mice ($n \geq 5$ per group) were administered respectively G2 and G2-Asp (15 mg/kg) dissolved in a mixture of 5% Cremophor, 5% ethanol in saline as dosing vehicle via the lateral tail vein at 10 mL/kg. For the solvent control group, only the dosing vehicle was given. Following dosing at fixed interval, mice were anesthetized by intraperitoneal injection of an anesthetic cocktail (25 mg/mL tiletamine-zolazepam, 80 mg/mL ketamine, 20 mg/mL xylazine) and PDT was performed after the onset of anesthesia. The tumor area was focally illuminated using the Lumacare LC-122A fiber optic light delivery system (Lumacare, Newport Beach, CA) fitted with a 665/32 bandpass filter. The total fluence delivery was 100−200 J/cm^2 with a fluence rate of 130 mW/cm^2 over a 12 mm diameter irradiation spot. Following illumination, animals were allowed to recover from anesthesia in a warm chamber. Animal weights and tumor volume were measured thrice weekly for 2 weeks or earlier when the mice were deemed necessary to be sacrificed owing to excessive tumor burden (tumor volume >2000 mm^3). The tumor volume (mm^3) was calculated from the measurements (mm) of two perpendicular dimensions, length and width, using the following formula for a prolate ellipsoid: tumor volume (mm^3) = 0.5 × length (mm) × width^2 (mm^2).

Statistical Analysis. Statistical significance was determined using one-way ANOVA *post hoc* with Bonferroni test (SPSS 16.0, IBM Corporation, Armonk, NY), and differences were considered significant when $P < 0.05$.

RESULTS

Photophysical Properties. The photophysical properties of G2 analogues assessed at 10 μM in ethanol or PBS pH 7.4 are summarized in Table 2. In ethanol, the conjugation of G2 with aspartyl or lysyl as well as G2 in acid form did not result in a shift in the absorption and fluorescence emission peaks (Figure 2). All the analogues had similar absorption spectrum shape with a B-band at approximately 400 nm and a major Q-band at 667 nm. However, the Q-band molar extinction coefficients of G2 acid (ε = 8400 M^{-1}cm^{-1}) and G2-Lys (ε = 6500 M^{-1}cm^{-1}) were appreciably lower compared to those of G2 (ε = 34 100 M^{-1} cm^{-1}) and G2-Asp (ε = 31 800 M^{-1} cm^{-1}). Meanwhile, the fluorescence emission wavelengths among the G2 analogues were very similar at ∼675 nm, and their fluorescence quantum yields (Φ_{fl}) in ethanol ranged from 0.14 to 0.19 as calculated by using PhA (Φ_{fl} = 0.28 in ethanol) as reference. On the other hand, the light absorption peaks in PBS pH 7.4 were very similar among the G2 analogues except for G2, which had a lower B-band but a red-shifted Q-band (Figure S1, in Supporting Information). In terms of absorption intensity, G2-Asp had a higher Q-band molar extinction coefficient (ε = 14 200 M^{-1} cm^{-1}) than the other G2 analogues.

Table 2. Photophysical Parameters of G2 Analogues in Ethanol and PBS pH 7.4[a]

	ethanol					PBS pH 7.4		
	λ_{max} (nm)					λ_{max} (nm)		
Ps	B-band	Q-band	Q-band ε (M^{-1} cm^{-1})	λ_{em} (nm)	Φ_{fl}	B-band	Q-band	Q-band ε (M^{-1} cm^{-1})
G2	398	667	34 100	675	0.16	370	683	9 400
G2 acid	400	666	8 400	672	0.18	399	668	6 400
G2-Asp	397	667	31 800	675	0.14	393	662	14 200
G2-Lys	399	667	6 500	672	0.19	396	663	4 500

[a]Φ_{fl}: Fluorescence quantum efficiency of photosensitizers (Ps) was calculated using pheophorbide-*a* in ethanol (Φ_{fl} = 0.28) as reference.

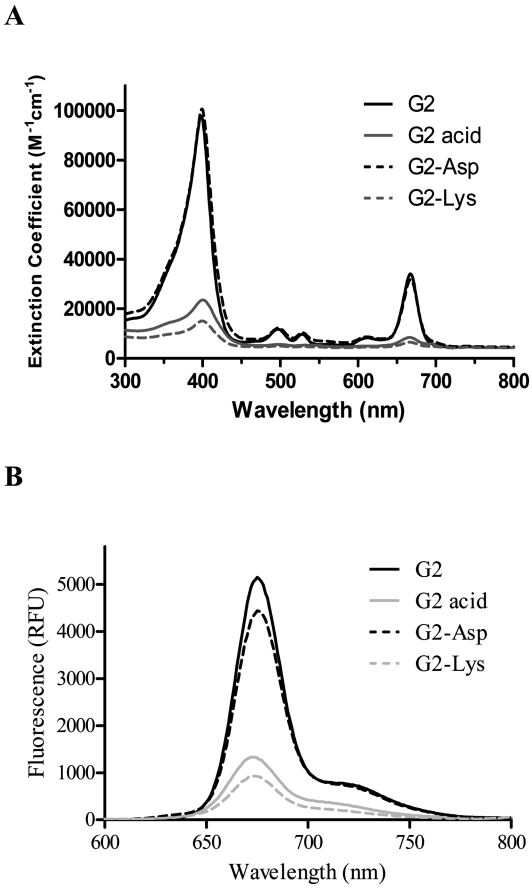

Figure 2. Photophysical properties of G2 analogues at 10 μM in ethanol. (A) UV−visible spectrum for G2 analogues. (B) Fluorescence emission spectra for G2 analogues when excited at B-band λ_{max}.

dx.doi.org/10.1021/mp500351s | *Mol. Pharmaceutics* 2014, 11, 3164−3173

Distribution Coefficient Log *D*. Distribution coefficient (Log *D*) is defined as the ratio of concentrations of a compound (ionized plus un-ionized) distributed in each phase of a mixture of two immiscible solvents, namely, an aqueous buffer and *n*-octanol, at equilibrium. From the shake flask experiment, G2-Lys and G2-Asp gave Log *D* values of 0.3 and −0.4 respectively, which were significantly lower ($P < 0.05$) compared to the unconjugated G2 with a value of 1.3 (Table 3). The lower Log *D* values for G2-Lys and G2-Asp compared to G2 indicated that the conjugation of the latter with aspartyl or lysyl amino acids had increased its solubility in the aqueous phase. The negative Log *D* value of G2-Asp reflects its preferential solubilization in the aqueous compared to the octanol phase. Meanwhile, the Log *D* value for G2 acid at 1.2 was similar to that for G2 ($P > 0.05$).

Table 3. Singlet Oxygen Quantum Yield, Log *D*, and Photocytotoxicity of G2 Analogues[a]

compounds	(Φ_Δ)	Log *D*	IC_{50} (μM)
G2	0.66 ± 0.03[§]	1.3 ± 0.2[§]	0.48 ± 0.02[§]
G2 acid	0.32 ± 0.01[†]	1.2 ± 0.1[§]	2.8 ± 0.1[†]
G2-Asp	0.32 ± 0.03[†]	−0.4 ± 0.1[‡]	0.91 ± 0.07[§]
G2-Lys	0.29 ± 0.02[†]	0.3 ± 0.1[†]	3.3 ± 0.4[†]

[a]Singlet oxygen quantum yields (Φ_Δ) determined in isopropanol using pheophorbide-*a* (Φ_Δ = 0.52 in ethanol) as reference. Distribution coefficient (Log *D*) of compounds determined using a modified shake flask method in *n*-octanol and PBS (pH 7.4). IC_{50} (half maximal inhibitory concentration) in HSC-2 cells determined using MTT assay following 24 h incubation with compounds (light dose 5.3 J/cm^2). No dark cytotoxicity was observed up to 10 μM. Values represent mean ± SD of three independent replicates. Values with different symbols were significantly different ($P < 0.05$) within each parameter.

Singlet Oxygen Generation Quantum Yields. The ability of a photosensitizer to generate singlet oxygen determines their efficiency as a photodynamic therapy agent. This event is essential because the singlet oxygen produced is the key cytotoxic agent that directly oxidizes biological molecules thereby causing damage to biological systems. The singlet oxygen quantum yield of G2 analogues was quantified by monitoring the bleaching of the singlet oxygen scavenger DPBF at an initial concentration of 50 μM in isopropanol over a period of 1 h of light irradiation. The irradiation was performed at 5.3 mW/cm^2 of light dose at room temperature. The singlet oxygen quantum yield was determined using PhA as reference. Under this experimental condition, G2 exhibited significantly higher Φ_Δ value ($P < 0.05$) at 0.66, which is at least 2-fold greater compared to G2 acid, G2-Asp, and G2-Lys (Table 3). In the meantime, reduction of DPBF was not observed in the negative control well, indicating that its reduction was not caused by photobleaching of the DPBF reagent.

Photostability. Degradation of photosensitizer following irradiation due to photobleaching reduces their availability to perform PDT. Photostability study was performed by irradiating 10 μM photosensitizers in PBS (pH 7.4) at 8.9 mW/cm^2 in order to mimic the *in vitro* assay settings. From Figure 3, G2 and G2-Asp were relatively stable to irradiation at wavelengths between 600 and 800 nm. Meanwhile, G2 acid and G2-Lys were found to be photodegraded within the first 20 min of irradiation by 8% and 15% from their initial concentrations, respectively. It is noteworthy that within the first 10 min of light irradiation—a duration that corresponded with that used for subsequent *in vitro* potency studies—the extent of photodegradation was minimal (<10%) for all the analogues.

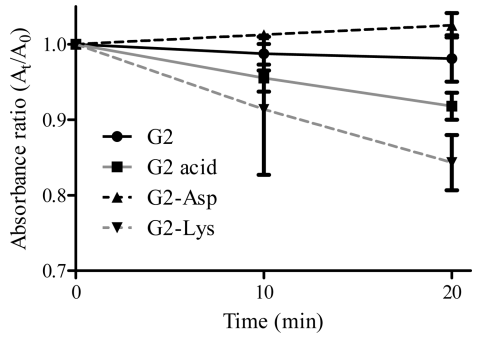

Figure 3. Photostability assessment via UV−visible spectra of 10 μM of compounds in PBS (pH 7.4) upon irradiation with 8.9 mW/cm^2 of light >580 nm in wavelength.

Cellular Uptake. The kinetics of cellular accumulation of G2 analogues was studied in HSC-2 cells. This was achieved by measuring the molar amount of photosensitizers taken up by cells following incubation with 10 μM photosensitizer in the dark. From the study (Figure 4), G2 exhibited the highest rate and amount of uptake among the analogues, whereby the accumulation of G2 increased significantly within the first 0.5 h ($P < 0.05$) and continued to rise to 150 nmol/mg protein at 24 h ($P < 0.05$). Meanwhile, the uptake rates and amounts for G2 acid, G2-Asp, and G2-Lys within the first 24 h were low with concentrations detected at approximately 18 nmol/mg protein.

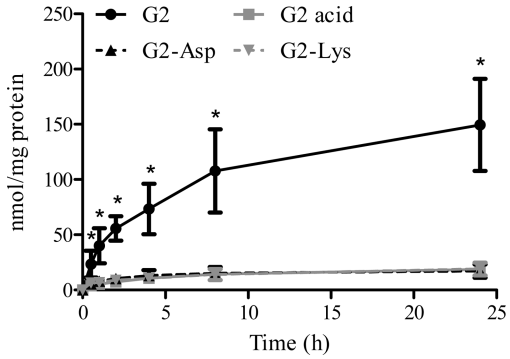

Figure 4. Intracellular uptake profiles of G2 analogues at 10 μM in HSC-2 cells. Intracellular accumulation of G2 increased rapidly within the first 4 h and continued to rise to 150 nmol/mg protein at 24 h. Meanwhile, the uptakes for G2 acid, G2-Asp, and G2-Lys within 24 h were approximately 18 nmol/mg protein. *Statistically significant differences compared to each group at their respective time point with $P < 0.05$.

In Vitro PDT Activity. To determine the photocytotoxicity of the G2 analogues, HSC-2 cells treated with the photosensitizers were irradiated with a light dose 5.3 J/cm^2. The cell viability following treatment was determined 24 h later using MTT assay. The MTT assay is based on the conversion of yellow tetrazolium salt to purple formazan by the mitochondrial dehyrogenase activity of viable cells. In this study, G2 was the most potent photosensitizer with an IC_{50} value of 0.48 μM followed by G2-Asp, G2 acid, and G2-Lys with IC_{50} values of 0.91, 2.8, and 3.3 μM respectively (Table 3). The reduction in *in vitro* PDT potency of G2-Asp was not significant ($P > 0.05$) when compared to G2, while for G2-Lys and G2 acid, their PDT potency was significantly reduced ($P < 0.05$) when

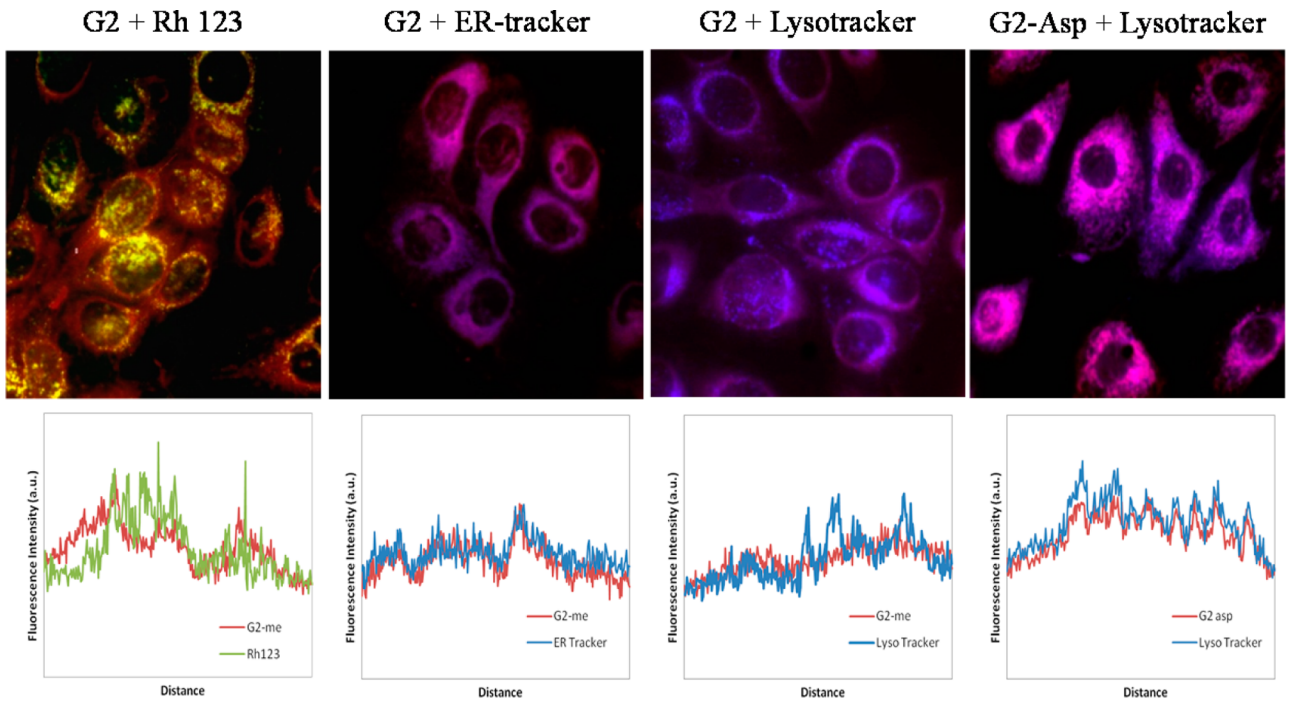

Figure 5. Intracellular localization of G2 and G2-Asp in HSC-2 cells. Spinning disk confocal fluorescence images and their respective fluorescence topographic profiles of HSC-2 cells double-stained with 100 nM G2/G2-Asp and organelle probes. Mitochondria were labeled with 100 nM Rh123 and excited at 494 nm. Endoplasmic reticulum were labeled with 100 nM ER-Tracker and excited at 365 nm. Lysosomes were labeled with 500 nM LysoTracker and excited at 365 nm. Both G2 and G2-Asp were excited at 420 nm. Topographic profiles revealed that G2 localized predominantly in the endoplasmic reticulum, while G2-Asp localized in the lysosomes. Objective magnification ×60.

compared to G2. Treatment of the cells with up to 10 μM photosensitizers without irradiation did not result in a significant loss of cell viability (data not shown).

Intracellular Localization. The intracellular localization of the G2 analogues was analyzed by confocal microscopy using dual staining techniques. Only G2 and G2-Asp were included in this study because these two photosensitizers had sufficiently high fluorescence intensities for live cell imaging. Costaining images of the photosensitizers with organelle-specific probes, namely, rhodamine 123 (mitochondria), Lyso-tracker (lysosome), and ER-Tracker (endoplasmic reticulum), were captured, and their localization topographic profiles were compared (Figure 5). The topography profiles revealed that G2 localized to a great extent in the endoplasmic reticulum. Meanwhile, G2-Asp was found to localize primarily in the lysosomes. No staining of the nuclei or plasma membrane was observed for both G2 and G2-Asp.

PDT-Induced Vascular Occlusion. One method to evaluate the PDT efficacy of a photosensitizer is by determining the ability of the agent to induce vasculature occlusion. Given that G2 and G2-Asp were the most potent based on the *in vitro* assays, they were selected for further evaluation for PDT-induced vascular occlusion (Figure 6). Using the CAM model, G2 at 6 nmol/embryo was able to induce closure of vessels below 30 μm diameter with an average occlusion score of 2.5 (according to the scoring system in Table 1) when irradiated with a light dose of 20 J/cm^2. At similar drug and light doses, G2-Asp only induced partial closures of capillaries of diameter below 10 μm with an average damage score of 1. When the light dose was increased to 40 J/cm^2, G2 at 6 nmol/embryo was able to induced complete closure of vessels with diameter <30 μm with an average occlusion score of 3.3, while G2-Asp induced an average occlusion score of 4.0 with total occlusion of vasculature observed for vessels with diameter <70 μm. Meanwhile, the control eggs that received 20 μL of dosing vehicle (2.5% CrEL, 2.5% EtOH in saline) and were exposed to a similar light dose showed no detectable vascular alteration in the treated area. This indicated that the vascular occlusion observed in embryos treated with G2 or G2-Asp neither was caused by the vehicle components nor was it a result of heat generated by the light irradiation.

PDT-Mediated Tumor Response in Vivo. A dose of 15 mg/kg was used in *in vivo* testing based on the maximum solubility of G2 in 5% CrEL, 5% EtOH in saline (1.5 mg/mL). This dosage of G2 or G2-Asp, when injected into mice but not irradiated by light, was found to be well tolerated by the mice over a two-week observation period (data not shown). First, a dose-finding experiment was conducted by administering 15 mg/kg of G2 or G2-Asp to Balb/C mice implanted with 4T1 tumor. PDT was performed with an irradiation dose of 100 or 200 J/cm^2 at two drug–light intervals of 1 and 24 h, respectively. Each treatment group consisted of two mice. Both mice in the group that received PDT with 200 J/cm^2 of light an hour following drug dosing resulted in an immediate functional loss of the limb close to the irradiation site, which was an undesirable adverse effect. In contrast, no clear evidence of PDT-induced antitumor response was detected for mice in the group with 24 h drug–light interval when irradiated with 200 J/cm^2 of light. Subsequently, the treatment regime was modified to incorporate 100 J/cm^2 of light dose and 1 h of drug–light interval. This time, the treated mice presented evidence of antitumor response with an observation of tumor cyanosis within 24 h after PDT, followed by the typical development of necrosis and eschars within 2–3 days (Figure 7A).

dx.doi.org/10.1021/mp500351s | *Mol. Pharmaceutics* 2014, 11, 3164–3173

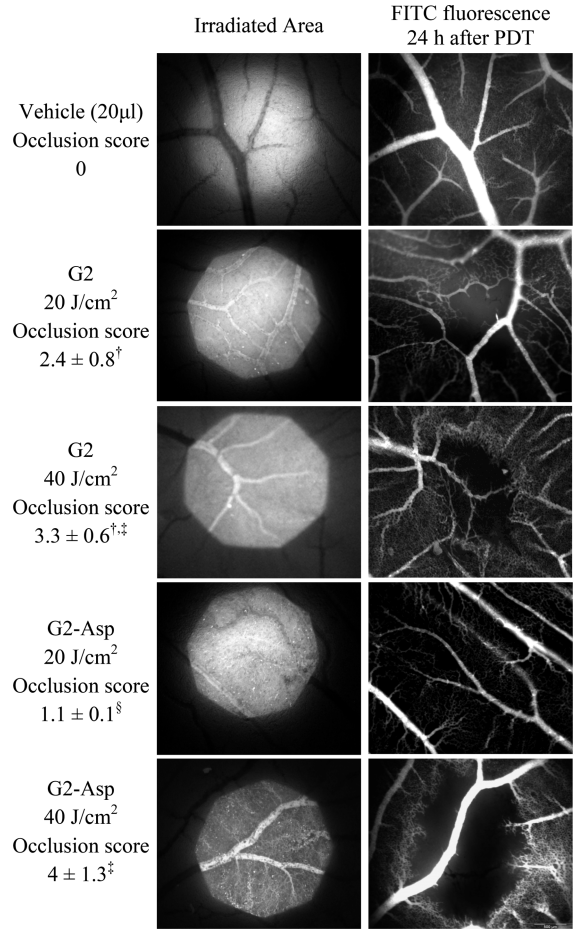

Figure 6. Representative angiographies of blood vessels supplying the CAM at the beginning and 24 h after PDT, illustrating the vascular occlusion efficacy induced by G2 and G2-Asp at 6 nmol/embryo. Irradiation was performed at 400−440 nm of excitation wavelength with 20 or 40 J/cm^2 of light dose. Occlusion score represents mean values from at least ten embryos. Score with different symbols indicate differences were statistically significant (P < 0.05). Objective magnification ×4.

In our tumor model, both G2 and G2-Asp at a dose of 15 mg/kg were effective to inhibit the growth of 4T1 cancer cells when the mice were irradiated with 100 J/cm^2 of light 1 h post drug injection (Figure 7B). At the end of a 14-day observation period, the tumor growth in mice receiving G2 + 100 J/cm^2 and G2-Asp + 100 J/cm^2 was inhibited by 41% (P < 0.05) and 43% (P < 0.05) respectively compared to the vehicle control group. There were no statistically significant differences in tumor growth between the two treatment groups. However, complete tumor regression was observed in two out of eight mice receiving 15 mg/kg G2-Asp + 100 J/cm^2 of light but not in the equivalent G2 + 100 J/cm^2 group. No tumor growth inhibition was observed in animals receiving 15 mg/kg of G2 or G2-Asp alone. There was no treatment-related toxicity or significant loss of animal body weight observed in all treatment groups exposed to 100 J/cm^2 of light 1 h post drug injection. Tumor growth was only monitored for 2 weeks before the experiments were terminated given the high risk of tumor metastasis of 4T1 tumors grown in mammary fat pad of Balb/C mice. A previous study conducted using the same murine tumor model has shown that no metastasis was detected up to 18 days following tumor cell inoculation.[20]

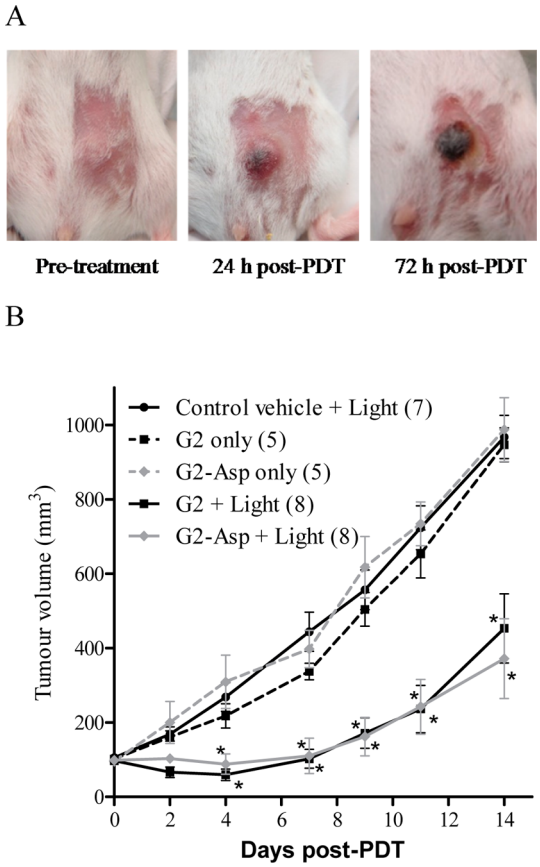

Figure 7. (A) Photographs of 4T1 syngeneic murine tumor implanted into the mammary fat pad at the lower left quadrant of the mice's abdomen before and 24 and 72 h after PDT (15 mg/kg of G2 + 100J/cm^2 light). Evidence of antitumor response was observed with the development of tumor cyanosis within 24 h after PDT and followed by the typical development of necrosis and eschars within days 2−3. (B) Effects of G2 and G2-Asp (15 mg/kg, respectively) on tumor growth of 4T1 *in vivo*. Treatment was initiated when tumors reach volume of ∼100 mm^3. For PDT, tumor site was irradiated 1 h after drug dosing with 665/32 bandpass filtered light with a light dose of 100 J/cm^2 at a fluence rate of 130 mW/cm^2. Mixture of 5% CrEL, 5% EtOH in saline was used as dosing vehicle, and number in parentheses indicates number of mice in each treatment group. *Statistically significant differences compared to control group at each time point with P < 0.05.

■ DISCUSSION

Data from our study suggest that the attachment of aspartyl or lysyl amino acids was able to improve the aqueous solubility of G2 as represented by the lower or negative Log D values in the resultant analogues. This is expected as Asp and Lys are highly polar such that, at physiological conditions, the acidic aspartyl moiety is set to lose an H^+ (proton) at its carboxylic side chain to become negatively charged and to engage in ionic bonding, whereas the amine side chain of the lysyl moiety accepts an H^+ to become positively charged and to engage in hydrogen bonding. In terms of photophysical properties, the conjugation did not affect the λ_{max} absorption wavelengths for both B- and Q-bands, but it reduced the Q-band extinction coefficients especially for G2-Lys. This observation is consistent with previous reports that also observed lower extinction coefficients with the conjugation of hydrophilic amino acids to porphyrins.[10,21] This reduction is generally undesirable for PDT agents because, in order to receive sufficient excitation energy

especially in deep-seated tissues, a photosensitizer should have a relatively intense absorption band (>20000−30000 M^{-1} cm^{-1}) at wavelength between 600 and 800 nm where light can penetrate effectively.[22]

The *in vitro* potency data revealed a decrease in PDT cytotoxicity following the conjugation of aspartyl or lysyl amino acids to G2. Factors such as singlet oxygen generation, photostability, cellular uptake, and the organelles in which the compound resides in the cells can influence the *in vitro* PDT efficacy.[23,24] When analyzed according to singlet oxygen generation ability, the photocytotoxicity of the G2 analogues decreased in accordance with decreasing singlet oxygen production following conjugation to aspartyl or lysyl group. This decrease in the singlet oxygen generation could be linked to the lower molar absorption coefficient of the more polar analogues, which would in turn affect the amount of light energy absorbable to generate singlet oxygen. When analyzed according to cellular uptake, we observed greater photocytotoxicity in analogues that showed higher level of cellular uptake. The higher cellular uptake by G2 compared to G2-Asp and G2-Lys was probably due to the greater lipophilicity of the former as lipophilic compounds can cross the membrane lipid bilayers more easily. While it is generally true that the uptake of compounds into cells is largely governed by their relative lipophilicity, several studies have shown that uptake of certain porphyrins demonstrated nonlinear correlation with their lipophilicity.[25−27] An example is demonstrated in extremely lipophilic porphyrins which tend to form aggregates in cell culture media thus preventing plasma membrane diffusion. In our study, even though G2-Asp and G2-Lys have similar cellular uptake patterns, poorer cytotoxicity is observed for G2-Lys, which could be due to lower photostability of this compound compared to the other analogues.

A singlet oxygen species generated following PDT illumination has a short half-life and could cover limited diffusion distance in the biological environment.[28] Therefore, different subcellular localization of a photosensitizer is known to produce different mechanisms of PDT-mediated cell toxicity depending on the targeted organelle, and this can affect its overall potency. In this regard, the accumulation of a photosensitizer in the mitochondria and reticulum endoplasm has been found to be more efficient in triggering cell death following PDT as compared to the accumulation in lysosomes. The mitochondrial damage by PDT has been shown to correlate with several cellular events which are associated with apoptosis, namely, rapid loss of mitochondrial membrane potential, cytochrome *c* release, and the activation of cytotoxic caspases.[29] Meanwhile in endoplasmic reticulum, PDT is observed to induce carbonylation of cellular proteins that causes oxidative stress to the organelle and this leads to apoptotic cell death.[30] On the other hand, the photosensitization of the lysosomes can either promote survival or facilitate death of the photodamaged cells. It was observed that lysosomal proteases were photoinactivated by certain photosensitizers and this had led to impaired autophagic processes leading to the survival of cells.[31] However, other studies have shown that lysosomal photodamage also triggers the cathepsin-mediated cleavage of Bid protein that leads to apoptosis via the mitochondrial pathway.[32−34]

In our study, the lipophilic G2 was shown to localize predominantly in the reticulum endoplasma whereas the localization of hydrophilic photosensitizer G2-Asp shifted to the lysosomes, as can be seen in Figure 5. Similar preference for lysosome localization was also reported for chlorin e6 conjugated with aspartyl moiety such as mono-L-aspartyl chlorin e6 (NPe6) and mono-*N*-aspartyl chlorin e6.[10,32] Broadly speaking, the observed subcellular localization of a photosensitizer may be attributed to the lipophilicity and the anionicity of the compound. Photosensitizers which are more lipophilic (e.g., G2) tend to accumulate in cellular compartments which have high lipid bilayer content such as mitochondria and endoplasmic reticulum, and PDT-induced damage to these major organelles is likely to amplify cellular toxicity.[35] In contrast, anionic photosensitizers (e.g., G2-Asp) diffuse poorly across the negatively charged plasma membrane but can be taken up by cells into lysosomes via endocytosis.[36]

To establish the PDT efficacy of G2 analogues in physiological setting, the CAM model and an *in vivo* tumor model in mice were used. CAM is a viable model that has been successfully used to evaluate the PDT-induced vascular occlusion efficacy of photosensitizers, some of which are currently in clinical trials or are already clinically approved.[37] The results from this study showed that both G2 and G2-Asp were able to occlude blood vessels of the CAM following PDT, with G2-Asp achieving similar photodamage compared to G2 ($P < 0.05$) when a higher light dose was used. Meanwhile in the mouse tumor model, G2 and G2-Asp showed similar effectiveness in inhibiting tumor growth although the former is 2-fold more potent *in vitro*. A possible explanation for this observation is that other than direct cell-killing, which may dominate in the G2 treated mice, the observed tumor shrinkage was probably also caused by shutting down of blood vessels servicing the tumor. Since the hydrophilic G2-Asp was able to occlude blood vessels well in the CAM model experiments, this phenomenon may have also positively influenced the treatment outcome in the mice. These findings are consistent with previous studies which reported that tumor regression induced by mono-L-aspartyl chlorin e6, a photosensitizer that closely resembles G2-Asp, resulted from both direct cytotoxicity and antivascular effects.[38,39] It is worth noting that complete tumor regression was observed in 2/8 mice treated with G2-Asp but none in the G2-treated mice.

In conclusion, this study has prepared chemically new derivatives of 15[1]-hydroxypurpurin-7-lactone based on known conjugation chemistry with two hydrophilic amino acids, aspartic acid and lysine. The resultant analogues showed altered photosensitizing potencies and efficacies through changes in multiple parameters including absorption extinction coefficient, singlet oxygen quantum yield, cellular uptake, photostability, and intracellular localization pattern. The conjugated G2-Asp is a promising candidate to develop as a PDT agent because it has ideal photophysical properties such as absorption maxima at far-red wavelength (675 nm) with a relatively high extinction coefficient, and it is able to achieve an antitumor response similar to that of G2 in the preclinical mouse model. Given the hydrophilic nature of G2-Asp, the photosensitizer is also a pharmaceutically advantageous candidate as it can be formulated easily for administration, thereby reducing the risk of aggregation in vascular system.

■ ASSOCIATED CONTENT

Supporting Information

General procedures for spectroscopic measurements, synthesis procedures, and characterization data for G2 analogues. This material is available free of charge via the Internet at http://pubs.acs.org.

AUTHOR INFORMATION

Corresponding Author

*Department of Pharmacy, Faculty of Medicine, University of Malaya, Lembah Pantai, 50603, Kuala Lumpur, Malaysia. E-mail: hongboon.lee@carif.com.my, hongboonlee@um.edu.my.

Notes

The authors declare no competing financial interest.

ACKNOWLEDGMENTS

This work is supported in part by Cancer Research Initiatives Foundation (CARIF) and by MoHE-HIR grants (UM.C/625/1/HIR/MOHE/MED/17 and UM.C/625/1/HIR/MOHE/MED/33) from the Ministry of Higher Education of Malaysia.

REFERENCES

(1) Chee, C. F.; Lee, H. B.; Ong, H. C.; Ho, A. S. Photocytotoxic pheophorbide-related compounds from Aglaonema simplex. *Chem. Biodiversity* **2005**, *2* (12), 1648−55.

(2) Kim, K. K.; Kawano, Y.; Yamazaki, Y. A novel porphyrin photosensitizer from bamboo leaves that induces apoptosis in cancer cell lines. *Anticancer Res.* **2003**, *23* (3B), 2355−61.

(3) Lim, S. H.; Nowak-Sliwinska, P.; Kamarulzaman, F. A.; van den Bergh, H.; Wagnieres, G.; Lee, H. B. The neovessel occlusion efficacy of 15-hydroxypurpurin-7-lactone dimethyl ester induced with photodynamic therapy. *Photochem. Photobiol.* **2010**, *86* (2), 397−402.

(4) Lim, S. H.; Lee, H. B.; Ho, A. S. A new naturally derived photosensitizer and its phototoxicity on head and neck cancer cells. *Photochem. Photobiol.* **2011**, *87* (5), 1152−8.

(5) Sternberg, E. D.; Dolphin, D.; Brückner, C. Porphyrin-based photosensitizers for use in photodynamic therapy. *Tetrahedron* **1998**, *54* (17), 4151−202.

(6) Liang, G.; Wang, L.; Yang, Z.; Koon, H.; Mak, N.; Chang, C. K.; Xu, B. Using enzymatic reactions to enhance the photodynamic therapy effect of porphyrin dityrosine phosphates. *Chem. Commun. (Cambridge)* **2006**, *48*, 5021−3.

(7) Chaloin, L.; Bigey, P.; Loup, C.; Marin, M.; Galeotti, N.; Piechaczyk, M.; Heitz, F.; Meunier, B. Improvement of porphyrin cellular delivery and activity by conjugation to a carrier peptide. *Bioconjugate Chem.* **2001**, *12* (5), 691−700.

(8) Alvarez, M. G.; Prucca, C.; Milanesio, M. E.; Durantini, E. N.; Rivarola, V. Photodynamic activity of a new sensitizer derived from porphyrin-C60 dyad and its biological consequences in a human carcinoma cell line. *Int. J. Biochem. Cell Biol.* **2006**, *38* (12), 2092−101.

(9) Hudson, R.; Carcenac, M.; Smith, K.; Madden, L.; Clarke, O. J.; Pelegrin, A.; Greenman, J.; Boyle, R. W. The development and characterisation of porphyrin isothiocyanate-monoclonal antibody conjugates for photoimmunotherapy. *Br. J. Cancer* **2005**, *92* (8), 1442−9.

(10) Roberts, W. G.; Shiau, F. Y.; Nelson, J. S.; Smith, K. M.; Berns, M. W. In vitro characterization of monoaspartyl chlorin e6 and diaspartyl chlorin e6 for photodynamic therapy. *J. Natl. Cancer Inst.* **1988**, *80* (5), 330−6.

(11) Pandey, R. K.; Jagerovic, N.; Ryan, J. M.; Dougherty, T. J.; Smith, K. M. Efficient syntheses of new classes of regiochemically pure benzoporphyrin derivatives. *Bioorg. Med. Chem. Lett.* **1994**, *3* (12), 2615−8.

(12) Wang, H. M.; Jiang, J. Q.; Xiao, J. H.; Gao, R. L.; Lin, F. Y.; Liu, X. Y. Porphyrin with amino acid moieties: a tumor photosensitizer. *Chem. Biol. Interact.* **2008**, *172* (2), 154−8.

(13) Kwitniewski, M.; Kunikowska, D.; Dera-Tomaszewska, B.; Tokarska-Pietrzak, E.; Dziadziuszko, H.; Graczyk, A.; Glosnicka, R. Influence of diamino acid derivatives of protoporphyrin IX on mouse immunological system: preliminary results. *J. Photochem. Photobiol. B* **2005**, *81* (3), 129−35.

(14) Kwitniewski, M.; Juzeniene, A.; Ma, L. W.; Glosnicka, R.; Graczyk, A.; Moan, J. Diamino acid derivatives of PpIX as potential photosensitizers for photodynamic therapy of squamous cell carcinoma and prostate cancer: in vitro studies. *J. Photochem. Photobiol. B* **2009**, *94* (3), 214−22.

(15) Röder, B.; Hanke, T.; Oelckers, S.; Hackbarth, S.; Symietz, C. Photophysical properties of pheophorbide a in solution and in model membrane systems. *J. Porphyrins Phthalocyanines* **2000**, *4* (1), 37−44.

(16) Hackbarth, S.; Horneffer, V.; Wiehe, A.; Hillenkamp, F.; Röder, B. Photophysical properties of pheophorbide-a-substituted diaminobutane poly-propylene-imine dendrimer. *Chem. Phys.* **2001**, *269*, 339−46.

(17) Lim, S. H.; Thivierge, C.; Nowak-Sliwinska, P.; Han, J.; van den Bergh, H.; Wagnieres, G.; Burgess, K.; Lee, H. B. In vitro and in vivo photocytotoxicity of boron dipyrromethene derivatives for photodynamic therapy. *J. Med. Chem.* **2010**, *53* (7), 2865−74.

(18) Lange, N.; Ballini, J. P.; Wagnieres, G.; van den Bergh, H. A new drug-screening procedure for photosensitizing agents used in photodynamic therapy for CNV. *Invest. Ophthalmol. Visual Sci.* **2001**, *42* (1), 38−46.

(19) Kessel, D. Properties of Cremophor EL micelles probed by fluorescence. *Photochem. Photobiol.* **1992**, *56* (4), 447−51.

(20) Wenzel, J.; Zeisig, R.; Fichtner, I. Inhibition of metastasis in a murine 4T1 breast cancer model by liposomes preventing tumor cell-platelet interactions. *Clin. Exp. Metastasis* **2010**, *27* (1), 25−34.

(21) Serra, V. V.; Zamarron, A.; Faustino, M. A.; Cruz, M. C.; Blazquez, A.; Rodrigues, J. M.; Neves, M. G.; Cavaleiro, J. A.; Juarranz, A.; Sanz-Rodriguez, F. New porphyrin amino acid conjugates: synthesis and photodynamic effect in human epithelial cells. *Bioorg. Med. Chem.* **2010**, *18* (16), 6170−8.

(22) Castano, A. P.; Demidova, T. N.; Hamblin, M. R. Mechanisms in photodynamic therapy: part one - photosensitizers, photochemistry and cellular localization. *Photodiagn. Photodyn. Ther.* **2004**, *1*, 279−93.

(23) Allison, R. R.; Sibata, C. H. Oncologic photodynamic therapy photosensitizers: a clinical review. *Photodiagn. Photodyn. Ther.* **2010**, *7* (2), 61−75.

(24) Garland, M. J.; Cassidy, C. M.; Woolfson, D.; Donnelly, R. F. Designing photosensitizers for photodynamic therapy: strategies, challenges and promising developments. *Future Med. Chem.* **2009**, *1* (4), 667−91.

(25) Margaron, P.; Gregoire, M. J.; Scasnar, V.; Ali, H.; van Lier, J. E. Structure-photodynamic activity relationships of a series of 4-substituted zinc phthalocyanines. *Photochem. Photobiol.* **1996**, *63* (2), 217−23.

(26) Huang, D. P.; Ho, J. H.; Poon, Y. F.; Chew, E. C.; Saw, D.; Lui, M.; Li, C. L.; Mak, L. S.; Lai, S. H.; Lau, W. H. Establishment of a cell line (NPC/HK1) from a differentiated squamous carcinoma of the nasopharynx. *Int. J. Cancer* **1980**, *26* (2), 127−32.

(27) Huang, Y. Y.; Mroz, P.; Zhiyentayev, T.; Sharma, S. K.; Balasubramanian, T.; Ruzie, C.; Krayer, M.; Fan, D.; Borbas, K. E.; Yang, E.; Kee, H. L.; Kirmaier, C.; Diers, J. R.; Bocian, D. F.; Holten, D.; Lindsey, J. S.; Hamblin, M. R. In vitro photodynamic therapy and quantitative structure-activity relationship studies with stable synthetic near-infrared-absorbing bacteriochlorin photosensitizers. *J. Med. Chem.* **2010**, *53* (10), 4018−27.

(28) Moan, J.; Berg, K. The photodegradation of porphyrins in cells can be used to estimate the lifetime of singlet oxygen. *Photochem. Photobiol.* **1991**, *53* (4), 549−53.

(29) Morgan, J.; Oseroff, A. R. Mitochondria-based photodynamic anti-cancer therapy. *Adv. Drug Delivery Rev.* **2001**, *49* (1−2), 71−86.

(30) Szokalska, A.; Makowski, M.; Nowis, D.; Wilczynski, G. M.; Kujawa, M.; Wojcik, C.; Mlynarczuk-Bialy, I.; Salwa, P.; Bil, J.; Janowska, S.; Agostinis, P.; Verfaillie, T.; Bugajski, M.; Gietka, J.; Issat, T.; Glodkowska, E.; Mrowka, P.; Stoklosa, T.; Hamblin, M. R.; Mroz, P.; Jakobisiak, M.; Golab, J. Proteasome inhibition potentiates antitumor effects of photodynamic therapy in mice through induction of endoplasmic reticulum stress and unfolded protein response. *Cancer Res.* **2009**, *69* (10), 4235−43.

(31) Reiners, J. J., Jr.; Agostinis, P.; Berg, K.; Oleinick, N. L.; Kessel, D. Assessing autophagy in the context of photodynamic therapy. *Autophagy* **2010**, *6* (1), 7−18.

(32) Reiners, J. J., Jr.; Caruso, J. A.; Mathieu, P.; Chelladurai, B.; Yin, X. M.; Kessel, D. Release of cytochrome c and activation of pro-caspase-9 following lysosomal photodamage involves Bid cleavage. *Cell Death Differ.* **2002**, *9* (9), 934−44.
(33) Wan, Q.; Liu, L.; Xing, D.; Chen, Q. Bid Is Required in NPe6-PDT-induced Apoptosis. *Photochem. Photobiol.* **2008**, *84* (1), 250−7.
(34) Chiu, S. M.; Xue, L. Y.; Lam, M.; Rodriguez, M. E.; Zhang, P.; Kenney, M. E.; Nieminen, A. L.; Oleinick, N. L. A requirement for bid for induction of apoptosis by photodynamic therapy with a lysosome- but not a mitochondrion-targeted photosensitizer. *Photochem. Photobiol.* **2010**, *86* (5), 1161−73.
(35) Kessel, D.; Reiners, J. J., Jr. Apoptosis and autophagy after mitochondrial or endoplasmic reticulum photodamage. *Photochem. Photobiol.* **2007**, *83* (5), 1024−8.
(36) Rosenkranz, A. A.; Jans, D. A.; Sobolev, A. S. Targeted intracellular delivery of photosensitizers to enhance photodynamic efficiency. *Immunol. Cell Biol.* **2000**, *78* (4), 452−64.
(37) Hammer-Wilson, M. J.; Cao, D.; Kimel, S.; Berns, M. W. Photodynamic parameters in the chick chorioallantoic membrane (CAM) bioassay for photosensitizers administered intraperitoneally (IP) into the chick embryo. *Photochem. Photobiol. Sci.* **2002**, *1* (9), 721−8.
(38) McMahon, K. S.; Wieman, T. J.; Moore, P. H.; Fingar, V. H. Effects of photodynamic therapy using mono-L-aspartyl chlorin e6 on vessel constriction, vessel leakage, and tumor response. *Cancer Res.* **1994**, *54* (20), 5374−9.
(39) Saito, K.; Mikuniya, N.; Aizawa, K. Effects of Photodynamic Therapy Using Mono-l-aspartyl Chlorin e6 on Vessels and Its Contribution to the Antitumor Effect. *Cancer Sci.* **2000**, *91* (5), 560−5.

Supporting Information

Photodynamic characterisation of amino acids conjugated 15[1]-hydroxypurpurin-7-lactone for cancer treatment

Siang Hui Lim[1,3], Mun Li Yam[1], May Lynn Lam[1], Fadzly Azhar Kamarulzaman[1], Norazwana Samat[1], Lik Voon Kiew[2], Lip Yong Chung[3], Hong Boon Lee[1,3*].

[1]Cancer Research Initiatives Foundation (CARIF), Sime Darby Medical Centre, Subang Jaya, Selangor, Malaysia. [2]Department of Pharmacology, Faculty of Medicine, University Malaya, Kuala Lumpur, Malaysia. [3]Department of Pharmacy, Faculty of Medicine, University Malaya, Kuala Lumpur, Malaysia.

*Corresponding author e-mail: hongboon.lee@carif.com.my; hongboonlee@um.edu.my (Hong Boon Lee)

1. Semi-synthesis and Spectroscopic Data for G2, G2 acid, G2-Asp and G2-Lys

General

Solvents (AR and HPLC grade) for purification of compounds were used as supplied by Merck. TLC was peformed on silica gel 60 F_{254} (Merck) precoated plastic sheets (20x 20 cm). Silica gel 60 (70-230 mesh, Merck) was used for column chromatography. ^{1}H-NMR spectra were recorded on Varian Unity INOVA 500 (500 MHz) spectrometer. Chemical shifts (δ) were reported in ppm relative to chloroform-*d* ($CDCl_3$) (7.26 ppm) or tetra methyl saline (TMS) (0.00 ppm). Coupling constant (*J*) were reported in Hertz and s, d, t, q, m and br refer to singlet, doublet, triplet, quartet, multiplet and broad respectively. The high-resolution mass spectrometry (HRMS) was performed using Waters UPLC system (model Acquity) coupled to Synapt High Definition Mass Spectrometer (HDMS). Analytical HPLC was performed using Shimadzu pump (model LC-10 AT) equipped with a photodiode array detector (PDA, Shimadzu model SPD-20AT *vp*) and a C-18 Chromolith (4.6x 100 mm, Merck) column.

Preparation of 15^1-hydroxypurpurin-7-lactone phytyl methyl ester (G2-Phytyl) from Spirulina extract[1]

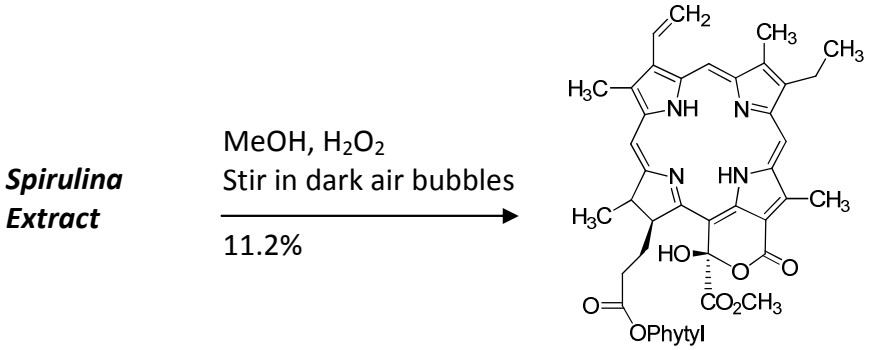

G2-Phytyl

Pigment was extracted from *S. Pacifica* (5g) dry powder with acetone (100 ml) according to literature procedure.[2] 350 mg of the acetone extract dissolved in 20 ml of MeOH was added 20 ml of H_2O_2 and 3 ml of H_2O. The mixture solution was refluxed overnight in the dark with a constant stream of air bubbles and a vigorously stirring magnetic stirrer. Three major spots were detected by TLC which co-eluted with pure pheophytin-*a*, hydroxypheophytin-*a* and G2-Phytyl

standard compounds (R_f = 0.47, 0.38 and 0.35 respectively). The reaction mixture was purified using silica gel column chromatography eluting with increasing polar mixtures of hexane and acetone to yield 39.2 mg of G2-Phytyl, which was used for subsequent reactions without further spectroscopic analyses.

Synthesis of 15[1]-hydroxypurpurin-7-lactone dimethyl ester (G2)[3-5]

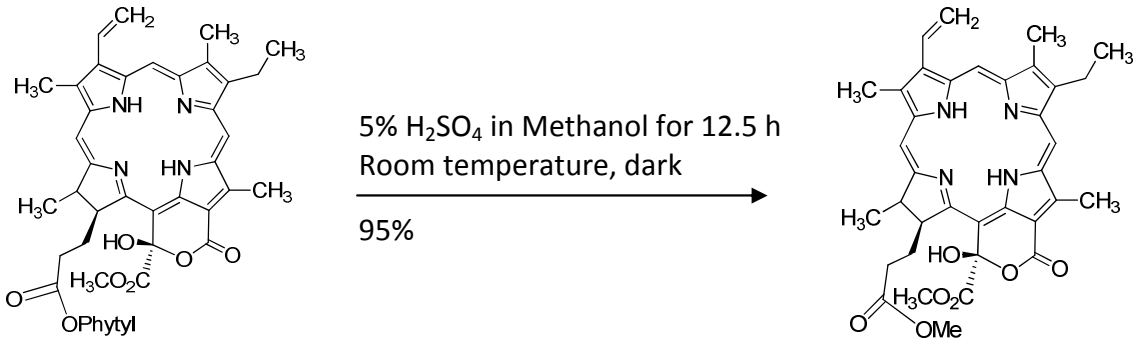

G2-Phytyl **G2**

15[1]-hydroxypurpurin-7-lactone phytyl methyl ester (G2-Phytyl, 50 mg, 0.05 mol) was treated with 5% sulphuric acid in methanol for 12.5 hours at room temperature while protected from light. The reaction mixture was diluted with dichloromethane, washed with water and then 10% saturated sodium bicarbonate. The aqueous layer was dried over sodium sulphate, filtered and then evaporated. Recrystalization of the residue from dichloromethane and methanol gave 36.43 mg of the title product ($C_{36}H_{38}N_4O_7$; 95% yield). UV- vis (acetone): λ_{max} nm 401, 665. ^{1}H-NMR ($CDCl_3$, 400MHz): δ 9.71 (1H, s, 10-H), 9.53 (1H, s, 5-H), 8.71 (1H, s, 20-H), 8.01 (1H, dd, J = 17.8 and 11.5 Hz, 3^1-H), 6.28 (1H, d, J = 18.0, 3^2-H_{cis}) 6.18 (1H, d, J = 11, 3^2-H_{trans}), 4.44 (1H, m, 17-H), 4.08 (1H, m, 18-H), 3.67 (2H, q, 8^1-H_2), 3.75 (3H, s, 15^1-H_3), 3.52 (3H, s, 12^1-H_3), 3.41 (3H, s, 2^1-H_3), 3.22 (3H, s, 7^1-H_3), 3.87 (3H, s, 17^3-H_3), 2.15 - 2.25 (2H, m, 17^1-H_2), 2.40 - 2.60 (2H, m, 17^2-H_2), 1.59 (3H, d, J = 7, 18^1-H_3), 1.68 (3H, t, 8^2-H_3). LCMS (ESI): *m/z* found 639.2813 (error 0.9ppm) calcd for $C_{36}H_{38}N_4O_7$: MH^+ 639.2819

1 **(a) UV chromatogram (b) Total ion chromatogram**

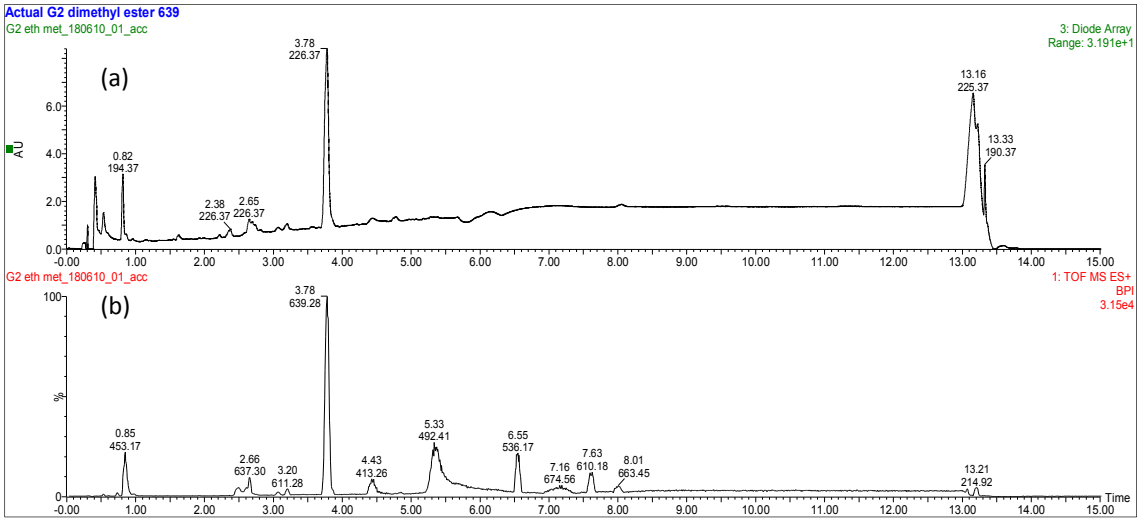

2 **(a) UV spectrum (b) Mass spectrum**

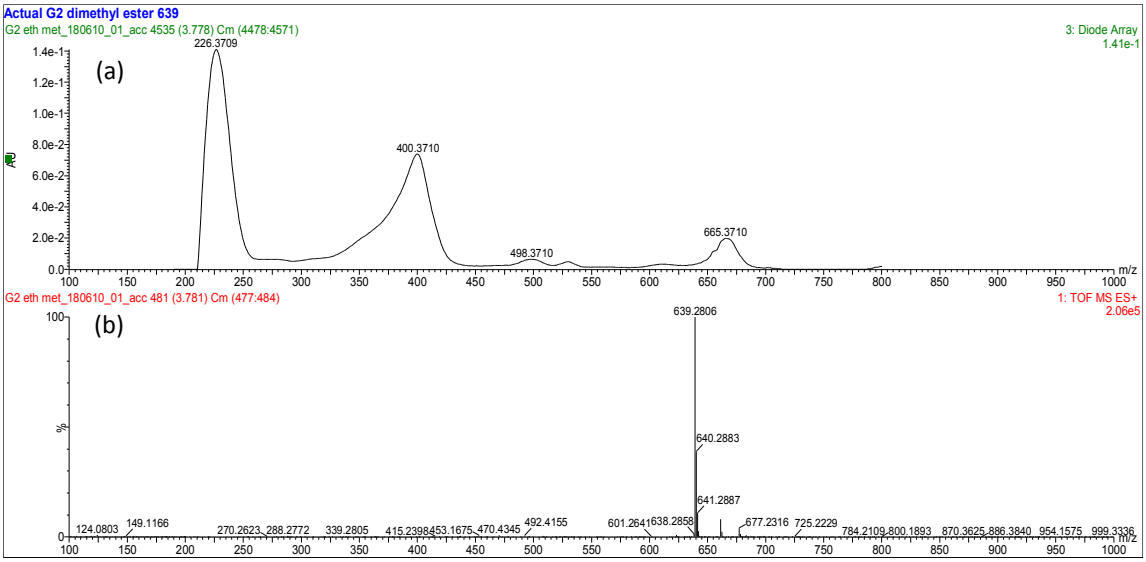

Synthesis of 15[1]-hydroxypurpurin-7-lactone methyl ester (G2 acid)[5]

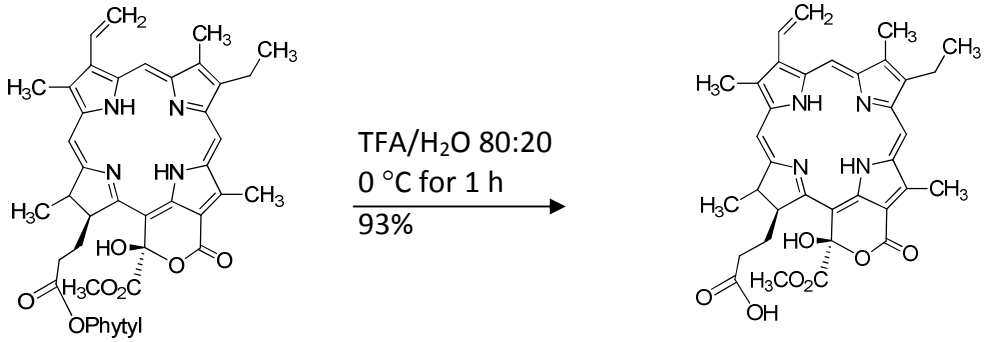

G2-Phytyll **G2 acid**

15^1-hydroxypurpurin-7-lactone dimethyl ester phytyl (G2-Phytyl, 208 mg, 0.23 mol) was selectively hydrolysed to the 17^3 carboxylic acid without affecting the 13^1 carbomethoxy group via the Wasielewski and Svec procedure which requires stirring pheophytin-*a* in 75 ml of degassed TFA/H_2O 80:20 at 0 °C for 1 h. The reaction mixture was poured in 100 ml of H_2O and partitioned with an equal amount of dichloromethane. The organic layer was purified with PTLC using 1:1:0.1% Hexane / Acetone / Acetic acid solvent system to yield 133mg of G2 acid ($C_{35}H_{36}N_4O_7$, 93% yield)

3 (a) UV chromatogram (b) Mass chromatogram

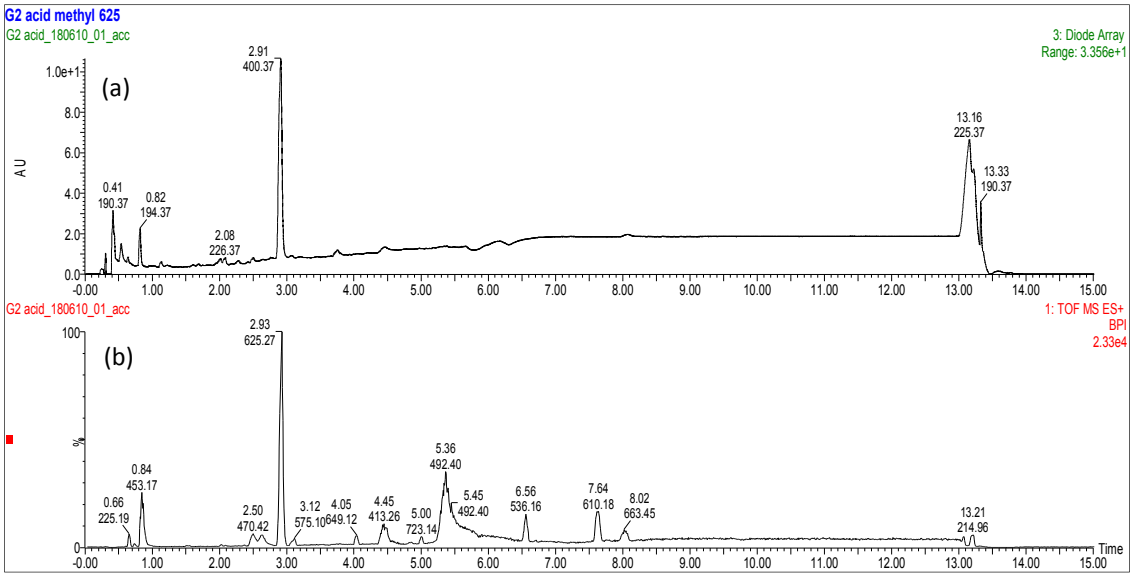

4 (a) UV spectrum (b) Mass spectrum

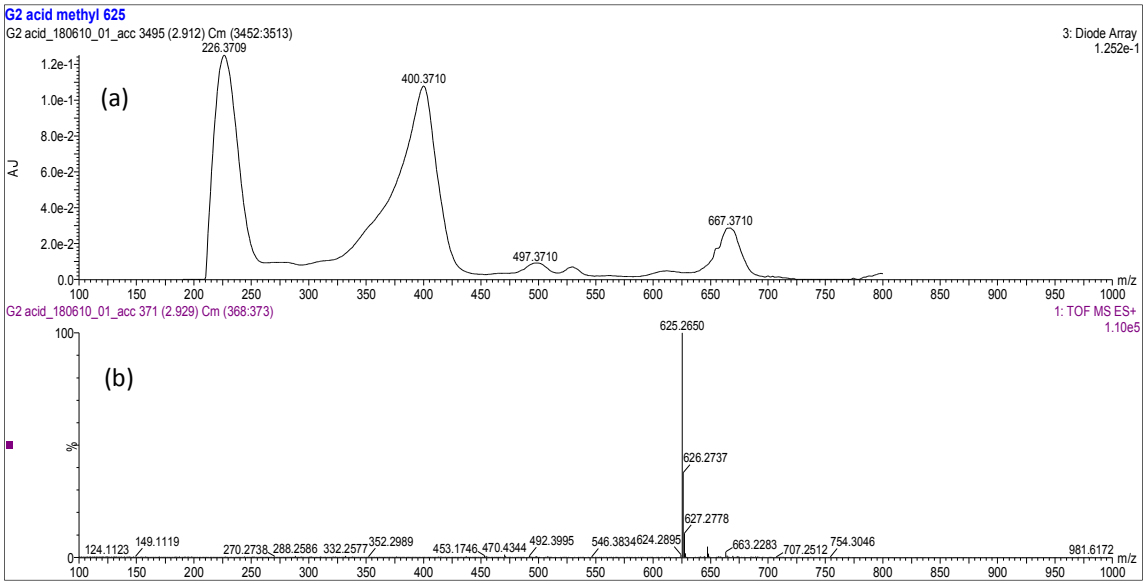

Synthesis of aspartyl-15[1]-hydroxypurpurin-7-lactone methyl ester (G2-Asp)[5]

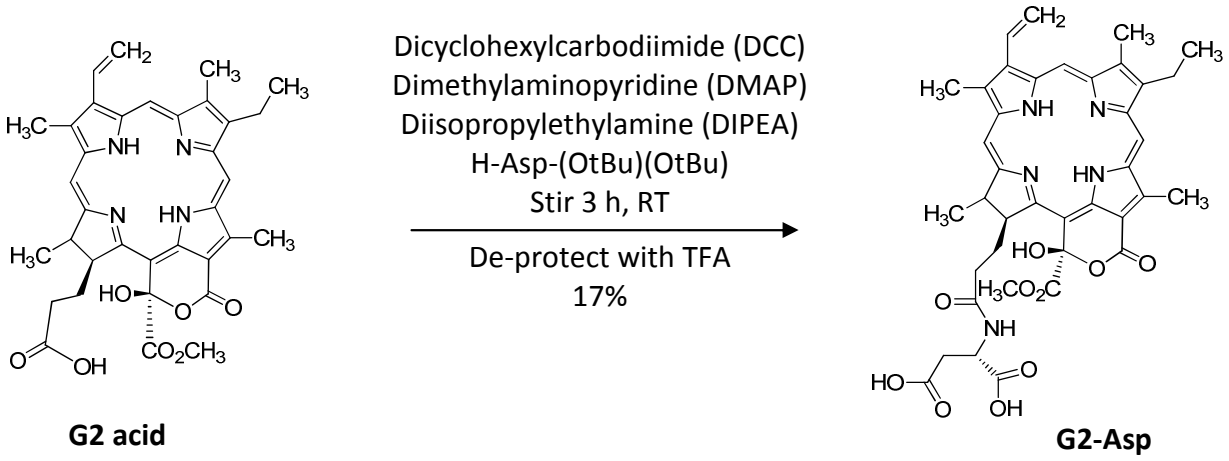

G2 acid **G2-Asp**

15[1]-hydroxypurpurin-7-lactone methyl ester (G2 acid, 67 mg, 0.11 mmol) was dissolve in a 40 ml solution containing DCC (24.2 mg, 0.11 mmol) and DMAP (14.1 mg, 0.11mmol) in dry $CHCl_2$. H-Asp-(OtBu)(OtBu) (31.7 mg, 0.11 mmol) and excess DIPEA (50 µl) was added into 40 ml of dry $CHCl_2$. Both solutions were allowed to dissolve separately by stirring for 10 minutes. After that both solutions were combined and the reaction mixture was stirred for 3 hours. The reaction mixture was washed with water and brine, dried over sodium sulphate and purified using PTLC (60:40 Hex / Acetone) solvent system. The purified compound was dissolved in cold acetonitrile and filtered. This step was repeated twice to remove DCC which precipitates in acetonitrile. Evaporation of acetonitrile gave 11.4 mg (17 %) of protected G2-Asp. The protecting group (OtBu) (16.6 mg) was deprotected by stirring with 10 ml of 1:1 DCM/TFA for 2 hours. 100 ml of H_2O was poured into the reaction mixture and then partitioned with an equal amount of dichloromethane. The organic layer was collected and was dried using rotary evaporator. 13 mg (92.5%) of G2-Asp ($C_{39}H_{41}N_5O_{10}$) was obtained. UV- vis (acetone): λ_{max} nm 400, 666. ^{1}H-NMR ($CDCl_3$, 400MHz): δ 9.75 (1H, s, 10-H), 9.50 (1H, s, 5-H), 8.90 (1H, s, 20-H), 8.05 (1H, dd, J = 18 and 12 Hz, 3^1-H), 6.35 (1H, d, J = 18.0, 3^2-H$_{cis}$) 6.15 (1H, d, J = 11, 3^2-H$_{trans}$), 3.70 (2H, q, 8^1-H$_2$), 3.81 (3H, s, 15^1-H$_3$), 3.72 (3H, s, 12^1-H$_3$), 3.39 (3H, s, 2^1-H$_3$), 3.15 (3H, s, 7^1-H$_3$), 1.27 (3H, d, J = 7, 18^1-H$_3$), 1.65 (3H, t, 8^2-H$_3$) for the chlorine skeleton and 4.76 (1H, ddd), 2.78 (2H, dd) for aspartyl side chain. LCMS (ESI): m/z found 740.2878

(error 7.3 ppm) calcd for $C_{39}H_{41}N_5O_{10}$: MH^+ 740.2932 . MS-MS: 722, 663, 646, 462, 530, **501***, 465, 421

5 (a) UV chromatogram (b) Mass chromatogram

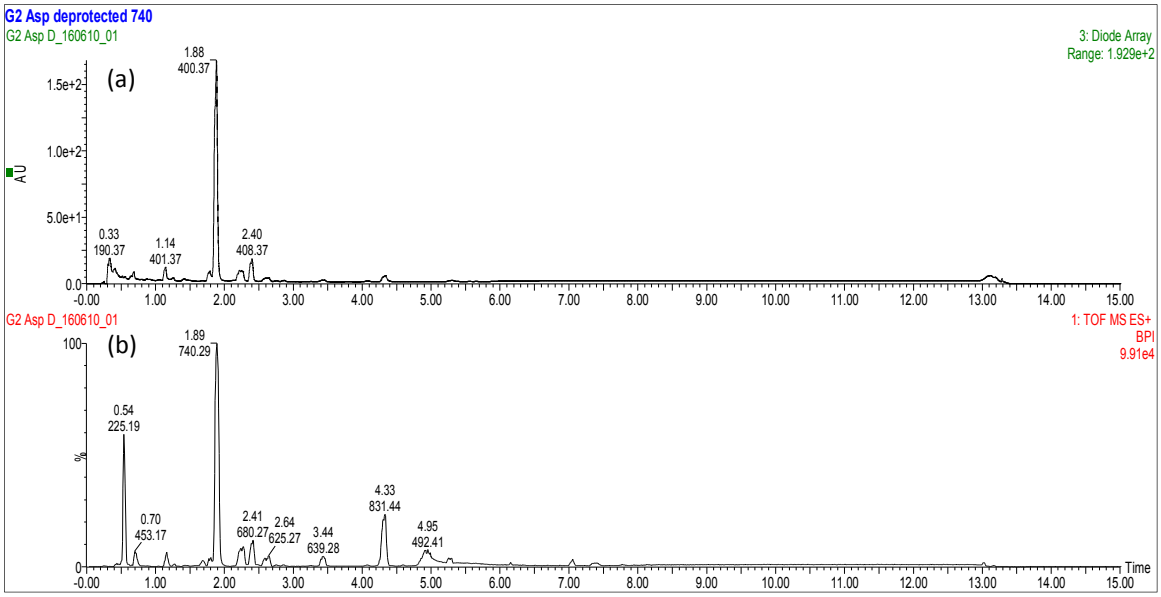

6 (a) UV spectrum (b) Mass spectrum

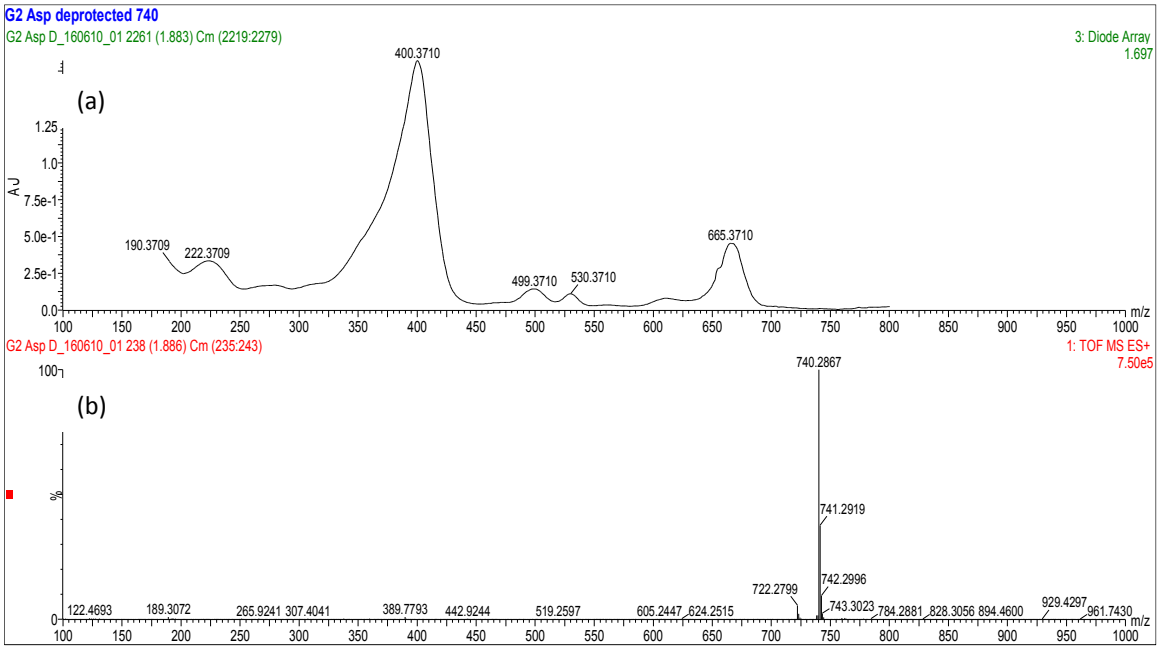

Synthesis of lysyl-15[1]-hydroxypurpurin-7-lactone methyl ester (G2-Lys)[5]

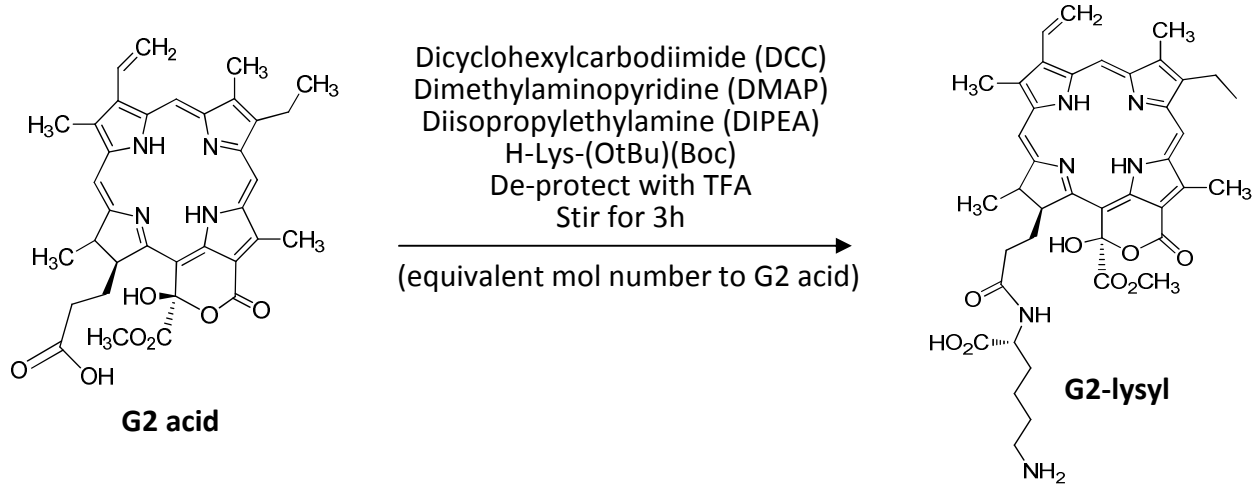

15[1]-hydroxypurpurin-7-lactone methyl ester (G2 acid, 94 mg, 0.15 mmol) was dissolve in a 50 ml solution containing DCC (32.9, 0.15mmol) and DMAP (20.7 mg, 0.15 mmol) in dry $CHCl_2$. H-Lys-(OtBu)(Boc) (50.7 mg,0.15 mmol) and excess DIPEA (19.4mg, 0.15 mmol, 65 µl) was added into 50 ml of dry $CHCl_2$. Both solutions were allowed to dissolve separately by stirring for 10 minutes. After that both solutions were combined and the reaction mixture was stirred for 3 hours, washed with water and brine, dried over sodium sulphate and purified using PTLC (60:40 Hex/Acetone) solvent system. The purified compound was dissolved in cold acetonitrile and filtered. This step was repeated twice to remove DCC which precipitates in acetonitrile. Evaporation of acetonitrile gave 18.5 mg (yield 13 %) of G2-Lys ($C_{50}H_{64}N_6O_{10}$). The protecting groups (OtBu) and (Boc) were removed by stirring with 10 ml 1:1 DCM/TFA for 4 hours. 100 ml of H_2O was poured into the reaction mixture and then partitioned with an equal amount of dichloromethane. The aqueous layer was collected and freeze-dried. UV- vis (acetone): λ_{max} nm 400, 666. ^{1}H-NMR ($CDCl_3$, 400MHz): δ 9.84 (1H, s, 10-H), 9.58 (1H, s, 5-H), 8.93 (1H, s, 20-H), 8.12 (1H, dd, J = 18 and 12 Hz, 3^1-H), 6.40 (1H, d, J = 18.0, 3^2-H_{cis}) 6.22 (1H, d, J = 11, 3^2-H_{trans}), 3.80 (2H, q, 8^1-H_2), 3.85 (3H, s, 15^1-H_3), 3.71 (3H, s, 12^1-H_3), 3.40 (3H, s, 2^1-H_3), 3.12 (3H, s, 7^1-H_3), 1.70 (3H, d, J = 7, 18^1-H_3), 1.70 (3H, t, 8^2-H_3) for the chlorine skeleton and 6.10 (1H, d, H-NH_a), 4.60 (1H, t, H-NH_b), 4.33 (1H, m, a1-H), 2.80 (1H, m, a5-H), 1.75 (1H, m, a2-H), 1.70 (1H, m, a4-H), 1.50 (1H, m, a4-H) for the lysyl side chain. LCMS (ESI): m/z found 753.3643 (error 1.46 ppm) calcd for $C_{41}H_{48}N_6O_8$: MH^+ 753.3612.

8 (a) UV chromatogram (b) Total ion chromatogram

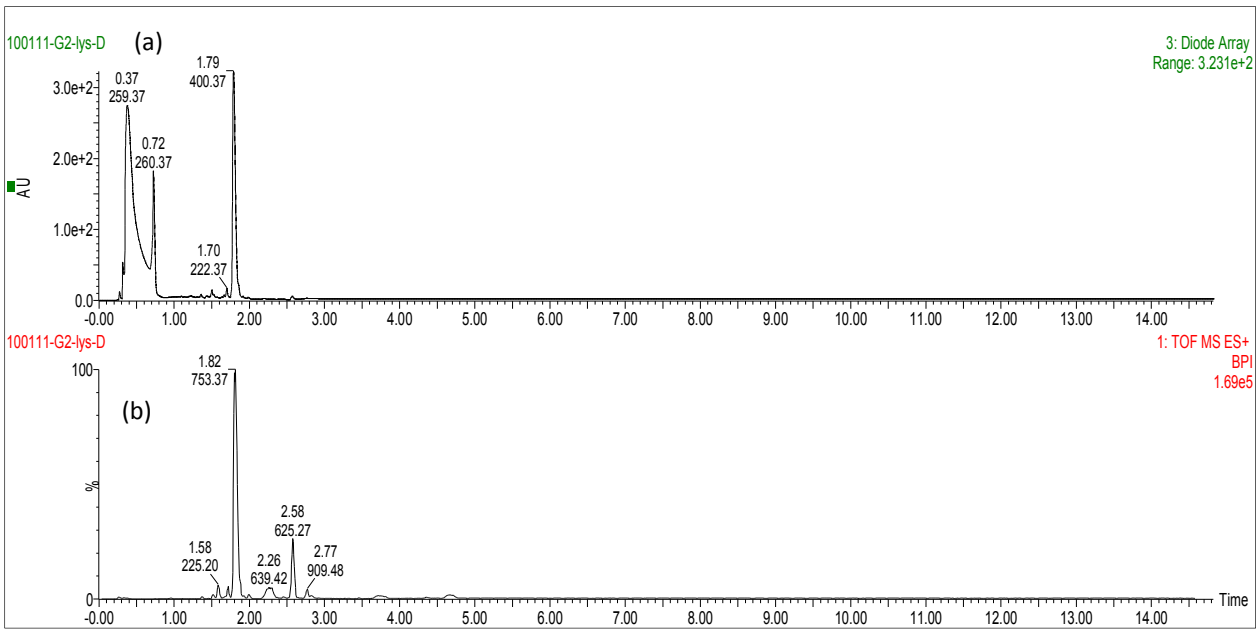

7 (a) UV spectrum (b) Mass spectrum

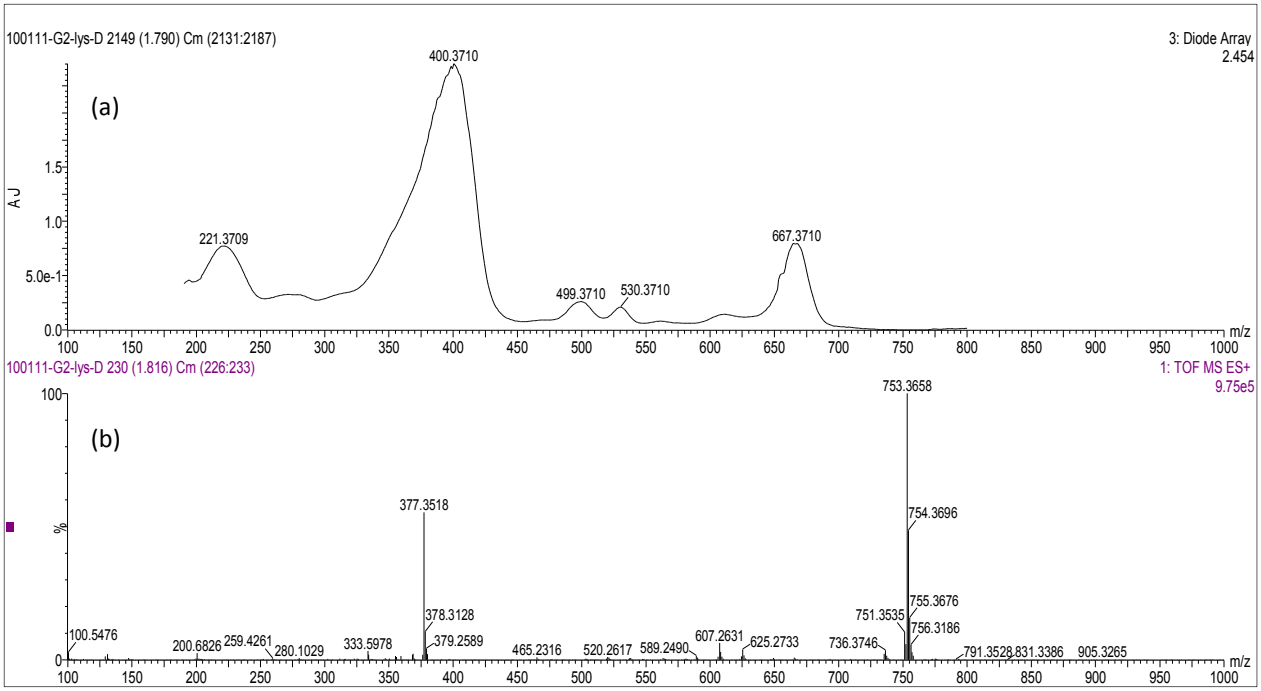

2. Figure S1: Photophysical properties of G2 analogues at 10 μM in ethanol

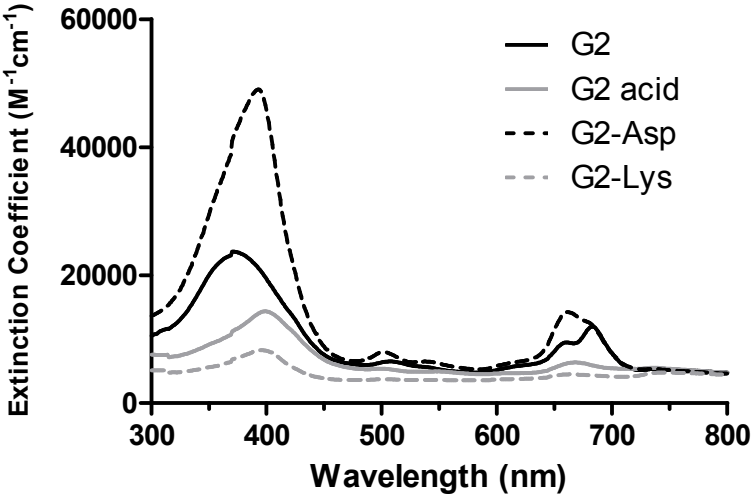

Reference

1. Woolley, P. S.; Andrea, M. J.; Ronald, H. E.; Brendan, K. J. A comparative study of the allomerization reaction of chlorophyll a and bacteriochlorophyll a. *Journal of the Chemical Society, Perkin Transactions 2* **1998**, (8), 1833-1840.
2. Hargus, J. A.; Fronczek, F. R.; Vicente, M. G.; Smith, K. M. Mono-(L)-aspartylchlorin-e6. *Photochem Photobiol* **2007,** *83*, (5), 1006-15.
3. Kozyrev, A. N.; Chen, Y.; Goswami, L. N.; Tabaczynski, W. A.; Pandey, R. K. Characterization of porphyrins, chlorins, and bacteriochlorins formed via allomerization of bacteriochlorophyll a. Synthesis of highly stable bacteriopurpurinimides and their metal complexes. *J Org Chem* **2006,** *71*, (5), 1949-60.
4. Ma, L.; Dolphin, D. Stereoselective Synthesis of New Chlorophyll a Related Antioxidants Isolated from Marine Organisms. *J Org Chem* **1996,** *61*, (7), 2501-2510.
5. Sternberg, E. D.; Dolphin, D.; Brückner, C. Porphyrin-based photosensitizers for use in photodynamic therapy. *Tetrahedron* **1998,** *54*, (17), 4151-202.

OPEN ACCESS Freely available online

PLOS ONE

Rosamines Targeting the Cancer Oxidative Phosphorylation Pathway

Siang Hui Lim[1,2], Liangxing Wu[3], Lik Voon Kiew[4], Lip Yong Chung[2], Kevin Burgess[3], Hong Boon Lee[1]*

1 Drug Discovery Laboratory, Cancer Research Initiatives Foundation (CARIF), Subang Jaya, Selangor, Malaysia, **2** Department of Pharmacy, University of Malaya, Kuala Lumpur, Malaysia, **3** Department of Chemistry, Texas A & M University, College Station, Texas, United States of America, **4** Department of Pharmacology, Faculty of Medicine, University of Malaya, Kuala Lumpur, Malaysia

Abstract

Reprogramming of energy metabolism is pivotal to cancer, so mitochondria are potential targets for anticancer therapy. A prior study has demonstrated the anti-proliferative activity of a new class of mitochondria-targeting rosamines. This present study describes *in vitro* cytotoxicity of second-generation rosamine analogs, their mode of action, and their *in vivo* efficacies in a tumor allografted mouse model. Here, we showed that these compounds exhibited potent cytotoxicity (average $IC_{50}<0.5$ μM), inhibited Complex II and ATP synthase activities of the mitochondrial oxidative phosphorylation pathway and induced loss of mitochondrial transmembrane potential. A NCI-60 cell lines screen further indicated that rosamine analogs **4** and **5** exhibited potent antiproliferative effects with $Log_{10}GI_{50}=-7$ ($GI_{50}=0.1$ μM) and were more effective against a colorectal cancer sub-panel than other cell lines. Preliminary *in vivo* studies on 4T1 murine breast cancer-bearing female BALB/c mice indicated that treatment with analog **5** in a single dosing of 5 mg/kg or a schedule dosing of 3 mg/kg once every 2 days for 6 times (q2d×6) exhibited only minimal induction of tumor growth delay. Our results suggest that rosamine analogs may be further developed as mitochondrial targeting agents. Without a doubt proper strategies need to be devised to enhance tumor uptake of rosamines, i.e. by integration to carrier molecules for better therapeutic outcome.

Citation: Lim SH, Wu L, Kiew LV, Chung LY, Burgess K, et al. (2014) Rosamines Targeting the Cancer Oxidative Phosphorylation Pathway. PLoS ONE 9(3): e82934. doi:10.1371/journal.pone.0082934

Editor: Siyaram Pandey, University of Windsor, Canada

Received June 13, 2013; **Accepted** October 30, 2013; **Published** March 12, 2014

Funding: This work was supported by grants from Cancer Research Initiatives Foundation, Malaysia Ministry of Higher Education's HIR-MOHE grants (UM.C/625/1/HIR/MOHE/MED/17 and UM.C/625/1/HIR/MOHE/MED/33), Universiti Malaya Post Graduate Research Grant (PS204/2010B), and by grants to KB from The National Institutes of Health (GM087981) and The Robert A. Welch Foundation (A-1121). The funders had no role in study design, data collection and analysis, decision to publish, or preparation of the manuscript.

Competing Interests: The authors have declared that no competing interests exist.

* E-mail: hongboon.lee@carif.com.my

Introduction

Conventional cancer chemotherapy depends on drugs that act by interrupting DNA replication, i.e. by inhibiting the synthesis or function of new nucleic materials, or by causing irreparable damage to vital nucleic acids through intercalation, alkylation or enzymatic inhibition. Lack of selectivity for neoplastic cells exhibited by these drugs typically limits their success as treatment agents. Contemporary chemotherapeutic strategies that target signaling pathways or particular gene products tend to be limited to cancers driven by a dominant oncogene and are often vulnerable to resistance via the multiplicity of tumorigenesis signaling pathways [1]. For example, most of the HER-2 positive metastatic breast cancer patients who initially responded to treatment with trastuzumab develop secondary trastuzumab resistance within a year after the treatment began [2]. Similar observations have been made for BRAF-targeted vemurafenib for melanoma therapy [3] and EGFR-targeted gefitinib or erlotinib for the treatment of non-small cell lung cancer [4].

A relatively new alternative to targeting DNA and enzymes in rapidly proliferating cells, or specific signaling pathways is to focus on organelles like the mitochondria. Mitochondria are the energy generators that maintain cell life and essential cell functions, including multiple signaling cascades that regulate cells, for instance, metabolism, cell cycle control, development, and cell death [5]. In cancer chemotherapy, mitochondria-targeting drugs interfere with cancer cell metabolisms by pertubing the mitochondrial transmembrane potential, inhibiting the electron redox chain complexes, interfering the mitochondria transmembrane permeability, and targeting mitochondrial-DNA [6,7]. The most common types of mitochondria-targeting drugs are lipophilic, cationic drugs; these are selective for cancer cells because they tend to have higher mitochondrial membrane potentials than normal epithelial cells [8,9].

We have previously reported structure-activity relationships (SARs) for the anticancer properties of a series of rosamines (Fig. 1A) [10,11]. These compounds are delocalized lipophilic cations (DLC) with peripheral cyclic amines and various groups at the *meso* position; the majority of these cations are substantially more potent than rhodamine-123 which is a well-studied delocalized lipophilic cation. Consistence with this, SAR data for the rosamines suggested good potencies correlated with hydrophobic cyclic amines and *meso*-aryl substituents. Thiofuryl and 4-iodophenyl *meso* substitution corresponded to approximately 5-fold improvement in potency compared to phenyl substitution. Additionally, the data indicated that significantly lower IC_{50} values were obtained for unsymmetrical compounds (X^1 not same as X^2), but the combination of unsymmetrical amine substituents with thiofuryl and 4-iodophenyl *meso* substitution was not explored. Intracellular imaging on representative examples indicated these

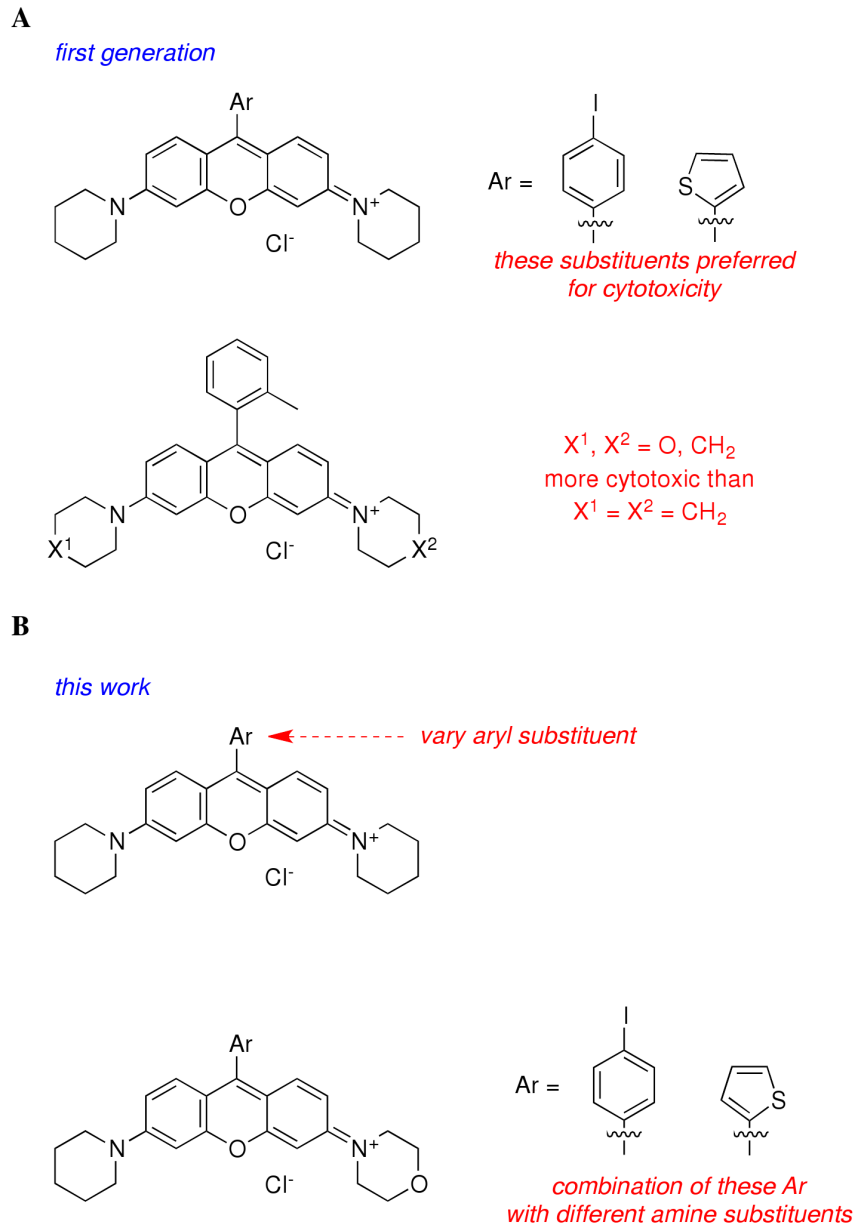

Figure 1. Structural variations of rosamine. (A) of the rosamine dyes variously functionalized at the *meso* position as previously reported by Lim et al. (Anticancer Drugs 2009, 20: 461–468), the ones shown here with *meso*- thiofuran or 4-iodophenyl had superior anticancer activities in cellular assays. (B) Second-generation targets featured in this work.
doi:10.1371/journal.pone.0082934.g001

compounds accumulate in the mitochondria. These compounds (i.e rosamine **2** and **5**) are also found to be more cytotoxic against cancer cells compared with immortalized normal epithelial cells of the same organ type [10].

The research reported here was undertaken to probe how two molecular modifications affect cytotoxicities in this series: (i) replacement of *para*-iodo or thiofuran groups with other *para*-halide or furan groups; and, (ii) combination of thiofuryl and 4-iodophenyl *meso* substitution with piperidine/morpholine combinations. Thus we report syntheses of second generation rosamines (Fig. 1B) and their cytotoxicities relative to a panel of solid tumor cell lines. Compounds with promising activity were further evaluated in the NCI-60 human tumor cell lines screen. Selected rosamines were also examined for their effect on cellular redox systems and for effects in an *in vivo* tumor model.

Materials and Methods

Ethics Statement

All animal experiments were conducted in accordance with protocols reviewed and approved by Dr. Haji Azizuddin Bin Haji Kamaruddin, Laboratory Animal Centre (LAC) Animal Care and Use Committee of Faculty of Medicine, University of Malaya (reference number FAR/14/07/2010/LSH). Female BALB/c mice aged between 6–8 weeks with a minimum weight of 17 g were maintained in a controlled environment of 12 h light-dark cycles with free access to food (standard pellet diet purchased from

Altromin International, Lage, Germany) and purified water. Female mice were used because the hormonal environment essential for development of implanted 4TI mouse mammary carcinoma would be present.

Materials

Minimum essential medium with Earl's salt and L-glutamine, RPMI 1640 medium with L-glutamine, fetal bovine serum, Pen-Strep (10 000 U/ml penicillin, 10 mg/ml streptomycin), trypsin 10× were supplied by GIBCO, Invitrogen (Auckland, New Zealand). JC-1 was purchased from Molecular Probes, Invitrogen (Oregon, USA). Dimethyl sulfoxide (DMSO), hydrochloric acid 37%, polyethylene glycol 400 (PEG 400) and 2-propanol were purchased from Merck (Hohenbrunn, Germany). Ethylene glycol-*bis*(aminoethylether)-*tetra*-acetic acid (EGTA), ethylenediaminetetraacetic acid (EDTA), 3-(*N*-morpholino)propanesulfonic acid (MOPS), potassium chloride, potassium dihydrogen orthophosphate, sodium chloride, sodium hydrogen carbonate, disodium hydrogen orthophosphate anhydrous, sucrose and Tris were purchased Fisher Scientific (Leicestershire, UK). Thiazoyl blue tetrazolium bromide (MTT) was purchased from Amresco (Ohio, USA). Saline (0.9% sodium chloride) was obtained from Duopharma Sdn. Bhd. (Selangor, Malaysia). Carbonyl cyanide 3-chlorophenylhydrazone (CCCP) was purchased from Sigma (Steinheim, Germany). Protein assay dye reagent concentrate was obtained from Bio-Rad Laboratories (California, USA). Complex I, Complex II, Complex IV and ATP synthase enzyme activity microplate assay kit were purchased from MitoSciences (Oregon, USA).

Syntheses of Rosamine Analogs

Rosamines were synthesized and purified as described previously [11]. The starting material of xanthone ditriflate was prepared in solution by triflation of the phenols, followed by animation of the triflate with piperidine to give symmetrical cyclic amines substitution (Fig. 2A) or by stepwise addition of piperidine and morpholine to give unsymmetrical cyclic amines substitution (Fig. 2B) [11]. The resulted 3,6-diamino-xanthen-9-one was reacted with organolithium or Grignard reagents to yield the desired rosamine structures.

In general, a Grignard reagent or lithium reagent (1.0 mmol) was added dropwise over 1 min to the solution of 0.2 mmol 3,6-diamino-xanthen-9-one in 5 ml of THF at 0°C. The reaction mixture was stirred for 12 h at room temperature. After completion of reaction, 2 ml of 2 M aqueous HCl was added, stirred for 10 min to quench the reaction and diluted with 20 ml of CH_2Cl_2. The organic layer was washed with water and brine, dried over anhydrous Na_2SO_4, and concentrated under reduced pressure. The residue was purified by flash chromatography (5% to 10% MeOH/CH_2Cl_2) to give the pure product.

Spectral data for the synthesized compounds are listed here except the synthesis and spectral data for rosamines **1**, **2** and **5** were as previously reported [11]. They are named below in a way that describes the *meso*-substituents and assumes the compound is symmetrical unless otherwise indicated.

4-Bromobenzene Rosamine 3. ^{1}H NMR (300 MHz, $CDCl_3$) δ 7.72 (d, 2H, J = 8.4 Hz), 7.27–7.21 (m, 4H), 7.09 (dd, 2H, J = 9.6, 2.6 Hz), 6.94 (d, 2H, J = 2.6 Hz), 3.74–3.70 (m, 8H), 1.74 (br, 12H); ^{13}C NMR (75 MHz, $CDCl_3$) δ 158.1, 156.3, 155.0, 132.2, 131.6, 130.9, 130.5, 124.9, 115.0, 113.3, 97.4, 49.1, 25.9, 24.0; $\lambda_{max\ abs}$ 570 nm, $\lambda_{max\ emiss}$ 590 nm, ε 110800 M^{-1} cm^{-1}, fwhm 38 nm, Φ 0.78±0.02 in CH_2Cl_2; HRMS (ESI) m/z calcd for (M-Cl)$^+$ $C_{29}H_{30}BrN_2O$ 501.1542; found 501.1539.

4-Chlorobenzene Rosamine 4. ^{1}H NMR (300 MHz, $CDCl_3$) δ 7.56 (d, 2H, J = 8.4 Hz), 7.30 (d, 2H, J = 8.4 Hz), 7.26 (d, 2H, J = 9.6 Hz), 7.09 (dd, 2H, J = 9.6, 2.4 Hz), 6.95 (d, 2H, J = 2.4 Hz), 3.74–3.70 (m, 8H), 1.74 (br, 12H); ^{13}C NMR (125 MHz, $CDCl_3$) δ 158.1, 156.3, 155.1, 136.7, 131.6, 130.8, 130.1, 129.3, 115.0, 113.4, 97.5, 49.2, 25.9, 24.1; $\lambda_{max\ abs}$ 570 nm, $\lambda_{max\ emiss}$ 590 nm, ε 119100 M^{-1} cm^{-1}, fwhm 38 nm, Φ 0.80±0.02 in CH_2Cl_2; HRMS (ESI) m/z calcd for (M-Cl)$^+$ $C_{29}H_{30}ClN_2O$ 457.2047; found 457.2052.

Furan Rosamine 6. ^{1}H NMR (500 MHz, $CDCl_3$) δ 7.97 (d, 2H, J = 9.7 Hz), 7.92–7.91 (m, 1H), 7.18 (dd, 2H, J = 9.7, 2.6 Hz), 7.15–7.14 (m, 1H), 6.90 (d, 2H, J = 2.6 Hz), 6.82–6.81 (m, 1H), 3.74–3.72 (m, 8H), 1.76 (br, 12H); ^{13}C NMR (125 MHz, $CDCl_3$) δ 158.2, 156.0, 147.3, 145.7, 142.2, 132.0, 120.5, 115.0, 113.3, 111.8, 97.5, 49.0, 25.9, 24.1; $\lambda_{max\ abs}$ 592 nm, $\lambda_{max\ emiss}$ 627 nm, ε 86900 M^{-1} cm^{-1}, fwhm 105 nm, Φ 0.38±0.01 in CH_2Cl_2; HRMS (ESI) m/z calcd for (M-Cl)$^+$ $C_{27}H_{29}N_2O_2$ 413.2229; found 413.2232.

Unsymmetrical 4-Iodophenyl Rosamine 7. ^{1}H NMR (300 MHz, $CDCl_3$) δ 7.96 (d, 2H, J = 8.3 Hz), 7.35–7.29 (m, 2H), 7.17–7.09 (m, 6H), 3.88 (t, 4H, J = 4.7 Hz), 3.78–3.71 (m, 8H), 1.77 (br, 6H); ^{13}C NMR (75 MHz, $CDCl_3$) δ 158.6, 157.9, 156.9, 156.7, 155.9, 138.2, 131.9, 131.5, 131.1, 131.0, 115.5, 114.6, 114.0, 113.7, 98.6, 97.9, 97.1, 66.4, 49.5, 47.4, 26.1, 24.0; $\lambda_{max\ abs}$ 565 nm, $\lambda_{max\ emiss}$ 586 nm, ε 80900 M^{-1} cm^{-1}, fwhm 39 nm, Φ 0.52±0.02 in CH_2Cl_2; HRMS (ESI) m/z calcd for (M-Cl)$^+$ $C_{28}H_{28}IN_2O_2$ 551.1195; found 551.1192.

Unsymmetrical Thiofuryl Rosamine 8. ^{1}H NMR (500 MHz, $CDCl_3$) δ 7.69 (dd, 1H, J = 4.8, 1.4 Hz), 7.62 (d, 1H, J = 9.7 Hz), 7.59 (d, 1H, J = 9.7 Hz), 7.26–7.22 (m, 2H), 7.19 (dd, 1H, J = 9.7, 2.5 Hz), 7.09 (dd, 1H, J = 9.7, 2.5 Hz), 7.00 (d, 1H, J = 2.5 Hz), 6.90 (d, 1H, J = 2.5 Hz), 3.78 (t, 4H, J = 4.9 Hz), 3.68–3.65 (m, 8H), 1.67 (br, 6H); ^{13}C NMR (75 MHz, $CDCl_3$) δ 158.1, 157.5, 156.6, 156.3, 149.8, 132.2, 132.0, 131.7, 130.6, 130.6 (two peaks: 130.62, 130.56), 128.2, 115.2, 114.6, 114.3, 114.0, 97.8, 97.2, 66.2, 49.1, 47.2, 25.9, 23.9; $\lambda_{max\ abs}$ 576 nm, $\lambda_{max\ emiss}$ 599 nm, ε 87600 M^{-1} cm^{-1}, fwhm 42 nm, Φ 0.30±0.01 in CH_2Cl_2; HRMS (ESI) m/z calcd for (M-Cl)$^+$ $C_{26}H_{27}N_2O_2S$ 431.1793; found 431.1795.

Cell Culture and *In Vitro* Cell Viability Assay

MCF-7 breast carcinoma and HCT-116 colon carcinoma cell lines were obtained from American Tissue Culture Collection (Virginia, USA) and maintained in RPMI 1640 medium supplemented with 10% FBS. HSC-2 oral cavity human squamous carcinoma cells were obtained from Health Science Research Resources Bank (Japan). HK-1, a previously characterized nasopharyngeal squamous carcinoma cells [12] is a gift by Prof. Wong Y.C. from the University of Hong Kong. Both cell lines were grown in MEM medium supplemented with 10% FBS. For cell viability assay, cells at 4000 cells/well in 80 µl of medium were inoculated in 96-well plates and were allowed to adhere overnight. Cells were then treated with each compound at concentrations ranging from 0.001–10 µM giving the final volume of 100 µl in each well. At the end of incubation period, 15 µl of 5.0 mg/ml MTT in phosphate buffered saline (PBS) was added and incubated for 4 h. Medium and excessive MTT were aspirated and the resulting formazan was solubilized with 100 µl of dimethyl sulfoxide. Absorbance was read at 570 nm with SpectraMax M4 microplate spectrophotometer (Molecular Devices, CA).

NCI-60 Human Tumor Cell Line Screen

NCI-60 cell panel screening was performed by the NCI/National Institutes of Health developmental therapeutics program

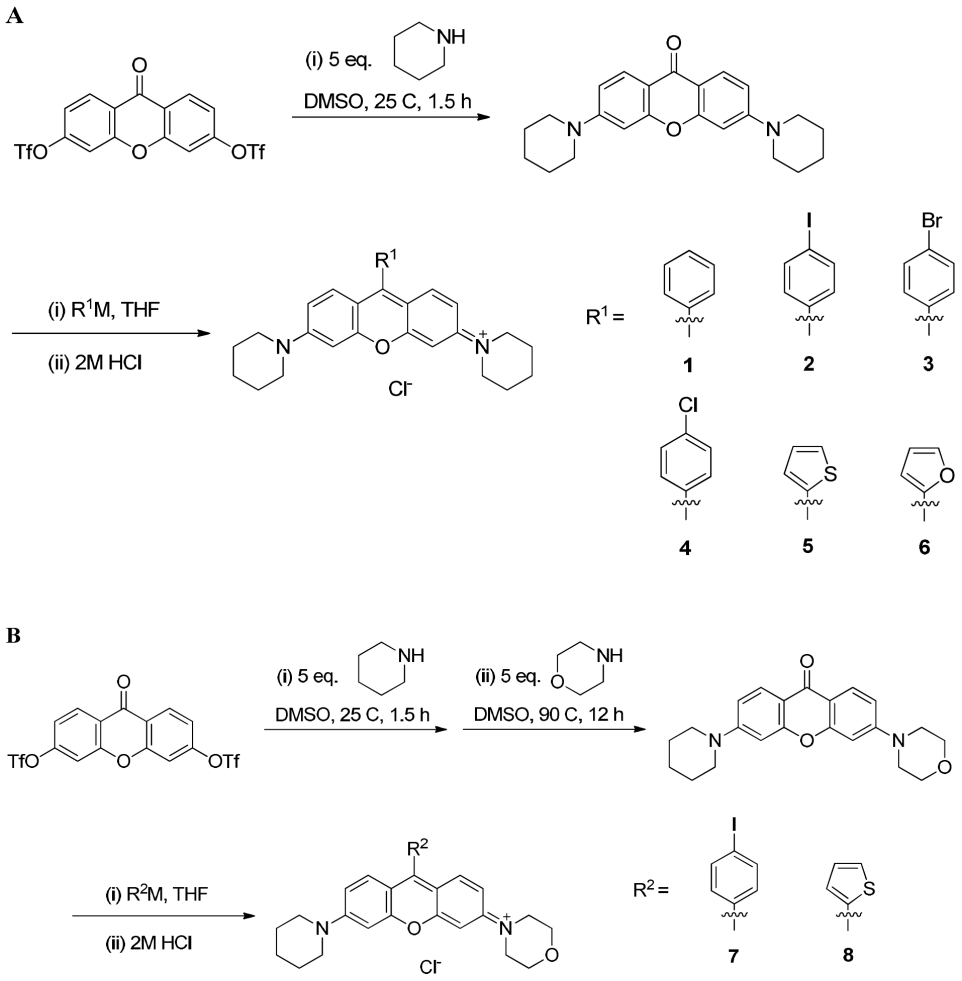

Figure 2. Schematic illustration of the synthesis of rosamines. (A) The starting material of xanthone ditriflate was prepared in solution by triflation of the phenols, followed by animation of the triflate with piperidine to give symmetrical cyclic amines substitution or; (B) by stepwise addition of piperidine and morpholine to give unsymmetrical cyclic amines substitution.
doi:10.1371/journal.pone.0082934.g002

(Bethesda, US). This platform allows the determination of growth inhibitory profiles of test compounds on 60 different human cancer cell lines, representing leukemia, melanoma and cancers of the lung, colon, central nervous system, ovary, breast, prostate, and renal subpanel. Sulforhodamine B assay was used to assess the cytotoxicity of test agents in a panel of 60 cell lines [13]. Briefly, the human tumor cell lines of the cancer screening panel were grown in RPMI 1640 medium containing 5% FBS and 2 mM L-glutamine. For a typical screening experiment, cells were inoculated into 96 well microtiter plates in 100 µl at plating densities depending on the doubling time of individual cell lines. After cell inoculation, the microtiter plates are incubated at 37°C, 5% CO_2 and 100% relative humidity for 24 h. Following incubation, aliquots of 100 µl of compound at different dilutions were added to the appropriate microtiter wells and were further incubated for 48 h. At the assay end-point, cells were fixed with trichloroacetic acid followed by Sulforhodamine B staining for cellular protein content. Sulforhodamine B absorbance was read at a wavelength of 515 nm as a measurement of cell density.

Mitochondria Isolation and Detergent Solubilization

Functional mitochondria were isolated from mouse liver by differential centrifugation method [14]. Briefly, a mouse (~30 g) was starved overnight before sacrificed by cervical dislocation. The liver was harvested promptly and rinsed with ice-cold mitochondria isolation buffer (10 mM Tris-MOPS, 1 mM EGTA/Tris, 0.2 M sucrose, pH 7.4) until blood-free. The liver was then cut into small pieces in a beaker using scissors while keeping in an ice-bath. The buffer was replaced with 5 ml of fresh isolation buffer and the liver was homogenized with a Polytron probe (Ultra-Turrax T8, Ika-Werke, Germany) until smooth. The homogenate was centrifuged at 1000 g for 15 min at 4°C. The pellet was discarded and the supernatant was centrifuged at 12000 g for 15 min at 4°C to pellet the mitochondria. The mitochondria were washed twice by resuspending in 4 volumes of isolation buffer containing 1 × protease cocktail inhibitor. The concentration of the mitochondrial protein was determined using the Bradford (Biorad protein assay) method. The mitochondria were frozen in 10 mg/ml aliquot at −80°C.

Detergent solubilization of the mitochondria proteins was done prior to measurement of the oxidative phosphorylation complexes activity. Mitochondria were diluted to 5.5 mg/ml with PBS and solubilized by addition of a 1/10th volume of detergent provided to give the final protein concentration of 5 mg/ml. The mixture was incubated on ice for 30 min and centrifuged at 17 000 g at 4°C for 20 min. The supernatant was collected and diluted to appropriate concentration for each oxidative phosphorylation complexes activity.

Table 1. Antiproliferative activities of rosamine analogs against a panel of cancer cell lines.

Rosamine	Activity IC_{50} (μM)[a]				
	MCF-7	HCT-116	HSC-2	HK-1	Mean[b]
1	1.2±0.7	0.60±0.41	0.09±0.00	0.61±0.07	0.63 †
2	0.59±0.12	0.39±0.07	0.35±0.05	0.29±0.03	0.41 ‡
3	0.29±0.04	0.30±0.08	0.19±0.11	0.34±0.00	0.28 ‡,§
4	0.15±0.04	0.22±0.14	0.09±0.01	0.25±0.01	0.18 ‡,§
5	0.18±0.02	0.07±0.02	0.09±0.01	0.10±0.00	0.11 §
6	0.31±0.14	0.10±0.03	0.09±0.00	0.31±0.08	0.20 ‡,§
7	0.26±0.07	0.24±0.07	0.22±0.10	0.44±0.01	0.29 ‡,§
8	0.17±0.10	0.07±0.02	0.22±0.11	0.53±0.00	0.25 ‡,§

[a]IC_{50}, the concentration of compound, which inhibits the viability by 50% as compared with control untreated cells. Values represent the mean ± SD of at least three determination assessed 48 h post-treatment using methylthiazolyldiphenyl-tetrazolium bromide assay.
[b]Different symbols (†, ‡, and §) indicate statistically significant differences ($P<0.05$) among the mean values.
doi:10.1371/journal.pone.0082934.t001

Measurement of Oxidative Phosphorylation Complexes Activity

Measurements of mitochondria oxidative phosphorylation activities for Complex I, II, IV and ATP-synthase were carried out using the microplate immunocapture ELISA assay kit according to their respective manufacturer's protocols [15]. In general, plate pre-coated with appropriate immunocapture antibody was incubated with mitochondria extract at recommended concentration to allow immobilization of their respective complexes. Complexes activity was measured by addition of substrates solution mix provided by the kit and compound was added at concentration ranging from 0.01–10 μM in triplicate. Control wells treated with only 0.1% DMSO (v/v) and wells without mitochondria extract incubation were included as background reference. The kinetic of the complexes activity was recorded with SpectraMax M4 microplate spectrophotometer reader using the suggested measurement parameters.

JC-1 Analysis of Mitochondrial Membrane Potential

The mitochondrial membrane potential was measured based on the potential–dependent accumulation of the cationic JC-1 dye which results in a shift of fluorescence emission from green (~525 nm) to red (~590 nm) due to the formation of J-aggregates [16]. Therefore, mitochondrial depolarization is indicated by a decrease in the red/green fluorescence intensity ratio. Briefly, cells were collected and suspended in 1 ml warm media at approximately 1×10^6 cell/ml. In a control tube, 1 μl of 50 mM CCCP was added and incubated at 37°C for 5 min. Then, 10 μl of 200 μM JC-1 was added into the cells and incubated at 37°C for 30 min. Cells were washed twice with warm PBS, resuspended in 500 μl of PBS and analyzed on a FACSCalibur flow cytometer using 488 nm excitation with 530/30 nm and 585/42 nm bandpass emission filters.

In Vivo Antitumor Efficacy

Tumor allografts were initiated by subcutaneous injection of 5×10^5 4T1 mouse mammary carcinoma in 0.1 ml RPMI 1640 media into the inguinal mammary fat-pads of mice [17]. Tumor growth was monitored and treatments were initiated when tumors reached volume of approximately 200 mm^3. To assess the tumor growth inhibition, 4T1 tumor bearing mice were randomized into groups with at least eight animals per group. Compound **5** was prepared at 0.3 mg/ml in normal saline and treatment was administered intravenously at 5 mg/kg on staging day or 3 mg/kg every other day for six treatments (q2dx6). For control group, normal saline was given. The animal weights and tumor volume were measured three times weekly for 14 d. The tumor volume was calculated using the equation: $(\text{length}\times\text{width}^2)/2$ and relative tumor volume (RTV) was calculated for every tumor volume at any given time (V_T) against the tumor volume at staging day (V_0) using the equation: V_T/V_0. The RTV – time profile for each group was plotted and tumor growth delay in attaining a specified number of doublings compared to control was determined [18,19]. Results were expressed as median ±95% confidence interval (n = 8).

Statistical Analysis

Statistical significance were performed using one-way ANOVA *post hoc* with Bonferroni test (SPSS 16.0, IBM Corporation, Armonk, NY) and difference were considered significant when $P<0.05$.

Results and Discussion

Rosamine Analogs

Our previous study indicated structures *meso*-substituted with 4-iodobenzene **2** and thiofuran **5** were 5-fold more active than the phenyl substituted compound **1**. Compounds **3**, **4** and **6** were synthesized to test if *meso*-replacement with 4-bromobenzene **3**, 4-chlorobenzene **4** or 2-furyl **6** groups would affect the anticancer activity. In addition, the 4-iodobenzene **7** or 2-thiofuran *meso* substituents **8** *and* unsymmetrical piperidine/morphine amine substituents were synthesized and investigated. Rosamines **1**–**4** and **7** were not appreciably water-soluble so they were reconstituted in DMSO at 10 mM as treatment stock. Rosamines **5**, **6** and **8** were readily solubilized in aqueous media at similar concentrations, so were used without DMSO.

In Vitro Antitumor Efficacy of Rosamine and NCI-60 Screen

The *in vitro* antitumor activity of rosamines was assessed using a 48 h endpoint cell viability methylthiazolyldiphenyl-tetrazolium bromide (MTT) assay against a panel of solid human tumor cell lines including breast carcinoma (MCF-7), colon carcinoma (HCT-116), oral squamous cell carcinoma (HSC-2) and nasopharyngeal carcinoma (HK-1). The IC_{50} values for these rosamines across the panel of cancer cell lines tested ranged from 0.07–1.2 μM as summarized in Table 1. From this study, rosamines bearing phenyl halide or heterocyclic moieties were significantly ($P<0.05$) more potent than phenyl substituted rosamine **1**. Halide substitution resulted in improvement of cytotoxicity; this was expected because substitution of *H* by halide is commonly used to increase compound lipophilicity that improves lipid-bilayer membrane permeability [20]. Within the halide series, cytotoxicities increase in the following order **4**>**3**>**2** (Cl>Br>I), although not statistically significant ($P>0.05$). The compounds with *meso*-heterocyclic substituents **5** and **6** were more potent than the aromatic halides **2**–**4**. Of the two compounds with *meso*-heterocycles the thiofuran-substituted **5** was slightly more active than **6**, the furan-substituted one.

Compounds **7** and **8** have a more polar combination of amine substituents than the symmetrical *bis*piperidine **2**, and they proved to be more cytotoxic (Table 1). This is consistent with our previous data for 2-methylbenzenes unsymmetrically substituted with

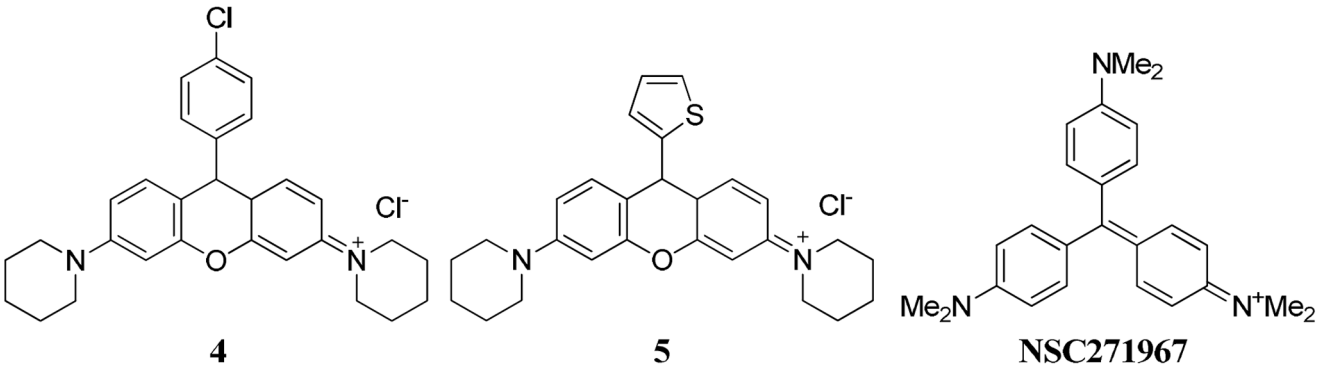

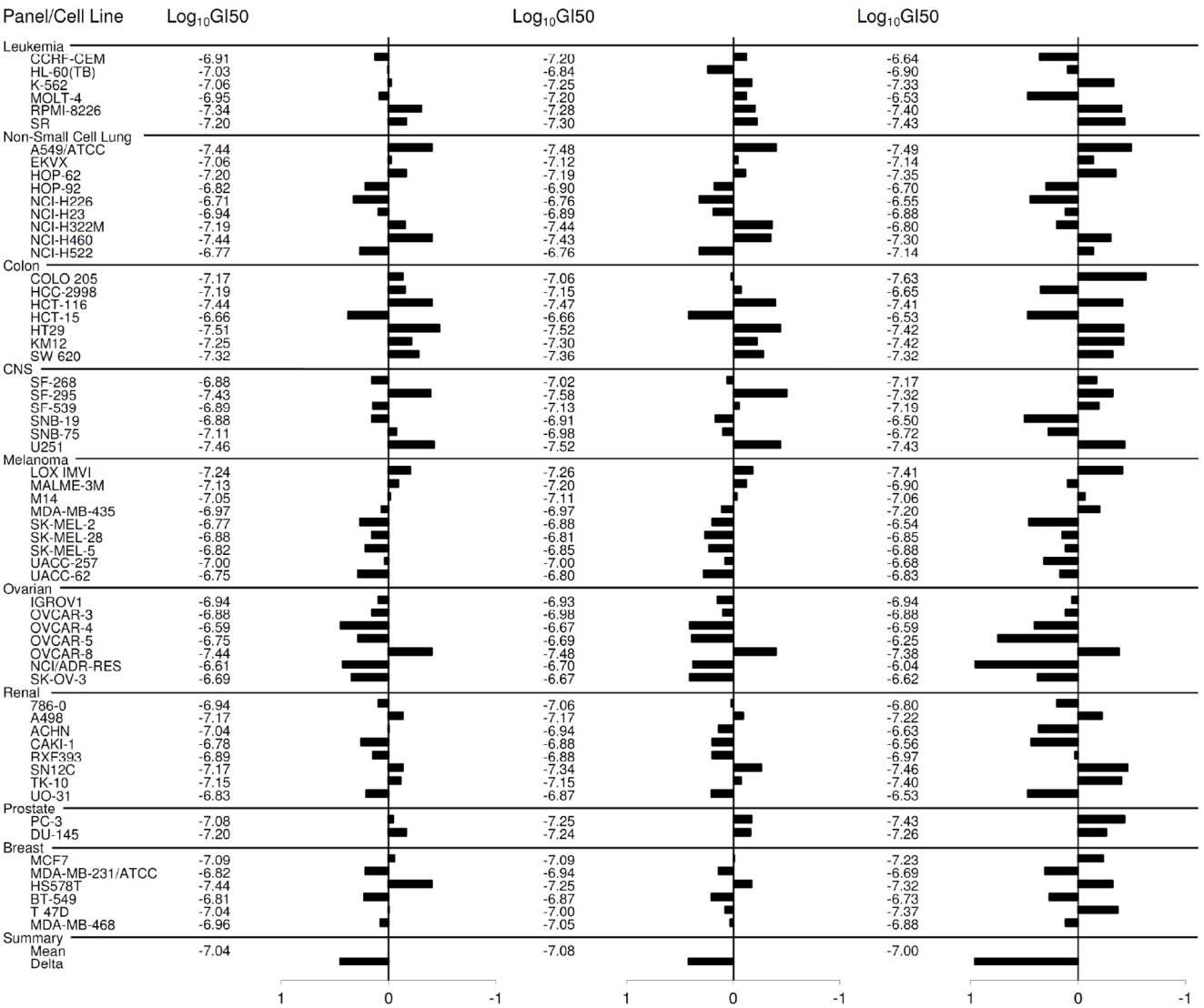

Figure 3. NCI-60 cell lines screen. GI_{50} (50% growth inhibition) mean graphs showing the activity patterns of **4**, **5** and methyl violet (NSC271967) in the NCI-60 cell line screens. Both the rosamines exhibited potent antiproliferative effects with $Log_{10}GI_{50} = -7$ ($GI_{50} = 0.1$ μM) and were particularly more effective against colorectal cancer panel. COMPARE analyses indicated **4** and **5** have similar pattern of activity as methyl violet with Pearson correlation coefficient values of 0.767 and 0.72, respectively.
doi:10.1371/journal.pone.0082934.g003

piperidine and morpholine which showed nearly 2-fold lower IC_{50} values compared with the symmetrical hydrophobic structure containing only piperidine [10]. Meanwhile for the *meso*-thiofuran **5**, substitution of one of the piperidine groups with morpholine gives **8**, which has a slightly *decreased* activity, contrary to our expectations.

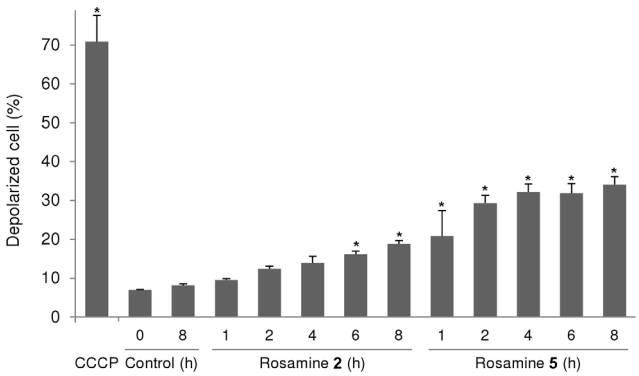

Figure 4. Loss of mitochondrial transmembrane potential. Representative event of mitochondrial transmembrane potential loss in HSC-2 cells treated with **2** and **5** at 0.1 μM. Following 8 h of treatment with **2** and **5**, the percentage of cell population with mitochondrial transmembrane potential loss increased to 19% and 34%, respectively. The percentage depolarized cell of untreated control at 8 h remains at 8%, while for positive control, cells treated with 5 μM of carbonyl cyanide 3-chlorophenylhydrazone (CCCP) for 5 min results in 70% depolarized cell population. *Difference with *P*-value<0.05 compared to control at 0 h.
doi:10.1371/journal.pone.0082934.g004

Rosamines can exhibit phototoxicity due to generation of reactive oxygen species in the presence of light. To test for this, a duplicate plate was irradiated with 5.3 J/cm^2 of broad spectrum light for 2 h after compound treatment in parallel with a plate maintained in the dark. There were no significant differences in IC_{50} values obtained between both irradiated and non-irradiated experiments (data not shown) indicating phototoxicity was not an issue.

On the basis of the findings above, rosamines **4** (NSC751819) and **5** (NSC751817) were submitted for NCI-60 human tumor cell lines screen to provide more information on the growth inhibitory profiles against 60 different human cancer cell lines, representing leukemia, melanoma and cancers of the lung, colon, central nervous system, ovary, breast, prostate, and renal subpanel. This platform allows the mode of action to be inferred by comparing with the drug-activity patterns of standard agents with known targeting characteristics using COMPARE (computerized pattern-recognition algorithm) analyses [21]. The GI_{50} values generated from the NCI-60 cell lines screen indicated that both rosamine **4** and **5** exhibited potent antiproliferative effects with $Log_{10}GI_{50} = -7$ ($GI_{50} = 0.1$ μM) and were particularly more effective against a sub-panel of colorectal cancer cell lines (Fig. 3). COMPARE analyses indicated that both these rosamines had similar patterns of activity with methyl violet (NSC271967), a cationic triarylmethane dye which has been formerly used in

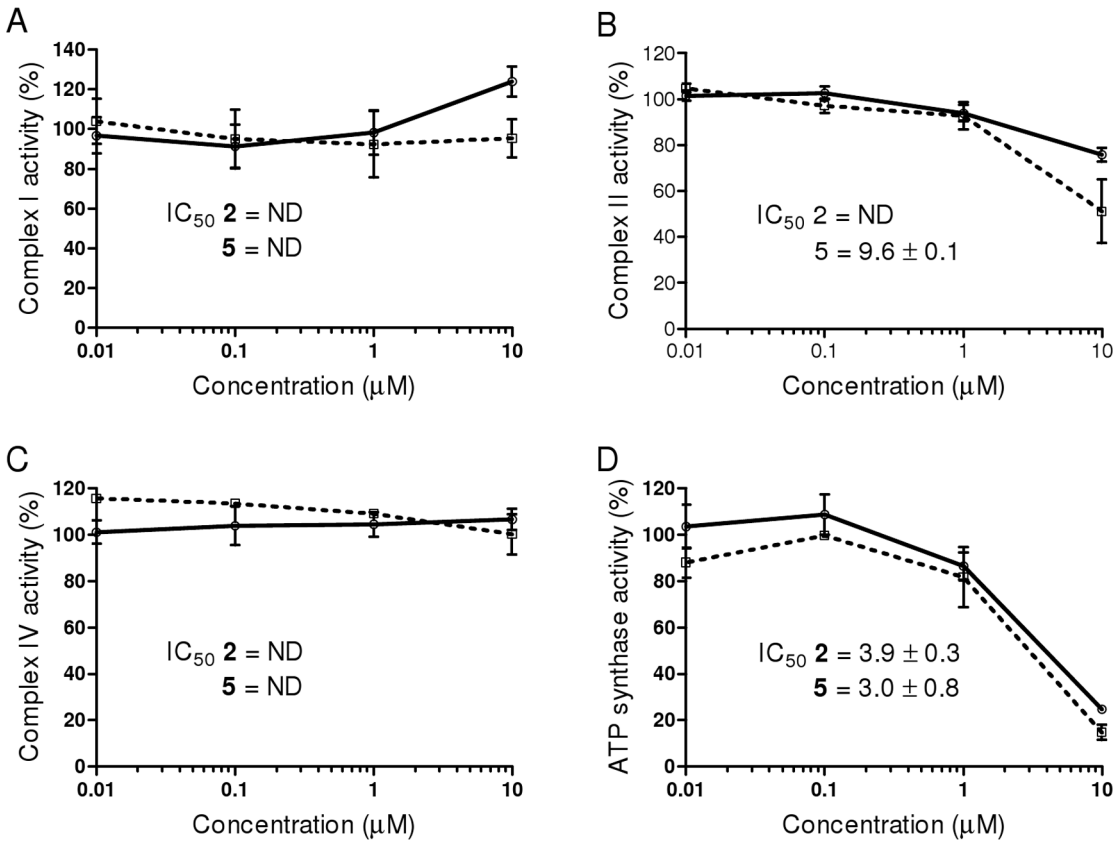

Figure 5. Inhibition of mitochondrial oxidative phosphorylation complexes. The dose-response inhibition of mitochondrial oxidative phosphorylation Complex 1 (A), Complex II (B), Complex IV (C) and ATP synthase (D) activities by rosamine **2** (solid line) and **5** (dotted line). The activity of Complex II was partially inhibited by **5** with IC_{50} value of 9.6±0.1 μM whereas for **2**, inhibition was observed but with undetermined IC_{50} value. Both **2** and **5** also inhibited the ATP synthase activities with IC_{50} values of 3.9±0.3 and 3.0±0.8 μM respectively. The activity of Complex I and Complex IV were not affected by the rosamines at the treated concentrations (highest at 10 μM). IC_{50} values depict concentration that inhibits the complexes activity by 50%. ND - indicate non-determined IC_{50} values based on the concentration used.
doi:10.1371/journal.pone.0082934.g005

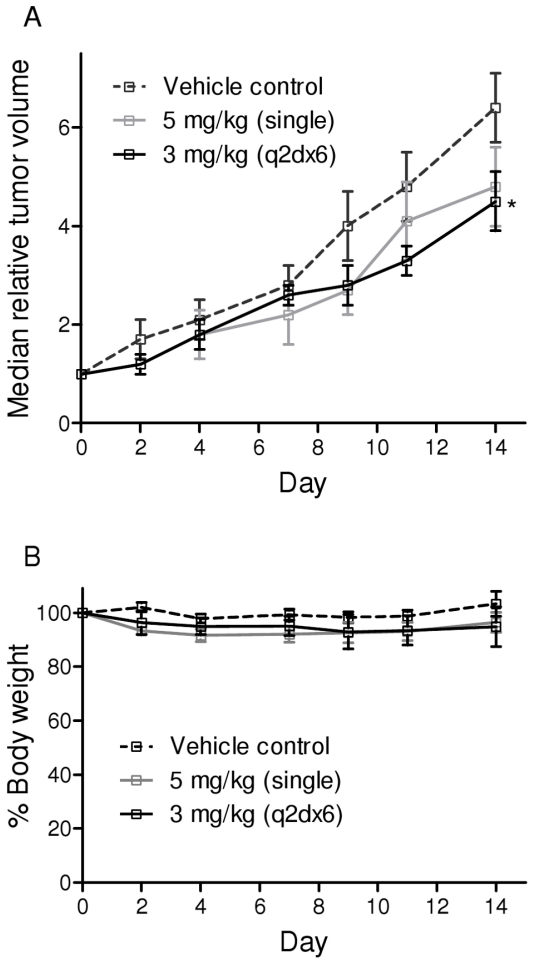

Figure 6. *In vivo* antitumor effects of rosamine. (A) The relative tumor volume (RTV) – time profile of 4T1 murine breast carcinoma in Balb/C mice following intravenous dosing of rosamine **5** or saline as vehicle control. Each point represents median ±95% confidence interval of RTV to staging day (n = 8). The terminal % T/C value for mice receiving 5 mg/kg and 3 mg/kg (q2d×6) of **5** were 72% and 66% respectively. The two doubling tumor growth delay (T-C)/C (dotted line, RTV = 4) for mice receiving a single bolus of 5 mg/kg and multiple doses of 3 mg/kg (q2d×6) of **5** were 22% and 38%, respectively. T and C refer to RTV for treatment and control groups, respectively. *Difference with *P*-value<0.05 compared to control animal. (B) Percentage of mean body weight of mice received 5 mg/kg or 3 mg/kg (q2d×6) of **5** compared to untreated mice. Body weight loss was observed in treatment groups but none of these mice experienced weight loss of more than 15%.
doi:10.1371/journal.pone.0082934.g006

medicine for its antimicrobial, antifungal and antihelmintic properties. This class of dyes had been shown to promote mitochondrial respiratory inhibition by inhibiting ATP synthesis, dissipating mitochondrial membrane potential and inducing mitochondrial permeability transition [22,23]. Thus the NCI-60 cell lines screen indicated the compounds tested had a signature unique to energy metabolism-targeting anticancer agents.

Rosamines Interfered the Energy Redox

We have previously demonstrated that rosamines primarily localize in the mitochondria [10] and that accumulation of cytotoxic DLC is known to alter mitochondrial transmembrane potentials [24,25]. Thus, alterations of mitochondrial membrane potential caused by rosamines **2** and **5** were monitored based on the accumulation of potential-dependent JC-1 dye which resulted in a shift of fluorescence emission from green (~525 nm) to red (~590 nm) due to the formation of J-aggregates. From the study, HSC-2 cells treated with **2** at 0.1 μM, 9% of the cell population exhibited the onset of mitochondrial transmembrane potential loss within 1 h after treatment and gradually increased to 19% ($P<0.05$) in 8 h (Fig. 4). Meanwhile, the mitochondrial transmembrane potential loss was more prominent in HSC-2 cells treated with **5** at 0.1 μM. Approximately 21% ($P<0.05$) of the cell population was affected in the first hour and the percentage increased drastically to 34% in 8 h. For the untreated control cells, the population of depolarized cells at 8 h remained at approximately 8%. Meanwhile, cells treated with 5 μM of CCCP for 5 min resulted in loss of membrane potential in 70% ($P<0.05$) of cell population. CCCP is an oxidative phosphorylation decoupling agent which acts as a positive control for the experiment.

To further understand the mitochondria inhibition featured by the rosamines, their effect on the oxidative phosphorylation pathway was investigated. Using immunocapture ELISA microplate assay, the enzyme kinetics of mitochondrial redox carriers Complex I, Complex II, Complex IV and ATP-synthase were monitored upon treatment with **2** or **5**. The activity of Complex II (Fig. 5B) was partially inhibited by **5** with IC_{50} value of 9.6±0.1 μM whereas for **2**, inhibition was observed but did not reach 50% up to maximum concentrations studied. Meanwhile, both **2** and **5** displayed inhibition of ATP synthase activities (Fig. 5D) with IC_{50} values of 3.9±0.3 μM and 3.0±0.8 μM respectively. The activity of Complex I and Complex IV (Fig. 5A and 5C) were not affected by the rosamines at concentrations up to the maximum used, 10 μM. These data suggest that rosamines **2** or **5** compromise mitochondrial bioenergetics primarily by inhibiting ATP synthase, a proton-driven enzyme that produces ATP from ADP and inorganic phosphate. Similar biochemical interaction was observed in rhodamine-123 and this effect is expected as the compound has close structural similarity with the rosamines [26].

In Vivo Antitumor Effect of Rosamines

Rosamine **5** was selected for further evaluation in *in vivo* tumor model given its *in vitro* potency and ability to achieve aqueous solubility large enough for preparing an intravenous injection without the need of formulation. As illustrated in Fig. 6A, tumor growth attenuation was observed at experimental end-point (day 14) when mice received single bolus of 5 mg/kg of **5** i.v. compared control group ($P = 0.08$). The tumor growth attenuation effect is further enhanced ($P = 0.029$) when mice received rosamine treatment regimen at 3 mg/kg, once every 2 day, for 6 times (q2d×6). The median day for 4T1 tumor in attaining two-doubling growth (RTV = 4) were approximately 9, 11 and 13 days in control mice, mice receiving 5 mg/kg and 3 mg/kg (q2d×6) respectively. The determined percentage of two-doubling tumor growth delay (T-C)/C in mice treated with 5 mg/kg and 3 mg/kg (q2d×6) of **5** were 22% and 38%, respectively.

Meanwhile, the terminal percent test/control (% T/C) values calculated at the end of experiment were 72% and 66% in mice receiving 5 mg/kg and 3 mg/kg (q2d×6) respectively. The antitumor efficacy of **5** is minimal as the % T/C attained after treatment had ended is not ≤40% activity, the minimal rating for a compound to be considered active [18]. Loss of body weight (Fig. 6B) was observed in mice treated with **5** throughout the experimental period, however the reduction at any time were not statistically significant compared to the untreated mice. None of the mice suffer weight loss more that 15%, the cut-off limit set in the experiment [27].

From this study, the *in vivo* anticancer effect shown by **5** is minimal, probably because 4T1 was an aggressive tumor cell line and the dose of compound **5** used was modest. However, use of a higher concentration was not possible because unacceptable adverse effects such as weight loss, diarrhea and sudden death were observed at 10 mg/kg dose.

Even though these rosamines (i.e **2** and **5**) are more cytotoxic against cancer cells compared with normal epithelial cells (previously published data [10]), their effects on normal cells could still lead to undesirable side effects as a result of increase lactic acid accumulation in cells following decreased ATP synthase activity and a shift in metabolic pathways from aerobic to anaerobic metabolism. Accumulation of lactic acid has been shown to cause depressive cardiovascular function, cardiac arrhythmias and multiple organ failure. Therefore, risk minimization measures to deal with lactic acidosis such as those employed in the management of patients prescribed with metformin, a commonly used antidiabetic drug with similar toxic side effects, need to be outlined to prevent this serious complication [28,29].

Another documented side effect commonly associated with DLC such as rosamines is selective accumulation of these compounds in cardiac muscle cells that can lead to fatal deterioration in the function of the heart muscle [30]. Studies have shown that cardiac muscle cells are similar to cancer cells in that both also exhibit high negative plasma membrane potentials which encourage increased uptake of DLC. In connection to this, doxorubicin which is a positively charged antracycline antitumor agent, was also shown to target the cardiac muscle cells and caused serious and occasionally fatal cardiotoxicity in a significant number of treated cancer patient [31]. However, following liposomal encapsulation of doxorubicin, cardiotoxicity was diminished in cancer patients receiving the formulation with no loss of efficacy [32]. It therefore remains to be investigated whether a similar encapsulation approach with the rosamines could also decrease their toxicity while maintaining the efficacy.

Conclusions

The *in vitro* results demonstrated that the rosamines investigated here inhibit the proliferation of cancer cell-lines with IC_{50} value at nanomolar concentrations, with rosamine **5** being the most active. NCI-60 cell lines screen showed that these compounds are particularly effective against the colorectal cancer panel of cells and COMPARE analysis revealed a strong correlation in growth inhibitory pattern exhibited by mitochondrial respiratory inhibitor i.e. crystal violet. The anticancer effects of these compounds may have been due to their ability to compromise mitochondrial membrane potential and to inhibit the oxidative phosphorylation complexes primarily the ATP synthase which were both experimentally observed in this study. Although the preliminary *in vivo* antitumor activity of **5** is moderate against 4T1 murine mammary tumor, it may be worthwhile to test the compound in colon cancer xenograft models, for example, models based on HCT-116 and HT-29 cell lines which are both more sensitive to **5** on NCI-60 cell line screen. However further study is needed to diminish the toxic effects observed for this compound.

Acknowledgments

The authors would like to thank the National Cancer Institute for NCI-60 tumor cell line screening and Prof. Wong Y.C. from the University of Hong Kong for providing the HK-1 cell line.

Author Contributions

Conceived and designed the experiments: SHL HBL LYC. Performed the experiments: SHL LW. Analyzed the data: SHL LVK. Contributed reagents/materials/analysis tools: HBL KB LVK LYC. Wrote the paper: SHL KB HBL.

References

1. Lemmon MA, Schlessinger J (2010) Cell signaling by receptor tyrosine kinases. Cell 141: 1117–1134.
2. Nahta R, Esteva FJ (2007) Trastuzumab: triumphs and tribulations. Oncogene 26: 3637–3643.
3. Alcala AM, Flaherty KT (2012) BRAF inhibitors for the treatment of metastatic melanoma: clinical trials and mechanisms of resistance. Clin Cancer Res 18: 33–39.
4. Ayoola A, Barochia A, Belani K, Belani CP (2012) Primary and acquired resistance to epidermal growth factor receptor tyrosine kinase inhibitors in non-small cell lung cancer: an update. Cancer Invest 30: 433–446.
5. McBride HM, Neuspiel M, Wasiak S (2006) Mitochondria: more than just a powerhouse. Curr Biol 16: R551–560.
6. Biasutto L, Dong LF, Zoratti M, Neuzil J (2010) Mitochondrially targeted anti-cancer agents. Mitochondrion 10: 670–681.
7. Wang F, Ogasawara MA, Huang P (2010) Small mitochondria-targeting molecules as anti-cancer agents. Molecular Aspects of Medicine 31: 75–92.
8. Modica-Napolitano JS, Aprille JR (2001) Delocalized lipophilic cations selectively target the mitochondria of carcinoma cells. Adv Drug Deliv Rev 49: 63–70.
9. Lampidis TJ, Hasin Y, Weiss MJ, Chen LB (1985) Selective killing of carcinoma cells "in vitro" by lipophilic-cationic compounds: a cellular basis. Biomed Pharmacother 39: 220–226.
10. Lim SH, Wu L, Burgess K, Lee HB (2009) New cytotoxic rosamine derivatives selectively accumulate in the mitochondria of cancer cells. Anticancer Drugs 20: 461–468.
11. Wu L, Burgess K (2008) Synthesis and spectroscopic properties of rosamines with cyclic amine substituents. J Org Chem 73: 8711–8718.
12. Huang DP, Ho JH, Poon YF, Chew EC, Saw D, et al. (1980) Establishment of a cell line (NPC/HK1) from a differentiated squamous carcinoma of the nasopharynx. Int J Cancer 26: 127–132.
13. Boyd MR, Paull KD (1995) Some practical considerations and applications of the national cancer institute in vitro anticancer drug discovery screen. Drug Dev Res 34: 91–109.
14. Frezza C, Cipolat S, Scorrano L (2007) Organelle isolation: functional mitochondria from mouse liver, muscle and cultured fibroblasts. Nat Protoc 2: 287–295.
15. Nadanaciva S, Bernal A, Aggeler R, Capaldi R, Will Y (2007) Target identification of drug induced mitochondrial toxicity using immunocapture based OXPHOS activity assays. Toxicol In Vitro 21: 902–911.
16. Reers M, Smith TW, Chen LB (1991) J-aggregate formation of a carbocyanine as a quantitative fluorescent indicator of membrane potential. Biochemistry 30: 4480–4486.
17. Jin W, Kim GM, Kim MS, Lim MH, Yun C, et al. (2010) TrkC plays an essential role in breast tumor growth and metastasis. Carcinogenesis 31: 1939–1947.
18. Plowman J, Dykes DJ, Hollingshead M, Simpson-Herren L, Alley MC (1997) Human tumor xenograft models. In: Teicher B, editor. Anticancer Drug Development Guide: Preclinical Screening, Clinical Trials, and Approval. Totowa, NJ: Humana Press. pp. 101–125.
19. Hollingshead MG (2008) Antitumor efficacy testing in rodents. J Natl Cancer Inst 100: 1500–1510.
20. Gerebtzoff G, Li-Blatter X, Fischer H, Frentzel A, Seelig A (2004) Halogenation of drugs enhances membrane binding and permeation. Chembiochem 5: 676–684.
21. Shoemaker RH (2006) The NCI60 human tumour cell line anticancer drug screen. Nat Rev Cancer 6: 813–823.
22. Moreno SN, Gadelha FR, Docampo R (1988) Crystal violet as an uncoupler of oxidative phosphorylation in rat liver mitochondria. J Biol Chem 263: 12493–12499.
23. Kowaltowski AJ, Turin J, Indig GL, Vercesi AE (1999) Mitochondrial effects of triarylmethane dyes. J Bioenerg Biomembr 31: 581–590.
24. Toogood PL (2008) Mitochondrial drugs. Curr Opin Chem Biol 12: 457–463.
25. Don AS, Hogg PJ (2004) Mitochondria as cancer drug targets. Trends Mol Med 10: 372–378.
26. Modica-Napolitano JS, Weiss MJ, Chen LB, Aprille JR (1984) Rhodamine 123 inhibits bioenergetic function in isolated rat liver mitochondria. Biochem Biophys Res Commun 118: 717–723.

27. Workman P, Aboagye EO, Balkwill F, Balmain A, Bruder G, et al. (2010) Guidelines for the welfare and use of animals in cancer research. Br J Cancer 102: 1555–1577.
28. Renda F, Mura P, Finco G, Ferrazin F, Pani L, et al. (2013) Metformin-associated lactic acidosis requiring hospitalization. A national 10 year survey and a systematic literature review. Eur Rev Med Oharmaco Sci 17 45–49.
29. Kraut JA, Madias NE (2012) Treatment of acute metabolic acidosis: a pathophysiologic approach. Nat Rev Nephrol 8: 589–601.
30. Kurtoglu M, Lampidis TJ (2009) From delocalized lipophilic cations to hypoxia: blocking tumor cell mitochondrial function leads to therapeutic gain with glycolytic inhibitors. Mol Nutr Food Res 53: 68–75.
31. Aiken MJ, Suhag V, Garcia CA, Acio E, Moreau S, et al. (2009) Doxorubicin-induced cardiac toxicity and cardiac rest gated blood pool imaging. Clin Nucl Med 34: 762–767.
32. Kesterson JP, Odunsi K, Lele S (2010) High cumulative doses of pegylated liposomal doxorubicin are not associated with cardiac toxicity in patients with gynecologic malignancies. Chemotherapy 56: 108–111.